PENTAFLUOROETHYL DERIVATIVES OF SULFUR(IV) FLUORIDES AND THE SF_4-DIAZABICYCLO[2.2.2]OCTANE LEWIS-ACID-BASE SYSTEM

NATHAN KOSTIUK
Bachelor of Science, University of Lethbridge, 2014

A Thesis
Submitted to the School of Graduate Studies
of the University of Lethbridge
in Partial Fulfilment of the Requirements for the Degree

MASTER OF SCIENCE

Department of Chemistry and Biochemistry
University of Lethbridge
LETHBRIDGE, ALBERTA, CANADA

PENTAFLUOROETHYL DERIVATIVES OF SULFUR(IV) FLUORIDES AND THE SF_4-DIAZABICYCLO[2.2.2]OCTANE LEWIS ACID-BASE SYSTEM

NATHAN KOSTIUK

Date of Defence: November 16th, 2017

Dr. Michael Gerken Supervisor	Professor	Ph.D.
Dr. Paul G. Hayes Thesis Examination Committee Member	Professor	Ph.D.
Dr. Stacey Wetmore Thesis Examination Committee Member	Professor	Ph.D.
Dr. Maik Finze External Examiner Julius-Maximilians-Universität Würzburg, Würzburg, Germany	Professor	Ph.D.
Dr. Peter Dibble Chair, Thesis Examination Committee	Associate Professor	Ph.D.

Dedicated to my parents, Greg and Valerie, whose parenting ensured my success and whose love shaped me into who I am.

Abstract

Pentafluoroethyl derivatives of sulfur(IV) fluorides were synthesized by reacting $Me_3SiC_2F_5$ with SF_4 and SOF_2 forming $SF_3C_2F_5$, $SF_2(C_2F_4)_2$, $SOFC_2F_5$, and $SO(C_2F_5)_2$, all of which were modelled by B3LYP/aug-cc-PVTZ calculations and characterized by high-resolution ^{19}F NMR spectroscopy including simulations of their complicated ^{19}F NMR spectra. The X-ray crystal structures of $SO(C_2F_5)_2$, $Me_3SiC_2F_5$, and $[S(OC_2H_5)_3][H_3F_4]$ were determined, the latter being formed by the low-temperature alcoholysis of some sulfur(IV) species.

The diazabicyclo[2.2.2]octane-SF_4 Lewis acid-base system was investigated using Raman spectroscopy, including the formation of $C_6H_{12}N_2$•$2SF_4$ that was characterized by X-ray crystallography. When precipitated at low temperature, the DABCO-SF_4 system incorporates additional non-adducted SF_4 in the solid. Removing some SF_4 under dynamic vacuum at –25 °C still left SF_4 in the sample, presumably yielding the DABCO•SF_4 adduct, based on Raman spectroscopy. The DABCO-SF_4 system can be solvolysed by HF that is produced by the hydrolysis of SF_4, forming crystals of $[C_6H_{12}N_2H]_2F[SF_5]$•$6SF_4$.

Acknowledgments

I would like to thank my supervisor, Dr. Michael Gerken, for his teaching and mentorship that ignited my interest for science and investigation. His Chem 1000 lecture was my first university class, and that day I saw his genuine kindness and passion for helping others succeed.

I would like to thank other members of my supervisory committee, Dr. Paul Hayes and Dr. Stacey Wetmore, for their participation and guidance over the course of my graduate education. My thanks to Dr. Peter Dibble for chairing my thesis examination and Dr. Maik Finze for participating as my external examiner.

My thanks to the entire Department of Chemistry and Biochemistry, especially Susan Hill whose work and organization keep the gears turning in this department. Thank you to Dr. Paul Hazendonk for his expertise and advice regarding the NMR spectroscopy and simulation presented in Chapters 3 and 4. Thank you to Tony Montina for helpful conversations, troubleshooting, and taking time to teach me the intricacies of NMR spectroscopy. Thank you to Kris Fischer for his ability to fix any hardware problem that I have presented him with.

Thank you everyone involved with Let's Talk Science at the University of Lethbridge, especially Dr. Ute Wieden-Kothe for her supervision and for always standing up for me.

Thank you to Waterhen Lake First Nation Chief and Council for their financial support and sense of community. Thank you to the Alberta Government for the Indigenous Graduate Award that was invaluable in terms of support and valuable in terms of sum. I hope that continued investment into the education of indigenous students may continue to produce the same opportunities that I have been lucky enough to receive.

Thank you to past and present members of the Gerken group, especially Doug Turnbull who has long-served as my human thesaurus and fact-checker, as well as Daniel Stuart for his friendship outside of regular work hours. I would also like thank members of the Hayes group for

their friendship and entertainment, especially Jackson Knott. I extend my thanks to fellow graduate student peers Rhys, David, Jalyce, and especially Sarah; our friendship made my years here bearable and quite often enjoyable. While too numerous to thank individually, I thank all my friends at the U of L – good luck on your thesis projects.

Finally, I thank my family Greg, Valerie, and Melissa who were my first teachers, friends, and mentors. Your presence, support, and love got me to where I am.

Table of Contents

List of Tables

List of Figures

List of Abbreviations

General

VSEPR	valence shell electron pair repulsion
IR	infrared
r_{vdW}	van der Waals radius
χ	electronegativity
o.d.	outer diameter
vide supra/infra	see above/below
ax/eq	axial/equatorial
σ	standard deviation

Computational methods

DFT	density functional theory
B3LYP	Becke, 3-parameter, Lee-Yang-Parr
aug-cc-pVTZ	augmented – correlation-consistent polarized – triple-zeta

Nuclear Magnetic Resonance

NMR	nuclear magnetic resonance
δ	chemical shift
J	scalar coupling constant in Hertz
ppm	parts per million
TMS	tetramethylsilane
ω	Larmor frequency

X-ray Crystallography

a, b, c,α, β, γ	cell parameters
V	cell volume
λ	wavelength
Z	molecules per unit cell
μ	absorption coefficient
R1	conventional agreement index
wR2	weighted agreement index
G.o.o.F.	goodness of fit

Compounds

THF	tetrahydrofuran
18-crown-6	1,4,7,10,13,16-hexaoxacyclooctadecane
t-BuO	tert-butoxide
DMF	dimethylformamide
FEP	copolymer of perfluoroethylene and perfluoropropylene
PTFE	polytetrafluoroethylene
Kel-F	chlorotrifluoroethylene
DABCO	diazabicyclo[2.2.2]octane
TMAF	tetramethylammonium fluoride
DMAP	dimethylaminopyridine
C_f	perfluorinated alkyl group

1 Introduction

1.1 Sulfur Tetrafluoride

Sulfur forms a number of binary neutral fluorides: SF_2, S_2F_2, SF_4, SF_6, and S_2F_{10}. Besides SF_6, which is used primarily as an insulator gas for electrical equipment, SF_4 is the next most used and studied binary sulfur fluoride.[1] Sulfur tetrafluoride is prepared by reaction of SCl_2 with NaF and Cl_2.[2] With a boiling point of –38 °C and a melting point of –121 °C, SF_4 must be stored in a high-pressure and corrosion-resistant vessel. Even at low temperature, SF_4 is hydrolytically sensitive, reacting with water to form thionyl fluoride and hydrogen fluoride. Structurally, SF_4 adopts a seesaw geometry as evidenced by vibrational spectroscopy,[3–5] electron diffraction,[6,7] and NMR spectroscopy.[8,9] Recently, the structure of SF_4 in the solid state has been elucidated by X-ray crystallography.[10] As predicted by VSEPR theory,[11] axial fluorine-sulfur bonds are longer, and more ionic (solid state: 1.635(4)–1.671(5) Å) compared to the equatorial S–F bonds (1.474(6)–1.553(4) Å).

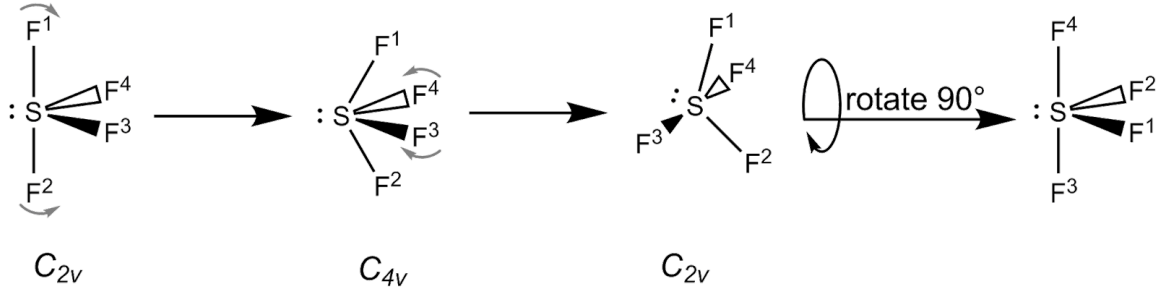

Figure 1.1 - Lewis diagram of sulfur tetrafluoride showing the seesaw geometry and the mechanism for the Berry pseudorotation causing exchange of axial and equatorial fluorine environments.

By ^{19}F NMR spectroscopy, SF_4 is observed as two triplets at 90 ppm and 34 ppm ($^2J_{F\text{-}F}$ = 79 Hz) that arise from the inequivalence of axial and equatorial fluorine environments at

low temperature. As temperature increases above approximately –30 °C Berry pseudorotation, the mechanism by which axial and equatorial environments can be exchanged (shown in Figure 1.1), becomes fast on the NMR timescale, causing the two fluorine resonances to coalesce into one broad singlet at approximately 62 ppm. The presence of fluoride or other donors will cause increased rate of exchange and will lower the coalescence temperature considerably. This is presumably due to an equilibrium that exists between adducted SF_4•D and SF_4 + D. The pseudo-octahedral SF_4•D can exist as either the *cis*- or *trans*- isomer, with respect to the lone pair and donor atom. The *trans* isomer exhibits C_{4v} symmetry with equivalent S–F bond distances that allow pseudorotation exchange with a reduced energy barrier.[12] Janzen argued that while this *trans* isomer is statistically disfavoured (1:4), only this isomer leads to the exchange of axial and equatorial ligands (see Equation 1.1).

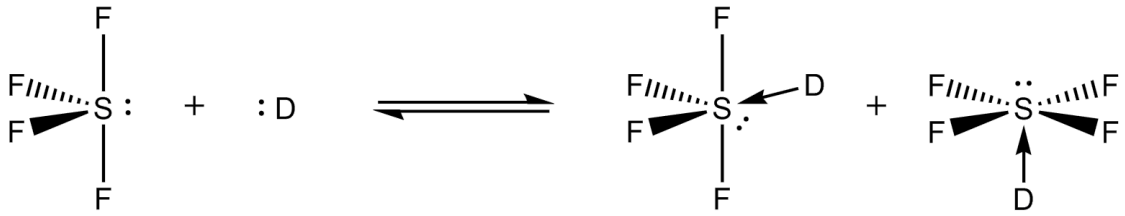

(1.1)

For this reason, the presence of a donor molecule will exacerbate SF_4 fluxionality caused by the Berry mechanism. This causes the coalescence of SF_4 resonances at a lower temperature than neat SF_4.[13] In their 1965 study, Redington and Berney proposed a

dimerization of pure SF_4 at low temperature (ca. 4 K),[14] featuring equatorial fluoride coordination to sulfur atoms of a neighboring molecule. Conversely, the solid-state crystal structure of SF_4 shows the more ionic and fluorobasic axial fluoride coordinating to sulfur centres at a distance of 2.954(5) – 3.261(6) Å.[10]

Sulfur tetrafluoride has been employed as a deoxyfluorination reagent, converting ketones, aldehydes, and carboxylic acids to their fluorinated analogues.[10] Several derivatives of SF_4 have been prepared and have become preferred deoxyfluorination reagents due to the toxic and corrosive nature of sulfur tetrafluoride and the hydrolysis product, hydrogen fluoride.[15]

1.1.1 Lewis-Acid Behavior of Sulfur Tetrafluoride

Sulfur tetrafluoride reacts with certain donor molecules to form Lewis acid-base adducts. The anionic pyramidal $[SF_5]^-$ is synthesized by the reaction of SF_4 with a sufficiently naked fluoride-ion source such as CsF (see Equation 1.2), $[N(CH_3)_4]F$, or by the cleavage of the S–C bond of $[SF_5C(CF_3)_2]^-$.[16-18]

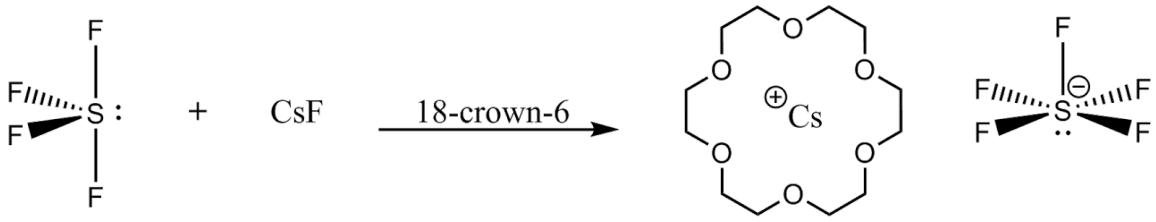

(1.2)

The $[SF_5]^-$ anion expectedly adopts a square pyramidal geometry; in their 1988 study, Seppelt and coworkers acquired the crystal structures of $Rb[SF_5]$ and $Cs_6[SF_5]_4[HF_2]_2$. Crystals of the $Cs[SF_5]$ salt were also synthesized but twinning prevented structural characterization.[17] Other salts containing $[SF_5]^-$ anions have been studied and include $[Cs(18\text{-crown-6})][SF_5]$,[19] $[(Me_2N)_3S][SF_5]$,[20] $[HNC_5H_3(CH_3)_2]F[SF_5]\bullet 4SF_4$,[10] $[HNC_5H_3(CH_3)_2][SF_5]\bullet SF_4$, and $[HNC_5H_4N(CH_3)_2]_2F[SF_5]\bullet CH_2Cl_2$.[21] Other Lewis acid-base adducts have been reported from reactions of organic bases with excess SF_4 allowing the characterization of these adducts by Raman spectroscopy and X-ray crystallography. Adducts of this type have been characterized with triethylamine,[22] pyridine (see Figure 1.2) and pyridine derivatives,[21,23] and the oxygen bases THF, cyclopentanone, dimethoxyethane, and caffeine.[24] A summary of some adducts between organic bases and SF_4 is tabulated in Table 1.1.

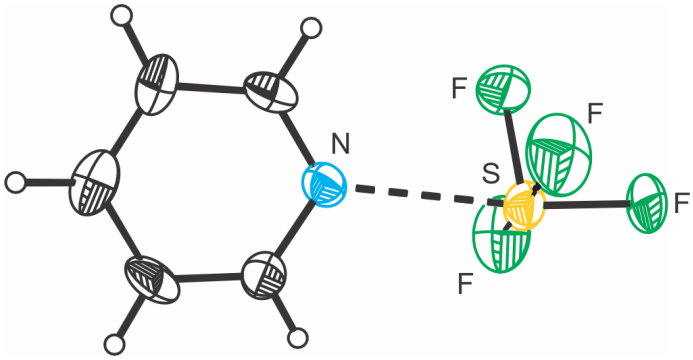

Figure 1.2 - X-ray crystal structure of $C_5H_5N\bullet SF_4$. Thermal ellipsoid plot drawn at 50% probability from Gerken and coworkers.[23] The 1:1 adduct is reversible and is stable to –40 °C. The S---N distance is 2.514(2) Å.

Table 1.1 - Tabulated data for some SF_4 acid-base adducts and their S---Donor distances as determined by X-ray crystallography

Adduct	Distance S---D (Å)
	S---N
SF_4•NEt_3[a]	2.384(2)
SF_4•NC_5H_5[b]	2.514(2)
SF_4•4-$NC_5H_5(CH_3)$[b]	2.513(3)
SF_4•4-$NC_5H_4N(CH_3)_2$[b]	2.141(2)
$[HNH_4C_5–C_5H_4N]F•2SF_4$[c]	2.614(3)
	S---O
$(SF_4•OC_4H_8)_2$[d]	2.777(2)–2.802(2)
$SF_4•(OC_4H_8)_2$[d]	2.662(2)–2.792(2)
$SF_4•CH_3OC_2H_4OCH_3$[d]	2.8692(9)
$C_8H_{10}N_4O_2•2SF_4•HF$[d]	2.8034(19)
$SF_4•(O{=}C_5H_8)_2$[d]	2.759(1) – 2.788(1)

[a] J.T. Goettel; P. Chaudhary; P. Hazendonk; H. P. A. Mercier; M. Gerken. *Chem. Commun.*, **2012**, *48*, 9120-9122.
[b] P. Chaudhary; J. T. Goettel; H. P. A. Mercier; S. Sowlati-Hashjin; P. Hazendonk; M. Gerken. *Chem. - Eur. J.*, **2015**, *21*, 6247–6256.
[c] J. T. Goettel; N. Kostiuk; M. Gerken. *Inorg. Chem.*, **2016**, *55* , 7126–7134.
[d] J. T. Goettel; M. Gerken. *Inorg. Chem.*, **2016**, *55* , 12441–12450

Whereas SF_4 adducts with triethylamine, pyridine, and pyridine derivatives are 1:1 adducts, those with THF, cyclopentanone, 1,2-dimethoxyethane, and caffeine feature two donor contacts to the sulfur tetrafluoride molecules.

Upon solvolysis by hydrogen fluoride, adducts of SF_4 with pyridine and pyridine derivatives incorporate HF into the crystal structures by protonation of the base and coordination of the fluoride counterion to SF_4, shown in Figure 1.3 and Equation 1.3. The $[SF_5]^-$ anion is distinct from F^----SF_4 moieties present in these solvolysed adducts because of the strong hydrogen bonding between the pyridinium cation and fluoride. In the cases of pyridine and 4-dimethylaminopyridine crystal structures were obtained which contain

$[HF_2]^-$ anions hydrogen-bonded to the protonated bases rather than fluoride. These structures reveal varied and intriguing bonding modalities between SF_4 and F^-: from $[SF_5]^-$ anion to much weaker F_4S---F^-, $F_4S(---F^-)_2$, and $F_4S(---FHF^-)_2$ dative bonds.[21]

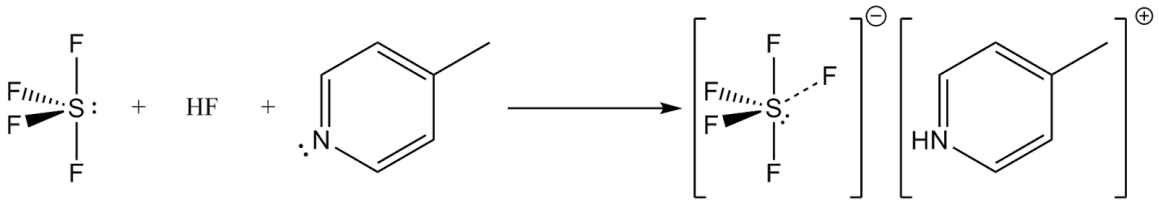

(1.3)

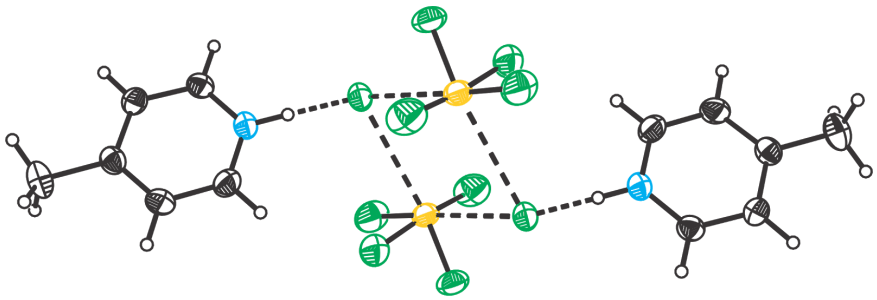

Figure 1.3 - Thermal ellipsoid plot of the X-ray crystal structure of the $([HNC_5H_4(CH_3)]F{\bullet}SF_4)_2$ dimeric structure from Goettel and coworkers[21] showing the solvolysis product of a SF_4 base adduct. Thermal ellipsoids are drawn to 50% probability.

Sulfur tetrafluoride can act as a Lewis base when reacted with strong Lewis acids to donate F^- and form $[SF_3]^+$ salts such as $[SF_3][AsF_6]$, shown in Equation 1.4.[25]

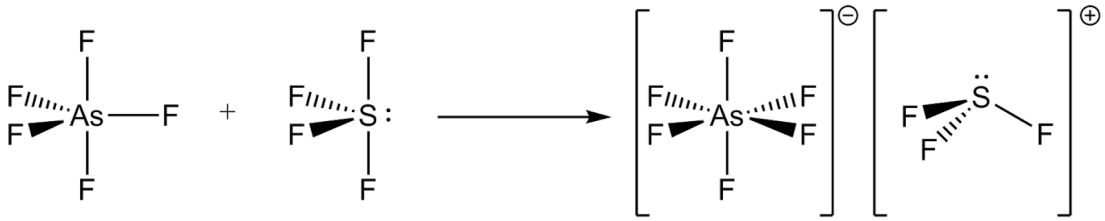

(1.4)

Gillespie and coworkers in their 1969 study synthesized adducts between SF_4 and Lewis acids BF_3, PF_5, SbF_5, and AsF_5. The adducts were found to be ionic in character of the form $[SF_3][EF_{4/6}]$ and were characterized by IR spectroscopy including isotopic effects, conductivity measurements, and ^{19}F NMR spectroscopy. A later 1972 study by Bartlett and coworkers reported the X-ray crystal structure of $[SF_3][BF_4]$ and confirmed the ionic salt nature of these adducts. [26] In these salts, the SF_3^+ cation adopts a trigonal pyramidal geometry with C_{3v} symmetry. Some adducts containing $[SF_3]^+$ have been synthesized with monodentate ligands pyridine, acetonitrile, and 4-dimethylaminopyridine form 1:2 adducts while the bidentate ligand 1,10-phenanthroline forms a 1:1 adduct.

1.2 Perfluoroalkyl Group

A perfluorinated alkyl group contains only carbon-fluorine and carbon-carbon bonds. This class of moiety lacks carbon-hydrogen bonds, offering interesting properties due to the unique nature of the C–F bond, the strongest single bond to carbon.[27–30] The polar nature of this bond ($\chi_{fluorine}$ = 3.98, χ_{carbon} = 2.55 on the Pauling scale)[31] gives it a significant ionic character creating a strong bond due to the electrostatic attraction introduced by the ionic feature. Comparison of bond enthalpies shows significantly increased C–F bond strength of methyl fluorides compared to the C–H or C–X (X = halogen) bond strengths, summarised in Table 1.2 with 2003 data from Blanksby and Ellison.[32]

Table 1.2 - Tabulated data comparing bond enthalpies of the C–R bond of H_3C–R at 298 K

R	CH_3–R Bond enthalpy, kJ mol^{-1} [a]
H	439
Cl	350
Br	302
I	241
F	481

[a]Data from S. J. Blanksby, G. Barney Ellison, *Acc. Chem. Res.* **2003**, *36*, 255–263 and references therein.

Fluorine can replace hydrogen atoms in an organic framework due to its similar size and valence. According to a report of van der Waals radii by Alvarez determined by survey of the Cambridge Structural Database, fluorine has a van der Waals radius of 1.46 Å ($r_{vdW(Hydrogen)}$ = 1.20 Å).[33] The combination of the C–F bond strength, polar nature, and the size of the F atom makes fluorine-containing functional groups very attractive building blocks for the synthesis of bioisosteres.[32,34] Adding a relatively stable and polar bond can have considerable effects on the electronic framework of the species and will consequently adjust the reactivity of that molecule.[35] The fluorosurfactant industry employs perfluoroalkyl chain tails attached to polar head groups to create non-stick coatings and membranes analogous to the phospholipid membranes found in living systems.[36]

Recently, there has been increased interest in the use of short-chain perfluoroalkyl compounds due to the persistence of long-chain analogues. Species such as perfluorooctanoic acid, PFOA, are so stable that it can bioaccumulate because it is not easily broken down by natural mechanisms.[37]

1.2.1 Trifluoromethyl Group

The trifluoromethyl group, $–CF_3$, is a functional group employed in organic chemistry. The group is strongly electron withdrawing, being called “halogen-like” by Sheppard in his 1962 study comparing electronic consequences of fluorine and fluoroalkyl substitutions.[38] In order to measure the effective electronegativity, True and coworkers devised a method comparing core-ionization potentials that offer good agreement with previous theoretical calculations of electronegativities. It was found that, the $–CF_3$ group has an effective electronegativity between 2.99 – 3.23 on the Pauling scale ($\chi_F = 3.98$, $\chi_{Cl} = 3.16$, $\chi_{Br} = 2.96$).[39,40] The addition of a trifluoromethyl group has been shown in some circumstances to largely change the reactivity of a molecule, changing nearby bond length, polarizability, and steric bulk.[39,41] As a specific example, trifluoromethyl groups can aid in creating molecules that are resistant to the metabolic mechanisms that living organisms use to break down molecules containing a reactive methyl group.[39,41,42] The trifluoromethyl group is significantly larger than a methyl group and will, therefore, impart substantial steric effects on the reactivity of the molecule. In their 2003 study, Timperley and White quantified the steric bulk added by trifluoromethyl groups by comparison to other substituents.[43]

The first evidence of a trifluoromethyl derivative of sulfur was reported by Bennett and coworkers in 1950 with the formation of $C_2S_2F_6$, believed to have the structure: $CF_3–S–S–CF_3$.[44] This novel product was formed by the reaction of CF_3HgI with sulfur. The production of trifluoromethyl derivatives of sulfur fluorides were reported by Silvey and Cady in their 1950 study on the fluorination of MeSH or CS_2 with

CoF_3 at high temperature or by fluorine gas in the presence of copper metal and silver fluorides.[45] This fluorination produced a novel volatile liquid after filtration at –78 °C followed by fractional distillation. The formula was determined by density and molecular weight to be CSF_8 and, while no structural investigation was undertaken, it was concluded that CF_3SF_5 was produced. It wasn't until 1952 that Kisliuk and Silvey acquired the microwave spectrum of what was believed to be CF_3SF_5 and provided positive evidence for its structure.[46]

A study by Brandt and coworkers provided evidence for reaction between CF_3I and sulfur at temperatures above 200 °C forming $S_2(CF_3)_2$ along with a mixture of unnamed products. By performing the synthesis in a steel container, Brandt *et al.* were able to produce high yields of $S_2(CF_3)_2$ allowing the investigation of reactivity, physical properties, and confirming the proposed structure.[47] The photolysis of $S_2(CF_3)_2$ caused the cleavage of the disulfide bond, forming bistrifluoromethyl sulfide. Trifluoromethyl derivatives of sulfur (IV) fluorides were synthesized by Tczkowski and Bigelow in their 1953 paper describing a new method for fluorination of CS_2 by F_2 yielding a mixture of fluoroalkyl derivatives including SF_3CF_3 and SF_5CF_3. [48] Upon synthesis, SF_3CF_3 and SF_5CF_3 were isolated using fractional distillation in relative purity. This study focussed on fluorination reactor design and proposed a mechanism by which CS_2 is converted to CSF_2 before further fluorination to CF_3SF_3 and then CF_3SF_5. The direct electrochemical fluorination of dimethyl sulfide and carbon disulfide was carried out as another method for the synthesis of CF_3SF_5 and resulted in the synthesis of novel $SF_4(CF_3)_2$. In this study, Clifford and coworkers fluorinated $S(CH_3)_2$ and CS_2 in anhydrous HF by applying an

electric current, producing CF_3SF_5, $SF_4(CF_3)_2$,[49] This electrochemical method for fluorination of alkyl sulfur compounds became a popular technique in the 1950s when it was used to synthesize many perfluoroalkylated sulfur compounds.[50–54]

1.2.2 Pentafluoroethyl Group

The pentafluoroethyl group, $–CF_2CF_3$, represents the next step in the extension of perfluorinated alkyl chains. Pentafluoroethyl is less electron withdrawing than trifluoromethyl and, therefore, does not affect the local electronic behavior to the same degree that a shorter perfluorinated substituent would. Pentafluoroethyl groups offer a larger steric effect than trifluoromethyl while maintaining chemical stability. Additionally, a $–C_2F_5$ groups can grant a lipophilic property similar to that of a $–SF_5$, a highly sought-after functional group that remains an important tool in organofluorine synthesis. Organic building blocks containing pentafluorosulfanyl substituents remain a popular method for synthesizing new organic frameworks containing $–SF_5$, because of the harsh reaction conditions associated with the introduction of $–SF_5$ using SF_5Cl. Research into pentafluoroethyl transfer reagents hopes to create a mild reaction condition that can transfer $–C_2F_5$ to important molecules.

1.2.3 Perfluoroalkyl Incorporation

Perfluoroalkyl chain addition reactions can proceed in four possible ways, (i) coupled aromatic, (ii) electrophilic, (iii) radical, and (iv) nucleophilic methods. Coupled aromatic reactions between perfluoroalkyl metal salts and aromatic organic substrates are

most commonly employed in trifluoromethyl addition to simple aromatic molecules. These reactions use perfluorinated alkyl iodides as the source of fluoroalkyl groups in the formation of perfluoroalkyl-metal complexes that allow introduction into organic substrates.

1.2.3.1 Coupled Aromatic Perfluoroalkylations

Metal-mediated perfluoroalkyl incorporation to aromatic systems was first patented by McLoughlin and Thrower in 1965. In these reactions, a perfluoroalkyl iodide (or bromide, but at the cost of lower yields) is reacted with an iodoarene substrate with stoichiometric copper metal at high temperature to form the perfluoroalkyl arene, shown in Equation 1.5.[55]

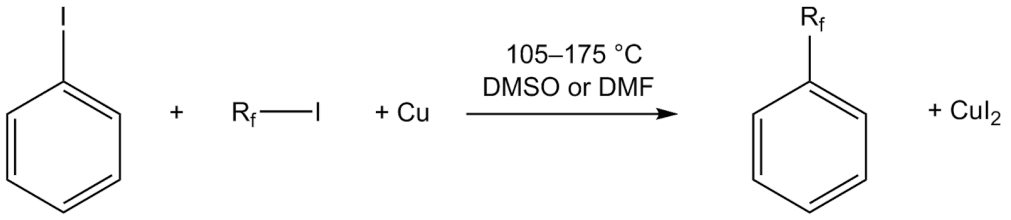

(1.5)

This method of trifluoromethylation features the formation of a metal trifluoromethyl complex and is important in the synthesis of perfluoroalkyl arenes that are used as building blocks in organofluorine chemistry. There has been extensive work optimizing these reactions and synthesizing metal complexes for the transfer of CF_3 groups. Some of these reactions employ catalytic metal while others require stoichiometric reactions. In 2006, Grushin and Marshall synthesized a Pd(II) complex that forms an Ar–CF_3 bond by

reductive elimination at the palladium centre.[56] Catalytic copper methods utilizing Cu(I) have been developed by Vicic in 2008,[57] and Oishi in 2009.[58] A 2015 review by Vicente and Rubio summarizes perfluoroalkyl gold complexes and their application in trifluoromethyl incorporation.[59] Many coupled aromatic trifluoromethylations have been surveyed by this method due to the variety of substrates available. Recent work focuses on the development of novel complexes allowing greater control over trifluoromethylation of particular substrates. This type of perfluoroalkyl introduction is popular for long-chain perfluoroalkyl arene derivatives, with *in situ* generation of R_fCu from R_fI and copper being the most popular method.[60]

1.2.3.2 Electrophilic Perfluoroalkylation

Electrophilic sources of perfluoroalkyl allow the generation of cationic perfluoroalkyl groups to add to electron-rich substrates. One electrophilic trifluoromethylation reagent was developed in 1984 by Yagupolskii and coworkers; this reagent, a shelf-stable diaryl(trifluoromethyl) sulfonium salt, allows the donation of a $–CF_3$ group upon the heterolytic cleavage of the heavily polarised S–C_f bond.[61] By adjusting the phenyl ring substitutions, this class of reagent can be tuned to optimize yields and/or reactivity. One trifluoromethylation from a study by Cheng and coworkers using a Yagupolskii-type reagent is shown in Equation 1.6.[62]

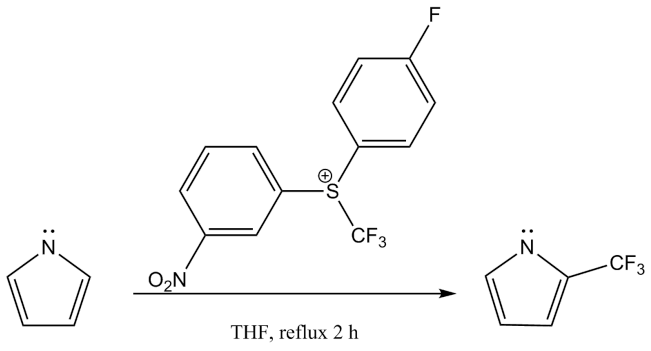

(1.6)

This transfer reagent is specialized for the trifluoromethylation of electron rich aromatic substrates. Umemoto reagents[63] feature a 5-membered heterocyclic ring containing a chalcogen (S, Se, or Te) also use a highly polarized chalcogen–carbon bond to transfer a $–CF_3$ group. The trifluoromethylating potential of these chalcogenium salts increase with lighter chalcogen centres in the order Te < Se < S. It is generally desirable to tune the perfluoroalkylating power of such reagents to match the nucleophilic substrate in order to optimize yields and suppress side reactions.[64] In order to tune the reactivity of the trifluoromethyl group, the heterocycle is flanked by electron withdrawing or donating groups, the general structure of such reagents is shown in Figure 1.4.

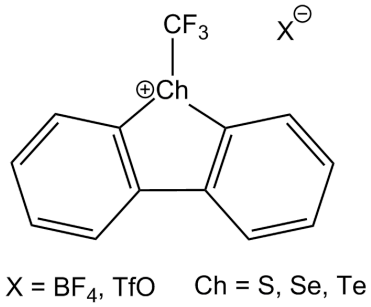

Figure 1.4 - Lewis diagram of Umemoto reagent containing a reactive trifluoromethyl group that can be transferred to a variety of substrates. Derivative salts can contain functional groups attached to phenyl ring positions in order to tune the reactivity of the Ch–S bond for specific substrates or reactions.

In 2010, a novel synthesis by Shibata and coworkers of benzothiophenium trifluoromethyl derivative salts allowed further expansion of electrophilic trifluoromethylation reagent development.[65] An example of such reagents is shown in Figure 1.5. The advantage of these extended Yagupolskii–Umemoto-type reagents is the ability to functionalize the 2-position of the benzothiophene ring allowing some enantioselective trifluoromethylations.

Shibata extended Yagupolskii–Umemoto-type reagent

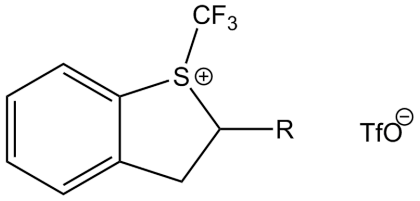

Figure 1.5 - Lewis diagram of a general Shibata-type extended Yagupolskii-Umemoto-type reagent used for electrophilic trifluoromethylations.

In their 2006 study, Togni and coworkers presented the synthesis of a new class of hypervalent iodine compound featuring an I–CF_3 bond that can be applied as a trifluoromethylating reagent.[66] Known as the Togni reagent, 3,3-dimethyl-1-(trifluoromethyl)-1,2-benziodoxole is a hypervalent iodine species that is produced using the Ruppert-Prakash reagent, Me_3SiCF_3, offering a mild electrophilic alternative for trifluoromethylations. A trifluoromethylation using the Togni reagent is shown in Equation 1.7. These –CF_3 sources are favorable because of their simple synthesis from the commercially available and relatively economical material, 1-chloro-1,3-dihydro-3,3-dimethyl-1,2-benziodoxole. Unlike similar tools, the Togni reagent is stable in air for short periods of time without significant hydrolysis. Other

derivatives of this class of compounds have been used for trifluoromethylations, such as Togni reagent II, 1-trifluoromethyl-1,2-benziodoxol-3-(1H)-one, shown in Equation 1.8.

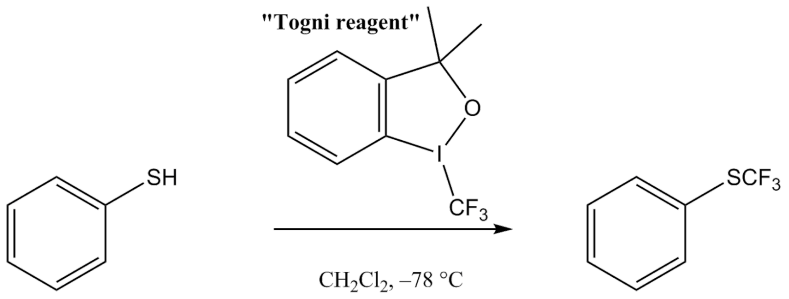

(1.7)

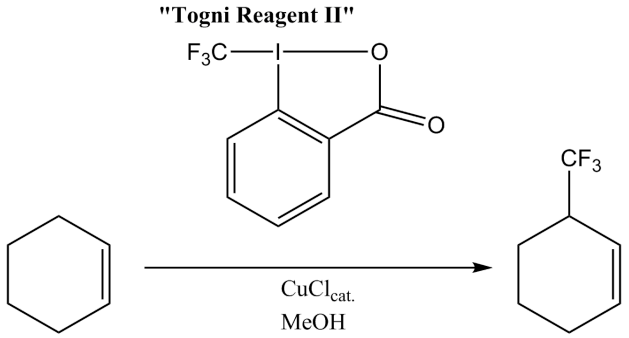

(1.8)

1.2.3.3 Radical Perfluoroalkylation

Thermally or photochemically generated perfluoroalkyl radicals can incorporate perfluoroalkyl groups into unsaturated organic frameworks. The photochemical generation of $\bullet CF_3$ radicals from CF_3I was reported in Haszeldine's 1949 article on the reactions of fluorocarbon radicals. Other methods for introducing trifluoromethyl radicals include a multitude of speciality reagents. One of the most common sources of radical perfluoroalkyl groups are the perfluoroalkyl iodides or bromides that are oxidized before reaction with a substrate. In their 1991 study, Langois *et al.* showed that sodium

trifluoromethanesulfinate ($Na[CF_3SO_2]$) is a source of trifluoromethyl radicals upon single-electron oxidation and can be used as a radical trifluoromethyl transfer reagent for substrates that bear reducible moieties.[67] This salt is commercially available and has been dubbed the Langois reagent, synthesized from $BrCF_3$ and $[SO_2]^{\bullet-}$. The sulfur dioxide radical anion is prepared from dithionite or a reaction between zinc and SO_2. Trifluoromethylations using the Langois reagent require a selective oxidizer to activate $Na[CF_3SO_2]$. Tert-butyl hydroperoxide is an oxidizer chosen to activate the Langois reagent selectively in order to avoid side reactions. Other oxidizers like potassium peroxydisulfate or some metal salts have been used for such purpose but are not as selective. These approaches offered advantages for particular systems but were not investigated for the pentafluoroethylation of sulfur fluorides since an electron-rich substrate was needed.

1.2.3.4 Nucleophilic Perfluoroalkylation

Nucleophilic perfluoroalkylation is a method by which new bonds to perfluorinated carbons can be formed with the use of an electron-rich fluoroalkyl species. For example, fluoroform has been used as trifluoromethyl source by first deprotonating CHF_3 using a strong organic or inorganic base to form an intermediate electron-rich $[CF_3]^-$. The challenge with these types of reactions is the instability of this trifluoromethanide anion. This type of species was long thought to be a short-lived intermediate that has since been confirmed to exist in a condensed state by Prakash and coworkers by bulk preparation of $[K(18\text{-crown-6})][CF_3]$ characterized by ^{19}F and ^{13}C

NMR spectroscopy at low temperature in THF.[68] Since this finding, Grushin and coworkers were able to present X-ray crystallographic and DFT computational evidence for the existence of a "naked" $[CF_3]^-$ ion in [K(crypt-222)][CF_3], although debate is still ongoing in contemporary literature.[69–71] Metal salts containing the trifluoromethanide ion can be of limited stability due to their tendency to form difluorocarbene, $:CF_2$, upon elimination of a metal fluoride salt.

A trifluoromethyl source that contains a highly polarizable bond to the desired perfluoroalkyl chain can also be used for nucleophilic perfluoroalkylation. This method allows the transfer of an electron-rich trifluoromethanide moiety with milder reaction conditions. An example of such a nucleophilic trifluoromethylation tools is Me_3SiCF_3, the Ruppert-Prakash reagent,[72] used for trifluoromethylation of organic substrates because of its shelf-stability, ease of use, and relative low cost.[73] This reagent is synthesized using $BrCF_3$, a persistent ozone-depleting molecule.[74] Trifluoromethylations using this Me_3SiCF_3 require the addition of some base to cause the weakening and reaction of the F_3C–Si bond. Upon polarization of this bond, the trifluoromethyl group is transferred to an electron-deficient substrate. A five-coordinate silicon species, $[Me_3Si(F)CF_3]^-$ has been observed by ^{19}F NMR spectroscopy in a 1999 study by Naumann and coworkers.[75] This pentacoordinate silicon species is observed when Me_3SiCF_3 reacts with a fluoride source such as CsF or $[Me_4N]F$. In the presence of an appropriate substrate, this species will rapidly transfer trifluoromethanide. However, anionic species $[Me_3Si(F)CF_3]^-$ will quickly degrade in solution due to the instability of the $[CF_3]^-$ ion as discussed above. An example trifluoromethylation using the Ruppert-Prakash reagent is shown in Equation 1.9.

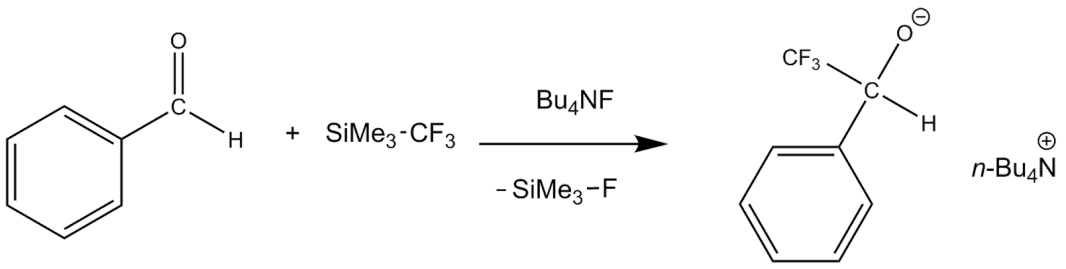

(1.9)

The extension of a perfluoroalkyl chain from $–CF_3$ to $–C_2F_5$ affords additional stability of the anionic perfluoroalkyl species. To use LiC_2F_5 for pentafluoroethyl additions, it must be kept at low temperature to avoid decomposition to LiF and C_2F_4, since the latter will exothermically and rapidly polymerize to polytetrafluoroethylene. In ethereal solution, decomposition is rapid at *ca.* –40 °C while some decomposition has been observed below –60 °C. Unlike the $LiCF_3$ analogue that forms a singlet carbene, difluorocarbene, upon decomposition, LiC_2F_5 instead decomposes into $F_3C(F)C$:. The formation of this latter carbene is significantly less favored and this distinction is likely why LiC_2F_5 is stable to higher temperatures than $LiCF_3$.[76] In their 2014 study, Mitzel and coworkers isolated neat LiC_2F_5 in the solid state. Without donor solvent, this salt decomposes below –100 °C.[76]

In their 2013 study, Lischynskyi and Grushin studied the cupration of C_2F_5H in order to introduce the pentafluoroethyl group.[77] This study found that C_2F_5H is deprotonated by first reacting potassium tert-butoxide in the presence of copper(II) chloride with dimethylformamide, which initially forms $[K(DMF)][(t\text{-}BuO)_2Cu]$ that then cuprates pentafluoroethane, shown in Equation 1.10. The salt that is formed by this

reaction was shown by X-ray crystallography to be K[(t-BuO)Cu(C_2F_5)] and can be used as a pentafluoroethylating reagent, converting aryl bromides, alkynes, and alkenes to their respective pentafluoroethyl derivatives.

$$\mathrm{CuCl} + 2\ \text{t-BuO}^-\mathrm{K}^+ \xrightarrow[-\ \mathrm{KCl}]{\mathrm{DMF}} [\mathrm{K(DMF)}][\mathrm{Cu(t\text{-}BuO)_2}]$$

$$[\mathrm{K(DMF)}][\mathrm{Cu(t\text{-}BuO)_2}] \xrightarrow[20\text{–}25\ ^\circ\mathrm{C}]{\mathrm{C_2F_5H}} [\mathrm{K(DMF)}][(\text{t-BuO})\mathrm{Cu}(\mathrm{C_2F_5})] + \text{t-BuOH} \qquad (1.10)$$

Like its analogous trifluoromethyl derivative, $Me_3SiC_2F_5$ can transfer a $[C_2F_5]^-$ moiety to an electron deficient substrate. Since the pentafluoroethyl group is less electron withdrawing than the trifluoromethyl group, it is expected that the pentacoordinate $[Me_3Si(F)CF_2CF_3]^-$ species should be more stable than the trifluoromethyl alternative. The use of other bases to initiate this reaction can also affect the stability of this intermediate. The reagent itself is a moisture-sensitive volatile liquid with a boiling point of 60 °C and a reported melting point of –111 °C. By ^{19}F NMR spectroscopy, $Me_3SiC_2F_5$ can be observed as two singlets at –133 ppm and –83 ppm because of the small $^3J_{FF}$ coupling (< 1Hz). Upon reaction with moisture, Me_3SiCF_3 has been shown by Ruppert and coworkers to polymerize forming mixed siloxane chains.[72] Recently, $Me_3SiC_2F_5$ has been used to synthesize tris(pentafluoroethyl)phosphane by Hoge and coworkers.[78] This pentafluoroethyl transfer reagent is commercially available in high purity and is shelf stable under the exclusion of moisture. These reagents of the form $Me_3Si[CF_2]_nCF_3$ have been prepared commercially up to heptadecafluorooctyl chains. While longer chains have

been studied.[79] Most longer chained derivatives are prepared from their perfluoroalkyl iodides and chlorosilane for specialized reactions.

1.3 Pentafluoroethyl Derivatives of Period three

Pentafluoroethyl derivatives of main group fluorides have been investigated for many systems with a variety of synthesis methods. Pentafluoroethyl derivatives in period three have been characterized for magnesium, silicon, phosphorus, and sulfur. Some of these species are summarized in Table 1.3 including the methods by which they were synthesized. Some salts, such as those of the form $[PF_{6-n}(C_2F_5)_n]^-$, have been extensively studied for their use as electrolytes in batteries. Such studies survey a multitude of salts containing this anion and are important industrially.

Table 1.3 - Summary of some period three pentafluoroethyl derivatives

Compound	Method of preparation	Methods of characterization[b]
	Magnesium	
$IMgC_2F_5$[80][a]	$C_2F_5I + Mg$	MW, reaction
	Silicon	
$SiF_2(C_2F_5)I$[81,82]	$C_2F_5I + SiF_2$	^{19}F NMR, MW, IR, MS
$SiF_3C_2F_5$[81,82]	$SiF_2(C_2F_5)I + SbF_3$ or AsF_3 or AgF	
$SiCl_3(C_2F_5)$[83]	i) $SiCl(OPh)_3 + LiC_2F_5$ ii) $PhCH_2COCl$ / $FeCl_{3\ cat.}$	$^{19}F/^{29}Si$ NMR
$[H(OH_2)_2]_2[SiF_5C_2F_5]$[83]	$SiCl_3(C_2F_5) + HF_{aq.}$	
$[H(OH_2)_2]_2[SiF_4(C_2F_5)_2]$[83]	$SiCl_2(C_2F_5)_2 + HF_{aq.}$	$^{19}F/^{29}Si$ NMR, SXD

Table 1.3 - (continued)

$Li[SiF_2(C_2F_5)_3]$[84]	$SiCl_4$ + 3 LiC_2F_5	$^{19}F/^{29}Si$ NMR, IR, MS
$Li_2[SiF_3(C_2F_5)_3]$[84]		
$SiF_2(C_2F_5)_2$[84]	$SiCl_2(C_2F_5)_2$ + SbF_3	$^{19}F/^{29}Si$ NMR, IR, MS, SXD
$Si(C_2F_5)_3NEt_2$[85]	$SiCl_3NEt_2$ + $3LiC_2F_5$	$^{19}F/^{29}Si$ NMR, IR, MS
$Si(C_2F_5)_3X$[85] (X = Br, Cl)	$Si(C_2F_5)_3NEt_2$ + HX	
$SiF(C_2F_5)_3$[85]	$Si(C_2F_5)_3X$ + SbF_3	$^{19}F/^{29}Si$ NMR, IR, MS, SXD
$Si(C_2F_5)_4$[85]	$Si(C_2F_5)_3C_2H_5$ + F_2	
Phosphorus		
$PF_2C_2F_5$[86]	i) C_2F_5I + red phosphorus + I_2 heat 70 Hr ii) SbF_3 12 Hr	$^{19}F/^{31}P$ NMR, MS, IR, MW
$(C_2F_5)_2PC_2H_4P(C_2F_5)_2$[87]	LiC_2F_5 + $Cl_2PC_2H_4PCl_2$ Or $Me_3SiC_2F_5$ + $(PhO)_2PC_2H_4P(PhO)_2$	$^{1}H/^{13}C/^{31}P/^{19}F$ NMR, MS, IR, EA
$PF(C_2F_5)_2$[88]	i) Cl_2PNEt_2 + LiC_2F_5 ii) HBr iii) SbF_3	$^{19}F/^{31}P$ NMR
$PF_2(C_2F_5)_3$[89,90]	i) PCl_3 + $BrMgCH_2CH_3$ ii) F_2 or e^- in HF	$^{19}F/^{31}P$ NMR, MS
$P(C_2F_5)_3$[89,90]	$PF_2(C_2F_5)_3$ + $PPh_2(SiMe_3)$	

[a]Grignard reagents of this form were used for synthesis of some organic pentafluoroethyl derivatives before being replaced due to their instability and complexity.[91]
[b]SXD = single crystal X-ray diffraction; MW = molecular weight; MS = mass spectrometry; IR = infrared spectroscopy; EA = elemental analysis; NMR = nuclear magnetic resonance spectroscopy

1.3.1 Pentafluoroethyl Derivatives of Sulfur

Pentafluoroethyl derivatives of sulfur fluorides were reported in 1971 by Sauer and Shreeve by reacting sulfur tetrafluoride with tetrafluoroethylene at 150–200 °C in the presence of cesium fluoride.[92] The reaction carried out synthesized $SF_2(C_2F_5)_2$ and is shown in Equation 1.11, including the proposed pyrolysis of bis(pentafluoroethyl)sulfur difluoride to form $SF_3C_2F_5$.

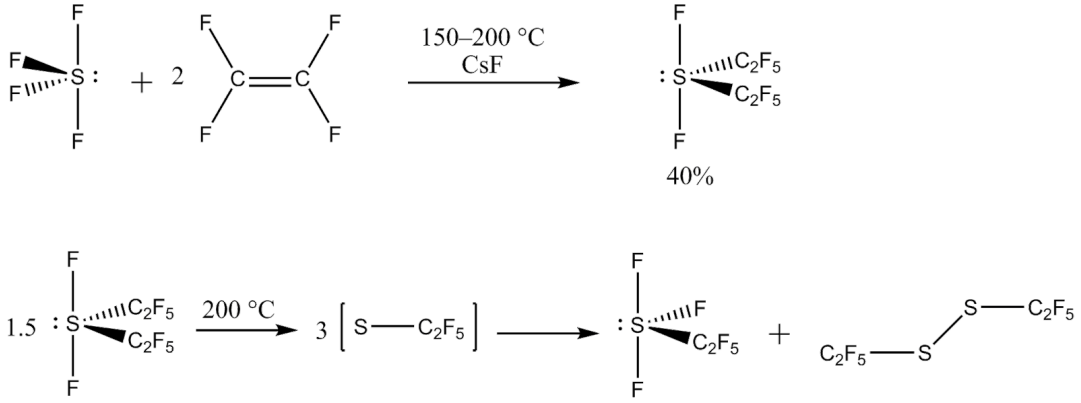

(1.11)

Bis(perfluoroalkyl)sulfides and bis(perfluoroalkyl)sulfoxides were also synthesized by photolysis of perfluoro sulfenic esters of the type $CF_3SOC(O)C_f$, where C_f is a perfluorinated alkyl group. Full NMR spectroscopic analyses of some bis(perfluoroalkyl)sulfoxides were rendered difficult by noted magnetically non-equivalent difluoromethylene environments flanking sulfoxide centers of $CF_3S(O)C_2F_5$, $CF_3S(O)CF_2CF_2CF_3$, and $CF_3CF_2S(O)CF_2CF_3$. Some of these sulfoxide centers are chiral, further complicating the NMR signal. The moisture sensitivity of $SF_2(C_2F_5)_2$ was investigated showing that this compound is stable at room temperature in the presence of water vapour. It was previously noted that another bisperfluoroalkyl disulfide, $((CF_3)_2CF)_2SF_2$ is also stable in the presence of water, which was explained by the steric bulk and shielding of the sulfur centre by the bulky perfluoroisopropyl groups. Comparatively, $SF_2(C_2F_5)_2$ is much less shielded by its pentafluoroethyl substituents. A 1968 study by Shreeve and coworkers provided a synthesis for the trifluoromethylsulfinyl analog, $CF_3S(O)F$, from the hydrolysis of CF_3SF_3 that offered a possible route to $C_2F_5S(O)F$ from $C_2F_5SF_3$.[93]

In their 1997 study,[94] Mews and coworkers synthesized pentafluoroethyl sulfur trifluoride, pentafluoroethyl sulfur pentafluoride, and pentafluorosulfinyl fluoride. This study employs a facile synthesis by cleavage of the disulfide bridge of bis(pentafluoroethyl) disulfide, a commercially available compound, with either AgF_2 or F_2. The reaction proceeds at 0 °C and forms a mixture of products that can be separated by fractional distillation. The X-ray crystal structure of $[SF_2C_2F_5][AsF_6]$, shown in Figure 1.6, was obtained by abstraction of one of the sulfur-bound fluorides by AsF_5, a strong Lewis acid with a fluoride affinity of 439.7 kJ mol^{-1}.

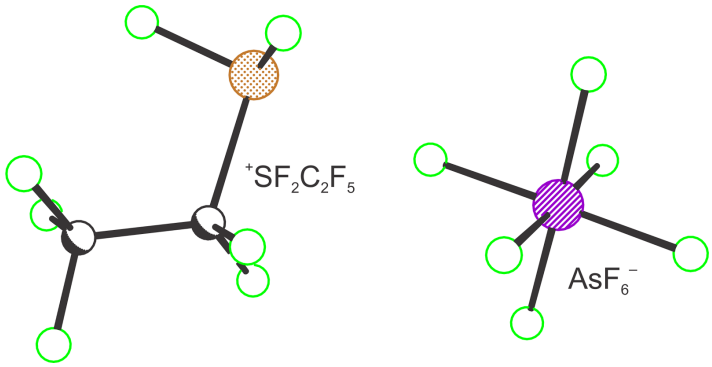

Figure 1.6 - A model of the X-ray crystal structure of $[SF_2C_2F_5][AsF_6]$ reported by Mews and coworkers by the abstraction of fluoride from $SF_3C_2F_5$ by AsF_5.[94]

1.4 Goal of Research

Recently, the Lewis acid behaviour of SF_4 has been studied primarily with respect to its adduct formation with organic Lewis bases. My goal was to expand our understanding of such adduct formation by including bicyclic systems such as diazabicyclo[2.2.2]octane, DABCO.

The DABCO-SF_4 Lewis acid-base system was studied by Raman spectroscopy. The goal of this investigation was to characterize the remarkably stable sulfur-containing DABCO•nSF_4 adduct in the solid state.

Interactions between SF_4 and nucleophilic pentafluoroethyl sources was investigated. The goal of this research was to create a better synthetic route to previously synthesized pentafluoroethyl derivatives of sulfur fluorides. A new synthetic route to these compounds could allow the investigation of characteristics that have been elusive in the past. Furthermore, isolation of these compounds may help in investigating their reactivity and pentafluoroethyl transfer reagent potential. Previous reports of pentafluoroethyl derivatives of sulfur(IV) fluorides have often focussed on creating a library of pentafluoroethyl derivatives of varying size and substitution rather than fully characterizing the individual components. For this reason some compounds have remained only partially characterized and synthetic routes remain unoptimized.

Upon synthesis of the compounds in question, this work focused on detailed characterization of compounds $SF_3C_2F_5$ and $SF_2(C_2F_5)_2$. The pentafluorosulfinyl analogs, $SOFC_2F_5$, and $SO(C_2F_5)_2$ were observed first in the reaction between $Me_3SiC_2F_5$ and SF_4, as well as the primary products of the reaction between $Me_3SiC_2F_5$ and SOF_2. A new route for synthesis of these compounds is presented, allowing the isolation of some products and high resolution NMR spectroscopic data.

References

[1] A. Dreveton, *Procedia Eng.* **2016**, *138*, 240–247.

[2] F. S. Fawcett, C. W. Tullock, C. I. Merrill, *Inorg. Synth.*, **1963**, pp. 119–124.

[3] R. E. Dodd, L. A. Woodward, H. L. Roberts, *Trans. Faraday Soc.* **1956**, *52*, 1052.

[4] K. D. Raffael, D. M. Smith, *J. Mol. Spectrosc.* **2002**, *214*, 21–27.

[5] K. D. Raffael, D. M. Smith, D. A. Newnham, *J. Mol. Spectrosc.* **2003**, *218*, 108–113.

[6] V. C. Ewing, L. E. Sutton, *Trans. Faraday Soc.* **1963**, *59*, 1241.

[7] K. Kimura, S. H. Bauer, *J. Chem. Phys.* **1963**, *39*, 3172–3178.

[8] C. A. Spring, N. S. True, *J. Am. Chem. Soc.* **1983**, *105*, 7231–7236.

[9] M. Pavone, V. Barone, I. Ciofini, C. Adamo, *J. Chem. Phys.* **2004**, *120*, 9167–9174.

[10] J. T. Goettel, N. Kostiuk, M. Gerken, *Angew. Chem., Int. Ed Engl.* **2013**, *52*, 8037–8040.

[11] R. J. Gillespie, I. Hargittai, *The VSEPR Model of Molecular Geometry*, Courier Corporation, **2013**.

[12] A. F. Janzen, *Coord. Chem. Rev.* **1994**, *130*, 355–426.

[13] E. L. Muetterties, W. D. Phillips, *J. Am. Chem. Soc.* **1959**, *81*, 1084–1088.

[14] R. L. Redington, C. V. Berney, *J. Chem. Phys.* **1965**, *43*, 2020–2026.

[15] F. Beaulieu, L.-P. Beauregard, G. Courchesne, M. Couturier, F. LaFlamme, A. L'Heureux, *Org. Lett.* **2009**, *11*, 5050–5053.

[16] R. Tunder, B. Siegel, *J. Inorg. Nucl. Chem.* **1963**, *25*, 1097–1098.

[17] J. Bittner, J. Fuchs, K. Seppelt, *Z. Anorg. Allg. Chem.* **1988**, *557*, 182–190.

[18] L. F. Drullinger, J. E. Griffths, *Spectrochim. Acta, Part A* **1971**, *27*, 1793–1799.

[19] M. Clark, C. J. Kellen-Yuen, K. D. Robinson, H. Zhang, Z. Y. Yang, K. V. Madappat, J. W. Fuller, J. L. Atwood, J. S. Thrasher, *Eur. J. Solid State Inorg. Chem.* **1992**, *24*, 809–833.

[20] W. Heilemann, R. Mews, S. Pohl, W. Saak, *Chem. Ber.* **1989**, *122*, 427–432.

[21] J. T. Goettel, N. Kostiuk, M. Gerken, *Inorg. Chem.* **2016**, *55*, 7126–7134.

[22] J. T. Goettel, P. Chaudhary, P. Hazendonk, H. P. A. Mercier, M. Gerken, *Chem. Commun.* **2012**, *48*, 9120-9122.

[23] P. Chaudhary, J. T. Goettel, H. P. A. Mercier, S. Sowlati-Hashjin, P. Hazendonk, M. Gerken, *Chem. - Eur. J.* **2015**, *21*, 6247–6256.

[24] J. T. Goettel, M. Gerken, *Inorg. Chem.* **2016**, *55*, 12441–12450.

[25] M. Azeem, M. Brownstein, R. J. Gillespie, *Can. J. Chem.* **1969**, *47*, 4159–4167.

[26] D. D. Gibler, C. J. Adams, M. Fischer, A. Zalkin, N. Bartlett, *Inorg. Chem.* **1972**, *11*, 2325–2329.

[27] R. E. Banks, B. E. Smart, J. C. Tatlow, *Organofluorine Chemistry: Principles and Commercial Applications*, Springer Science & Business Media, **2013**.

[28] G. Villalba, R. U. Ayres, H. Schroder, *J. Ind. Ecol.* **2008**, *11*, 85–101.

[29] D. O'Hagan, *Chem. Soc. Rev.* **2008**, *37*, 308–319.

[30] D. M. Lemal, *J. Org. Chem.* **2004**, *69*, 1–11.

[31] L. Pauling, *Phys. Rev. Lett.* **1987**, *59*, 225–227.

[32] S. J. Blanksby, G. Barney Ellison, *Acc. Chem. Res.* **2003**, *36*, 255–263.

[33] S. Alvarez, *Dalton Trans.* **2013**, *42*, 8617–8636.

[34] N. A. Meanwell, *J. Med. Chem.* **2011**, *54*, 2529–2591.

[35] H.-J. Böhm, D. Banner, S. Bendels, M. Kansy, B. Kuhn, K. Müller, U. Obst-Sander, M. Stahl, *Chembiochem* **2004**, *5*, 637–643.

[36] A. B. Lindstrom, M. J. Strynar, E. L. Libelo, *Environ. Sci. Technol.* **2011**, *45*, 7954–7961.

[37] M. Houde, J. W. Martin, R. J. Letcher, K. R. Solomon, D. C. G. Muir, *Environ. Sci. Technol.* **2006**, *40*, 3463–3473.

[38] W. A. Sheppard, *J. Am. Chem. Soc.* **1963**, *85*, 1314–1318.

[39] J. E. True, T. D. Thomas, R. W. Winter, G. L. Gard, *Inorg. Chem.* **2003**, *42*, 4437–4441.

[40] L. Pauling, *The Nature of the Chemical Bond and the Structure of Molecules and Crystals: An Introduction to Modern Structural Chemistry*, Cornell University Press, **1960**.

[41] H. Oberhammer, *J. Fluorine Chem.* **1982**, *21*, 88.

[42] G. D. Diana, P. Rudewicz, D. C. Pevear, T. J. Nitz, S. C. Aldous, D. J. Aldous, D. T. Robinson, T. Draper, F. J. Dutko, C. Aldi, *J. Med. Chem.* **1995**, *38*, 1355–1371.

[43] C. M. Timperley, W. E. White, *J. Fluorine Chem.* **2003**, *123*, 65–70.

[44] F. W. Bennett, G. R. A. Brandt, H. J. Emeleus, R. N. Haszeldine, *Nature* **1950**, *166*, 225.

[45] G. A. Silvey, G. H. Cady, *J. Am. Chem. Soc.* **1950**, *72*, 3624–3626.

[46] P. Kisliuk, G. A. Silvey, *J. Chem. Phys.* **1952**, *20*, 517–517.

[47] G. A. R. Brandt, H. J. Emeléus, R. N. Haszeldine, *J. Chem. Soc.* **1952**, 2198–2205.

[48] E. A. Tyczkowski, L. A. Bigelow, *J. Am. Chem. Soc.* **1953**, *75*, 3523–3526.

[49] A. F. Clifford, H. K. El-Shamy, H. J. Emeléus, R. N. Haszeldine, *J. Chem. Soc.* **1953**, 2372–2375.

[50] R. N. Haszeldine, F. Nyman, *J. Chem. Soc.* **1956**, 2684–2689.

[51] T. Gramstad, R. N. Haszeldine, *J. Chem. Soc.* **1956**, 173–180.

[52] F. W. Hoffmann, T. C. Simmons, R. B. Beck, H. V. Holler, T. Katz, R. J. Koshar, E. R. Larsen, J. E. Mulvaney, F. E. Rogers, B. Singleton, et al., *J. Am. Chem. Soc.* **1957**, *79*, 3424–3429.

[53] R. D. Dresdner, J. A. Young, *J. Am. Chem. Soc.* **1959**, *81*, 574–577.

[54] J. Young, R. Dresdner, *J. Org. Chem.* **1959**, *24*, 1021–1022.

[55] V. C. R. Mcloughlin, J. Thrower, *Manufacture of Organic Compounds Containing Fluorine*, **1968**, 3408411 A.

[56] V. V. Grushin, W. J. Marshall, *J. Am. Chem. Soc.* **2006**, *128*, 12644–12645.

[57] G. G. Dubinina, H. Furutachi, D. A. Vicic, *J. Am. Chem. Soc.* **2008**, *130*, 8600–8601.

[58] M. Oishi, H. Kondo, H. Amii, *Chem. Commun.* **2009**, 1909–1911.

[59] J. Gil-Rubio, J. Vicente, *Dalton Trans.* **2015**, *44*, 19432–19442.

[60] O. A. Tomashenko, V. V. Grushin, *Chem. Rev.* **2011**, *111*, 4475–4521.

[61] L. M. Yagupol'skii, N. V. Kondratenko, G. N. Timofeeva, *Zh. Org. Khim.* **1984**, *20*, 115–118.

[62] M. Li, X.-S. Xue, J. Guo, Y. Wang, J.-P. Cheng, *J. Org. Chem.* **2016**, *81*, 3119–3126.

[63] T. Umemoto, E. Magnier, in *Encyclopedia of Reagents for Organic Synthesis*, **2011**.

[64] N. Shibata, A. Matsnev, D. Cahard, *Beilstein J. Org. Chem.* **2010**, *6*, 65.

[65] A. Matsnev, S. Noritake, Y. Nomura, E. Tokunaga, S. Nakamura, N. Shibata, *Angew. Chem., Int. Ed Engl.* **2010**, *49*, 572–576.

[66] P. Eisenberger, S. Gischig, A. Togni, *Chem. - Eur. J.* **2006**, *12*, 2579–2586.

[67] B. R. Langlois, E. Laurent, N. Roidot, *Tetrahedron Lett.* **1991**, *32*, 7525–7528.

[68] G. K. S. Prakash, F. Wang, Z. Zhang, R. Haiges, M. Rahm, K. O. Christe, T. Mathew, G. A. Olah, *Angew. Chem., Int. Ed Engl.* **2014**, *53*, 11575–11578.

[69] A. Lishchynskyi, F. M. Miloserdov, E. Martin, J. Benet-Buchholz, E. C. Escudero-Adán, A. I. Konovalov, V. V. Grushin, *Angew. Chem., Int. Ed Engl.* **2015**, *54*, 15289–15293.

[70] F. M. Miloserdov, A. I. Konovalov, E. Martin, J. Benet-Buchholz, E. C. Escudero-Adán, A. Lishchynskyi, V. V. Grushin, *Helv. Chim. Acta* **2017**, *100*, e1700032.

[71] S. Becker, P. Müller, *Chem. - Eur. J.* **2017**, *23*, 7081–7086.

[72] I. Ruppert, K. Schlich, W. Volbach, *Tetrahedron Lett.* **1984**, *25*, 2195–2198.

[73] X. Liu, C. Xu, M. Wang, Q. Liu, *Chem. Rev.* **2015**, *115*, 683–730.

[74] S. Solomon, D. L. Albritton, *Nature* **1992**, *357*, 33–37.

[75] N. Maggiarosa, W. Tyrra, D. Naumann, N. V. Kirij, Y. L. Yagupolskii, *Angew. Chem., Int. Ed Engl.* **1999**, *111*, 2392–2393.

[76] B. Waerder, S. Steinhauer, B. Neumann, H.-G. Stammler, A. Mix, Y. V. Vishnevskiy, B. Hoge, N. W. Mitzel, *Angew. Chem., Int. Ed Engl.* **2014**, *53*, 11640–11644.

[77] A. Lishchynskyi, V. V. Grushin, *J. Am. Chem. Soc.* **2013**, *135*, 12584–12587.

[78] S. A. Hayes, R. J. F. Berger, B. Neumann, N. W. Mitzel, J. Bader, B. Hoge, *Dalton Trans.* **2010**, *39*, 5630–5636.

[79] S. S. Dua, R. D. Howells, H. Gilman, *J. Fluorine Chem.* **1974**, *4*, 409–413.

[80] R. N. Haszeldine, *Nature* **1951**, *167*, 139–140.

[81] K. G. Sharp, T. D. Coyle, *Inorg. Chem.* **1972**, *11*, 1259–1264.

[82] K. G. Sharp, S. Li, R. B. Johannesen, *Inorg. Chem.* **1976**, *15*, 2295–2297.

[83] N. Schwarze, S. Steinhauer, B. Neumann, H.-G. Stammler, B. Hoge, *Angew. Chem., Int. Ed Engl.* **2016**, *55*, 15528–15530.

[84] N. Schwarze, B. Kurscheid, S. Steinhauer, B. Neumann, H.-G. Stammler, N. Ignat'ev, B. Hoge, *Chem. - Eur. J.* **2016**, *22*, 17460–17467.

[85] S. Steinhauer, J. Bader, H.-G. Stammler, N. Ignat'ev, B. Hoge, *Angew. Chem., Int. Ed Engl.* **2014**, *53*, 5206–5209.

[86] K. G. Sharp, I. Schwager, *Inorg. Chem.* **1976**, *15*, 1697–1701.

[87] M. F. Ernst, D. M. Roddick, *Inorg. Chem.* **1989**, *28*, 1624–1627.

[88] A. V. Zakharov, Y. V. Vishnevskiy, N. Allefeld, J. Bader, B. Kurscheid, S. Steinhauer, B. Hoge, B. Neumann, H.-G. Stammler, R. J. F. Berger, et al., *Eur. J. Inorg. Chem.* **2013**, *2013*, 3392–3404.

[89] J. J. Kampa, J. W. Nail, R. J. Lagow, *Angew. Chem., Int. Ed Engl.* **1995**, *34*, 1241–1244.

[90] N. Ignat'ev, P. Sartori, *J. Fluorine Chem.* **2000**, *103*, 57–61.

[91] N. Thoai, *J. Fluorine Chem.* **1975**, *5*, 115–125.

[92] D. T. Sauer, J. M. Shreeve, *J. Fluorine Chem.* **1971**, *1*, 1–11.

[93] C. T. Ratcliffe, J. M. Shreeve, *J. Am. Chem. Soc.* **1968**, *90*, 5403–5408.

[94] D. Viets, E. Lork, R. Mews, U. Behrens, *Z. Anorg. Allg. Chem.* **1997**, *623*, 1892–1896.

2 Experimental

2.1 General Procedures

Since most reactants and products used herein are highly moisture sensitive, all reactions were performed using air-free techniques such as vacuum-line and dry-box techniques to sustain a dry and oxygen-free atmosphere. Nitrogen (99.99%, Praxair) was dried by passing it through anhydrous calcium sulfate (cobalt chloride indicator), and activated 4 Å molecular sieves. Dryness was maintained using sealed reactors, glass and metal vacuum lines, and a nitrogen-atmosphere dry box (Omni Lab, Vacuum Atmospheres), as well as rigorous drying procedures before the addition of reagents by distillation.

For distillations of non-corrosive materials, Pyrex-glass vacuum lines, such as shown in Figure 2.1, were used which were evacuated using Edwards two-stage direct-drive RV8 vacuum pumps. All glass vacuum lines were fitted with glass traps immersed in liquid nitrogen for the capture of volatile materials. Valves on glass vacuum lines are grease-free 6-mm J. Young glass stopcocks with PTFE (polytetrafluoroethylene) barrels. The vacuum achieved was approximately 10^{-5} Torr, measured by a McLeod gauge (Labconco) and monitored using Varian model 801 thermocouple gauges. Heise gauges (model CC, 0-1000 mmHg, beryllium/copper Bourdon tube, Dresser Instruments) were used to monitor pressures while the vacuum manifold was closed.

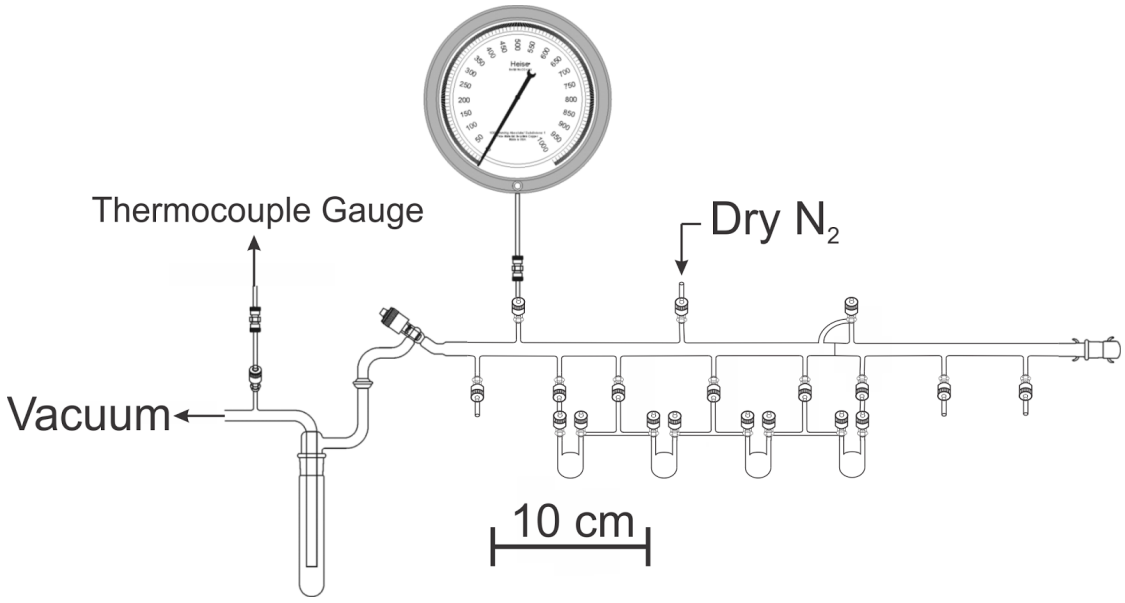

Figure 2.1 - Glass vacuum line equipped with J. Young PTFE/glass stopcocks, a Heise and thermocouple gauge, and vacuum/nitrogen manifolds.

The distillation of corrosive materials such as SF_4 that would otherwise react with glass vessels were performed with a metal vacuum line constructed from nickel, 316 stainless-steel, and fitted with 316 stainless steel valves (Autoclave Engineers Inc.). Pressures were monitored using Baratron capacitance manometers (MKS, Type 626A, effective range 0-1000 mmHg) with inert wetted surfaces constructed of Inconel, connected to digital readouts. Polytetrafluoroethylene tube fitting connectors (Swagelok) were used to connect ¼ in. o.d. FEP reactors to the metal line. A diagram of the metal line is shown in Figure 2.2. The vacuum manifold was evacuated using one of two Edwards two-stage direct-drive RV8 vacuum pumps fitted with liquid-nitrogen-cooled volatile traps. One pump was preceded by a small activated charcoal scrubber, this pump was used to maintain the final vacuum, while the second pump was preceded with a large (75 cm length by 17 cm outer diameter) stainless-steel tower packed with soda lime absorbent

(EMD, 4 mesh), used for removal and disposal of reactive gases including SF_4 and elemental fluorine.

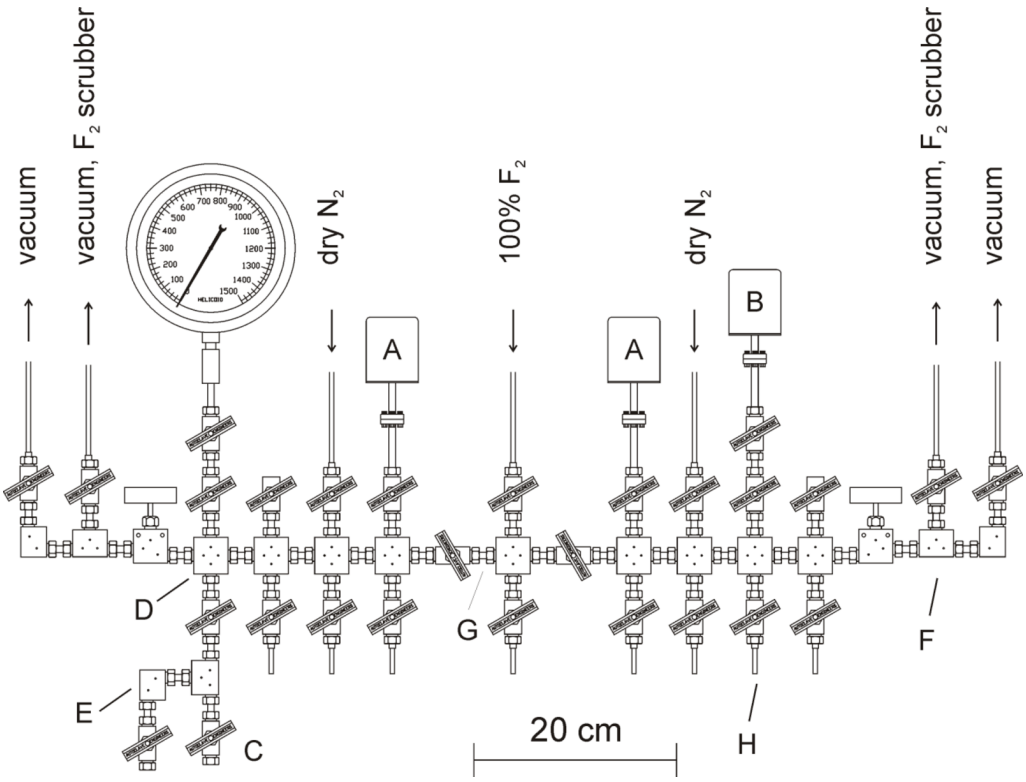

Figure 2.2 - Metal vacuum system; (A) MKS type 626A capacitance manometer (0-1000 Torr), (B) MKS Model PDR-5B pressure transducers (0-10 Torr), (C) 3/8-in. stainless-steel high-pressure valves (Autoclave Engineers, 30VM6071), (D) 316 stainless-steel cross (Autoclave Engineers, CX6666), (E) 316 stainless-steel L-piece (Autoclave Engineers, CL6600), (F) 316 stainless steel T-piece (Autoclave engineers, CT6660), (G) 3/8-in o.d., 1/8-in. i.d. nickel connectors, (H) 1/8-in o.d., 1/8-in. i.d. nickel tube. (from Jared Nieboer's M.Sc. thesis).

Reactors were crafted from FEP, a perfluorinated ethylene-propylene copolymer, shown in Figure 2.3. This plastic allows easy fabrication by heat-molding tubes while remaining relatively inert to the harsh reaction conditions described. The primary reactor design consists of a ¼-inch outer diameter straightened tube that is taper sealed at one end and flared at either 45° or 33° for connection to either a Kel-F or stainless steel valve,

respectively. Reactions destined to be characterized using NMR spectroscopy were performed in reactors crafted from straightened and sealed 4-mm o.d. tubing that was joined to a short, flared ¼ in. FEP connecting piece. After preparing the sample contents, the 4-mm tube was sealed using a heat gun while being under dynamic vacuum and cooling the contents of the reactor with liquid nitrogen. This sealed 4-mm tube can then be inserted into a thin-walled 5-mm glass NMR tube before being lowered into the NMR magnet for characterization.

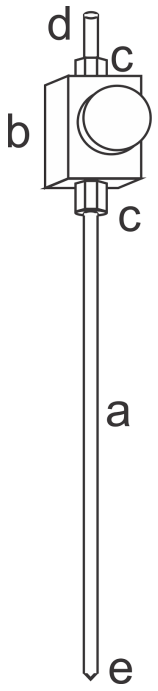

Figure 2.3 - Diagram of a typical FEP reactor fitted with a Kel-F valve. a) ¼ in. o.d. straightened FEP tubing; b) Kel-F valve; c) brass nut; d) ¼ in. o.d. FEP tubing; e) tapered seal formed by heat molding

Samples were primarily stored in their respective reactors unless otherwise stated. When required, samples were stored at low temperature by packing the sample tube into

powdered dry ice (–78 °C) or submerged into an ethanol bath cooled by liquid nitrogen to the desired temperature (range: room temperature to –120 °C). Long term storage of samples required heat-sealing of the FEP tube under dynamic vacuum before storing the sealed sample tube immersed in liquid nitrogen.

2.2 Purification of Starting Materials

Significant care was taken to ensure dryness of all reagents due to the moisture sensitivity of SF_4, SOF_2, and $Me_3SiC_2F_5$. In order to maintain the dryness of reagents, distillation setups were evacuated for upwards of 12 hours before performing the distillation.

2.2.1 Purification of SF_4, SOF_2, and BF_3

Sulfur tetrafluoride was received in a lecture bottle (Ozark-Mahoning Co.) containing impurities such as SOF_2, SF_6, and possibly S_2F_{10}. The impure SF_4 was passed through a U-Trap containing dry activated carbon, removing any traces of disulfur decafluoride from the mixture as S_2F_{10} may interfere with some reactions. The purified SF_4 was stored in a stainless steel can fitted with a steel valve. Thionyl fluoride (PCR Research Chemicals Inc.) was used as received in a lecture bottle cylinder. Boron trifluoride was used as received in a lecture bottle (Sigma Aldrich) fitted with a steel valve.

2.2.2 Purification of $(CH_3)_3SiC_2F_5$, CH_3CN, NC_5H_5, $CFCl_3$, $O(C_2H_5)_2$, CH_2Cl_2, and $CDCl_3$

Pentafluoroethyltrimethyl silane, $(CH_3)_3SiC_2F_5$ (Synquest Chemicals) was transferred using a dry-nitrogen glove-bag into a glass bulb equipped with a J. Young PTFE stopcock, followed by distillation onto 4 Å molecular sieves into a new glass bulb. Acetonitrile (Sigma-Aldrich) was purified according to the procedure reported by Winfield[1] and was stored over 4 Å molecular sieves in a glass flask fitted with a J. Young PTFE stopcock.

Pyridine (99.8%, Sigma Aldrich) was distilled upon CaH_2 in a dry Pyrex flask fitted with J. Young PTFE stopcock. Trichlorofluoromethane was distilled upon CaH_2, degassed by freeze-pump-thaw and then distilled into a new dry glass bulb fitted with a J. Young PTFE stopcock. Diethylether and dichloromethane were dispensed by an MBraun dry solvent system and stored upon 4 Å molecular sieves in a dry Pyrex glass bulb fitted with a J. Young PTFE stopcock after being degassed by the freeze-pump-thaw method.

Deuterated chloroform (99.8%, Sigma Aldrich) was transferred to a dry Pyrex glass bulb with a J. Young PTFE stopsock containing activated 4 Å molecular sieves inside a dry-nitrogen atmosphere glove-bag before being degassed by the freeze-pump-thaw method.

2.2.3 Purification of $[(CH_3)_4N]F$, CsF, DABCO, and t-BuLi

Tetramethylammonium fluoride tetrahydrate (>98%, Fluka) was dried according to literature.[2] Cesium fluoride (Sigma-Aldrich, 99.99%) was dried according to the

procedure outlined by Seppelt.[3] This drying procedure involved fusing wet CsF in a platinum crucible at ~800 °C before pouring the molten salt onto a pre-heated stainless-steel plate followed by immediate transfer into the dry-box antechamber and evacuation of the antechamber. Cesium fluoride and TMAF were stored in Kel-F vials in the dry-box. Tert-butyllithium (Sigma Aldrich, 1.6-3.2 M in heptane) was separated from solvent by dynamic vacuum at room temperature and the resultant solid was stored in an amber-glass bottle inside a dry box. Diazabicyclo[2.2.2]octane (≥99%, Sigma Aldrich) was used as received and stored inside a nitrogen-atmosphere dry-box.

2.3 Single-Crystal X-Ray Diffraction

2.3.1 Low-Temperature Crystal Mounting

Samples containing thermally unstable or moisture-sensitive crystals were manipulated using a low-temperature crystal-mounting setup shown in Figure 2.4. Dry gaseous nitrogen was passed through a 5 L Dewar of liquid nitrogen. This cooled nitrogen gas was passed over an aluminium trough that was used as a stage for crystal manipulation. Transferring solid samples from a ¼ in. o.d. FEP reactor starts by positioning the sealed end of the reactor inside the aluminium trough while nitrogen flows around the FEP tube. By cutting the FEP tubing to a length shorter than the aluminium trough, individual crystals may be selected and harvested from the tube while maintaining a blanket of cold and dry nitrogen over the sample. The temperature of the nitrogen gas can be controlled by regulating the flow rate entering the Dewar and was monitored using a copper/constantan thermocouple with digital readout. Depending on the temperature of

the trough, crystals were fixed to a goniometer tip by Z-15 or Z-25 Fomblin perfluoropolyether (PFPE) oil (Ausimont Inc.), differing in their pour points. These PFPE oils are resistant to aggressive chemical environments and remain viscous and viscid at low temperature in order to prevent crystal movement during data acquisition. Crystals were mounted on a CryoLoop (Hampton Research) attached to a metallic pin that was mounted magnetically to a wand that allowed fine manipulation inside the stream of nitrogen. The metal goniometer tip was transported to the goniometer using metal cryotongs that were precooled in liquid nitrogen. Transportation of the mounted crystal was done quickly (1-2 seconds) to avoid decomposition of the crystal. Once at the X-ray instrument, the goniometer tip was magnetically attached to the goniometer head.

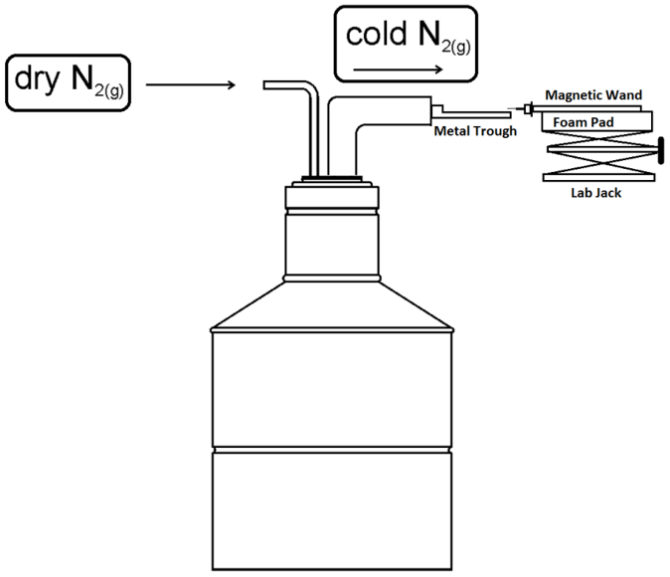

Figure 2.4 - Low-temperature crystal-mounting setup, consisting of a 10.5-L Dewar, equipped with a foam stopper, a glass nitrogen inlet, a silvered glass cold nitrogen outlet with an 11-cm long aluminium trough (2-cm o.d.). (Adapted from Jared Nieboer's M.Sc. thesis)

2.3.2 Collection and Reduction of X-Ray Data

Crystals of $SO(C_2F_5)_2$, $(CH_3)_3SiC_2F_5$, and $[S(OC_2H_5)_3][H_3F_4]$ were centered on a Rigaku SuperNova diffractometer equipped with a Dectris Pilatus 3R 200K-A hybrid-pixel-array detector, a four-circle κ goniometer, and sealed, graphite-monochromated Mo K_α and Cu K_α X-ray sources. Data were collected using the Cu K_α source (λ = 1.54184 Å) at 100 K. A pre-experiment was run to determine the unit cell, and a data collection strategy was calculated based on the determined unit cell and the quality of the preliminary data. The data were processed using *CrysAlisPro*,[4] which applied necessary Lorentz and polarization corrections to the integrated data and scaled the data. A numerical (Gaussian-grid) absorption correction was generated based upon the indexed faces of the crystal.

Diffraction data for crystals of $C_6H_{12}N_2 \cdot 2SF_4$ and $[C_6H_{12}N_2H]_2F[SF_5] \cdot 6SF_4$ were collected at −120 °C on a Bruker SMART APEX II X-ray diffractometer. The Apex II 4K charge-coupled device (CCD) area detector was positioned 6.120 cm away from the crystal. The Kα radiation (λ = 0.71073 Å) of a Mo source X-ray tube was used with a graphite monochromator. Cell reduction was carried out using the program *SAINT* which applied Lorentz and polarization corrections to three-dimensionally integrated diffraction spots.[5]

2.3.3 Solution and Refinement of Structures

The structure solutions for $SO(C_2F_5)_2$, $(CH_3)_3SiC_2F_5$, and $[S(OC_2H_5)_3][H_3F_4]$ were obtained using the *ShelXT*[6] intrinsic phasing method. Atom positions were refined using *ShelXL*[7,8] least-squares refinement. The *SCALE3 ABSPACK*[9] scaling algorithm was used for empirical absorption correction using spherical harmonics. The crystal structures were solved using the *Olex2* program.[10]

Crystal structures for $C_6H_{12}N_2 \bullet 2SF_4$ and $[C_6H_{12}N_2H]_2F[SF_5] \bullet 6SF_4$ were solved with the *Apex2* program using the *SHELXTL-plus v.6.14 package* for structure determination, refinement and molecular graphics.[11,12] The program *SADABS* was used for scaling of diffraction data, the application of a decay correction, and a multi-scan absorption correction.

Xprep was used to confirm unit cell dimensions and Bravais crystal lattice. The structures were minimized by least squares refinement based on the square of the structure factors, F^2 (equivalent to intensity, I). Atom positions were refined anisotropically and the extinction coefficient was calculated for the crystal structure. If the error in the extinction coefficient was on the same order of magnitude as the extinction coefficient, it was omitted from the refinement. Both residual values, R_1 based on F, the structure factor (Equation 2.1),

$$R_1 = \frac{\Sigma||F_o|-|F_c||}{\Sigma|F_o|} \tag{2.1}$$

and the weighted residual values wR_2 based on F^2 (Equation 2.2),

$$wR_2 = \sqrt{\frac{\Sigma[w(F_o^2 - F_c^2)^2]}{\Sigma[w(F_o^2)^2]}} \tag{2.2}$$

are available in their respective structure refinement tables along with the goodness of fit (Equation 2.3),

$$GooF = \sqrt{\frac{\Sigma[w(F_o^2 - F_c^2)]}{(n-p)}} \tag{2.3}$$

based on intensity where n is the number of reflections and p is the number of parameters defined.

2.4 Raman Spectroscopy

Raman spectra were recorded on a Bruker RFS 100 FT Raman spectrometer with a quartz beam splitter, liquid nitrogen-cooled Ge detector, and a low-temperature accessory when necessary. The backscattered (180°) radiation was sampled. The useable Stokes range was 50-3500 cm^{-1} with a spectral resolution of 2 cm^{-1}. A Nd:Yag laser with a 1064-nm line was used for excitation of the sample. Spectra consisting of approximately 1000 scans were recorded on powdered samples in ¼-in. o.d. FEP using powers between 100 and 150 mW. Samples were collected at temperatures between –100 and 20 °C. Spectra were visualized and analysed using *OPUS 4.2*.[13]

2.5 NMR Spectroscopy

Nuclear magnetic resonance spectra were recorded unlocked on either a 300.13 MHz (7.05 T) Bruker Avance II NMR spectrometer equipped with a BBFO probe or a 700 MHz (16.4 T) Bruker Avance III HD spectrometer equipped with a triple resonance Bruker TXO-Z (C/F-H-2H) Probe. Both probes have variable-temperature capabilities from +150 to –150 °C. *Bruker Topspin 3.5* was used for data refinement and visualization.[14] Fluorine-19 NMR spectra were referenced externally to neat $CFCl_3$ at room temperature. Proton and ^{13}C NMR spectra were referenced to an external sample of neat TMS at room temperature. Shimming on the NMR samples was performed manually or using *TopShim*,[15] when possible. All NMR spectroscopic samples were contained in 4 mm sealed FEP tubes that were inserted into 5 mm thin-walled glass NMR tubes. Initial ^{19}F NMR experiments were performed with a spectral window of 603.55 ppm centred at –50 ppm, a default pre-scan delay of 6 μs, and a relaxation delay of 1 s. After acquiring an initial spectrum, the spectral window was adjusted to include the signals of interest. The acquisition time, number of FID points, and number of scans were optimized for each sample in order to achieve good signal-to-noise, linewidth, and digital resolution. Variable delay relaxation experiments were performed to determine the T_1 relaxation times whenever possible. The relaxation delays and acquisition times were adjusted to approximately five times the longest determined T_1 values for each system in order to insure the full relaxation of nuclei.

T_1 time (ω_{19F}: 658.78 MHz) : $SF_3C_2F_5$ (CF_2: 1.9 s, CF_3: 1.9 s), $SF_2(C_2F_5)_2$ (SF_2: 2.4 s, CF_2: 2.6 s, CF_3: 2.7 s), $SO(C_2F_5)_2$ (CF_2: 2.2 s, CF_3: 2.7 s).

2.5.1 Spectral Simulation

Simulations of ^{19}F NMR spectra were performed using *SpinWorks 4* and *MestreNova 9.0.1*.[16,17] For the simulation of ^{19}F NMR spectra of $SOFC_2F_5$, *SpinWorks* was used to assign and optimize chemical shifts and *J*-coupling constants using the NUMMRIT algorithm. *Spinworks* allows the perturbation and optimization of NMR parameters if most transitions are visible and assigned. Otherwise, MestreNova was used to determine and visualize coupling constants and chemical shifts.

2.6 Computational Details

All DFT calculations were performed using the B3LYP functional and the aug-cc-pVTZ basis set was used for all systems. This basis set and level of theory were chosen due to good agreement between computational geometries and the crystal structures of similar systems.[20] In their study of $P(C_2F_5)_3$ geometry,[21] Hoge and coworkers found this basis set and a closely related functional to be well-suited for calculating relative conformer energies with significantly lower computational cost. In their study, this method was shown to slightly (< 10 kJ mol^{-1}) underestimate conformer energies, therefore a more robust level of theory and basis set should be used if more accurate energies are required. Geometry optimizations were performed using analytic gradient methods, and the vibrational frequency calculations were performed using the geometries optimized at the same level of theory. Calculations were performed using

Gaussian 09 (revision D.01).[18] The GaussView program was used to visualize and analyse the predicted geometries.[19]

2.7 Preparation of Pentafluoroethyl Derivatives of SF_4

2.7.1 Pentafluoroethylation of SF_4 using LiC_2F_5

A ¼ in. o.d. FEP reactor was loaded with 0.012 g of solid tert-butyllithium (0.19 mmol) in a dry box. Pentafluoroethane (0.024 g, 0.19 mmol) was distilled upon the solid followed immediately by addition of *ca.* 0.5 mL of Et_2O at –197°C. Slow warming to –75 °C caused the dissolution of t-BuLi and the generation of LiC_2F_5. While being cooled to –197 °C by liquid nitrogen, SF_4 (0.014g, 0.126 mmol) was distilled upon the frozen sample using a vacuum line. Slow warming to –75 °C with constant mixing caused a vigorous reaction yielding a viscous clear yellow mixture. Volatiles were condensed at –75 °C into a 4 mm FEP tube by static vacuum (*ca.* 10 minutes). The tube was sealed and the sample was characterized using ^{19}F NMR spectroscopy (see Figure 3.3), showing the formation of small quantities of $SF_2(C_2F_5)_2$, $SF_3C_2F_5$, and $SO(C_2F_5)_2$, with significant quantities of decomposition.

^{19}F NMR (ppm from $CFCl_3$, Et_2O, 223 K, $\omega_o(^{19}F)$ = 282 MHz)

Major component – C_2F_5H: –140.7 (CF_2, d of q, J = 52 Hz J = 3.5 Hz), –87.8 (CF_3, m); SF_4: 32.5 ($SF_{2\ eq}$, t, J = 78.3 Hz), 85.7 ($SF_{2\ ax}$, t, J = 78.3 Hz); SOF_2: 72.5 (SF_2, s); SF_6: 56.1 (s, J_{SF} = 253.1 Hz)

Minor component – $SF_3C_2F_5$: 49.4 ($SF_{2\ ax}$, m), –52.3 (SF_{eq}, m), –109.0 (CF_2, m), –79.7 (CF_3, m); $SF_2(C_2F_5)_2$: –14.5 ($SF_{2\ ax}$, m), –100.7 (CF_2, m), –81.4 (CF_3, t); $SO(C_2F_5)_2$: –113.9 & –120.7 (CF_2, AB pattern), –81.8 (CF_2, s).

2.7.2 Pentafluoroethylation of SF_4 with $Me_3SiC_2F_5$

2.7.2.1 Pentafluoroethylation of SF_4 with $Me_3SiC_2F_5$ using Fluoride Activator

A ¼ in. o.d. reactor was loaded with 0.006 g (0.04 mmol) of CsF inside a nitrogen-atmosphere dry box. The white solid was dissolved in 0.397 g (9.67 mmol) of CH_3CN, added by distillation using a glass vacuum line. Upon brief (<1 minute) warming to room temperature the solid dissolved, afterwards, care was taken to keep the sample below –40 °C in order to avoid decomposition of acetonitrile by fluoride. Sulfur tetrafluoride (0.241 g, 2.2 mmol) was distilled upon the solution using the metal vacuum line. The reactor was kept at low temperature (below –35 °C) in order to avoid overpressurization of SF_4 gas. Pentafluoroethyltrimethyl silane (0.355 g, 1.85 mmol) was vacuum distilled upon the solution at –197 °C and caused an immediate reaction upon warming to approximately –50 °C. The reactor was kept at room temperature for 12 hours, during which it developed a slightly yellow colour. The contents of the ¼ in. FEP reactor were transferred in a static vacuum to a 4 mm reactor and the contents were characterized using ^{19}F NMR spectroscopy (Figure 3.2). The product distribution favored the formation of $SF_2(C_2F_5)_2$, however, significant quantities of $SF_3C_2F_5$ were produced in addition to small quantities of $SOFC_2F_5$, and $SO(C_2F_5)_2$.

^{19}F NMR (ppm from $CFCl_3$,CH_3CN, 293 K, $\omega_o(^{19}F)$ = 282 MHz)

Major component – $SF_2(C_2F_5)_2$: –13.3 ($SF_{2\ ax}$, m), –99.2 (CF_2, m), –80.4 (CF_3, t); $SF_3C_2F_5$: 52.0 ($SF_{2\ ax}$, m), –51.1 (SF_{eq}, m), –108.0 (CF_2, m), –78.9 (CF_3, m); Me_3SiF: –158.2 (decet); SF_4: 34.9 ($SF_{2\ eq}$, br, s), 87.6 ($SF_{2\ ax}$, br, s); SOF_2: 74.5 (SF_2, s); SF_6: 56.7 (s).

Minor component – $SOFC_2F_5$: –18.8 (SF, m), –126.2 (CF, ddt), –124.6 (CF, ddt), –80.0 (CF_3, dt); $SO(C_2F_5)_2$: –113.2 to –118.9 (CF_2, AB pattern), –80.9 (CF_2, s); C_2F_5H: –139.8 (CF_2, dq), –87.1 (CF_3, m).

Alternative Method: In attempt to control and slow the addition of $Me_3SiC_2F_5$ to a solution containing a fluoride activator, a T-reactor fitted with a Swagelok ¼ in. T-connector was crafted, as shown in Figure 2.5. This specialty reactor allowed the slow addition of $Me_3SiC_2F_5$ to the straight vertical arm containing the SF_4 solution containing the activator. In the dry box, 0.002 g of CsF was loaded into the straight arm of the reactor. An excess of SF_4 solvent was distilled into the same arm and the solid was dissolved using a vacuum line. The sample was cooled below –35 °C because overpressurization of the reactor can cause leaks in the T-connector. While the bent sidearm of the reactor was turned downwards, 0.04 g of $Me_3SiC_2F_5$ was distilled into this arm. By backfilling the reactor with nitrogen and cooling the straight arm of the reactor to –80 °C, $Me_3SiC_2F_5$ slowly condensed into the SF_4 solution containing CsF. Over the course of 24 hours, the solution in the straight arm developed a yellow colour. Volatiles were distilled into an FEP NMR tube using a glass vacuum line and were characterized by ^{19}F NMR spectroscopy, showing that a similar product distribution was formed as in

the method described before. During the distillation of $Me_3SiC_2F_5$, a small amount was likely condensed into the straight arm because it was cooled by liquid nitrogen during the distillation.

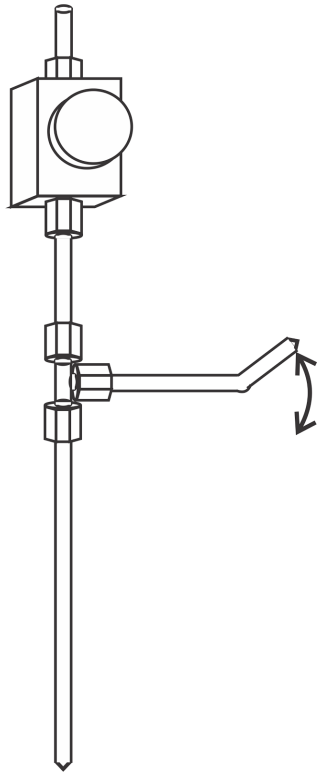

Figure 2.5 - Schematic of a specialty t-connector reactor designed for the slow addition from the bent-arm to a solution in the straight-arm. The bent-arm can be rotated to aid the transfer of a solution while maintaining a seal.

Alternative Method: In order to use tetramethylammonium fluoride as activator for $Me_3SiC_2F_5$, a ¼ in. o.d. reactor was loaded with 0.003 g (0.03 mmol) of $[NMe_4]F$ in the dry box. The fine white powder was then dissolved in a large excess of SF_4 (*ca.* 0.5 g, 4.6 mmol) at –197°C raising temperature to approximately –30 °C in order to dissolve. While

the sample was frozen at –197 °C, 0.006 g (0.03 mmol) of $Me_3SiC_2F_5$ was distilled upon the solid. The mixture was subsequently melted at approximately –50 °C, producing a vigorous reaction and developing a dark yellow colour over approximately 1 hour. Volatiles were removed under dynamic vacuum at –110 °C. Upon warming the remaining solution to room temperature, the sample separated into two immiscible phases. The larger and denser phase was volatile at room temperature and was characterized by ^{19}F NMR spectroscopy and contained small amounts of $SF_3C_2F_5$ and unidentified impurities. Reproductions of this method revealed that any undissolved $[NMe_4]F$ will float above the SF_4 solution and will immediately and vigorously react with $Me_3SiC_2F_5$ evolving gas and forming a dark solid. Care must be taken to completely dissolve $[NMe_4]F$ before distillation of $Me_3SiC_2F_5$.

^{19}F NMR (ppm from $CFCl_3$, SF_4, 208 K, $\omega_o(^{19}F) = 282$ MHz)

Major component – $SF_3C_2F_5$: –109.8 (CF_2, s), –80.8 (CF_3, s); Me_3SiF: –158.4 (decet); SF_4: 34.3 ($SF_{2\ eq}$, br, s), 79.2 ($SF_{2\ ax}$, br, s); SOF_2: 70.4 (SF_2, s); SF_6: 55.1 (s).

Minor component – $SF_2(C_2F_5)_2$: –17.0 ($SF_{2\ ax}$, br, s), –101.9 (CF_2, m), –81.9 (CF_3, s); $SOFC_2F_5$: –24.2 (SF, br, s), –126.8 (CF, ddt), –129.0 (CF, ddt), –81.4 (CF_3, s); $Me_3SiC_2F_5$: –134.5 (CF_2, s), –84.7 (CF_3, s).

Alternative Method: In order to completely dissolve $[NMe_4]F$, acetonitrile was used to dissolve approximately 0.002 g of $[NMe_4]F$. Stoichiometric amounts of the SF_4 substrate were distilled upon this solution, followed by addition of $Me_3SiC_2F_5$ using a glass vacuum line. Upon mixing, the solution was kept below –40 °C, close to the melting point of

CH_3CN in order to avoid fluoride attack on CH_3CN. The reduced temperature caused the reaction to proceed slowly, requiring 2-4 hours before the solution developed a yellow colour. The product distribution was determined using ^{19}F NMR spectroscopy and favored the formation of $SF_2(C_2F_5)_2$ with minimal quantities of $SF_3C_2F_5$ and small amounts of $SO(C_2F_5)_2$.

2.7.2.2 Pentafluoroethylation of SF_4 with $Me_3SiC_2F_5$ using Pyridine as Activator

A ¼ in. o.d. FEP reactor was loaded with $Me_3SiC_2F_5$ (0.110 g, 0.572 mmol) by vacuum distillation on a glass line. Sulfur tetrafluoride (0.506 g, 4.7 mmol) was distilled upon the frozen $Me_3SiC_2F_5$. The two liquids were mixed at –70 °C before adding pyridine (0.019 g, 0.24 mmol), that caused an immediate reaction upon mixing and warming to room temperature, at which point the mixture developed a yellow colour. While being cooled to –50 °C, volatiles were condensed into a liquid nitrogen cooled trap under dynamic vacuum. The volatiles were distilled into a 4 mm o.d. FEP tube that was heat sealed and the contents were characterized by ^{19}F NMR spectroscopy. While a small amount of $SF_2(C_2F_5)_2$ was observed, the reaction strongly favored the formation of $SF_3C_2F_5$ and $SOFC_2F_5$ formed by hydrolysis.

^{19}F NMR (ppm from $CFCl_3$, $CFCl_3$, 203 K, $\omega_o(^{19}F) = 282$ MHz)

Major component – $SF_3C_2F_5$: 51.0 ($SF_{2\ ax}$, m), –52.0 (SF_{eq}, m), –108.0 (CF_2, m), –78.5 (CF_3, m); SF_4: 34.1 ($SF_{2\ eq}$, t), 89.2 ($SF_{2\ ax}$, t); SOF_2: 74.1 (SF_2, s); $SOFC_2F_5$: –20.9 (SF, br, s), –124.5 (CF, ddt), –126.6 (CF, ddt), –79.6 (CF_3, d); Me_3SiF: –158.4 (decet).

Minor component – $SF_2(C_2F_5)_2$: –13.6 ($SF_{2\ ax}$, br, s), –100.0 (CF_2, m), –80.3 (CF_3, s); C_2F_5H: –139.1 (CF_2, d), –86.6 (CF_3, s); SF_6: 57.6 (s).

2.7.3 Attempted Isolation of $SF_3C_2F_5$

Sulfur tetrafluoride was pentafluoroethylated according to the procedure described in 2.7.2.2 using a large excess of SF_4 substrate (*ca.* 7:1). Upon condensation of volatile products into a liquid-nitrogen-cooled U-trap, the trap was warmed to –80 °C and evacuated. The remaining non-volatile liquid was characterized by ^{19}F NMR spectroscopy and contained $SF_3C_2F_5$.

^{19}F NMR (ppm from $CFCl_3$,$CDCl_3$, 293 K, $\omega_o(^{19}F)$ = 282 MHz)

Major component – $SF_3C_2F_5$: –105.0 (CF_2, s), –76.9 (CF_3, s)

Minor component – $SOFC_2F_5$: –17.4 (SF, br, s), –78.0 (CF_3, dt), –122.3 (CF, m), –123.8 (CF, m); SF_4: 86.0 ($SF_{2\,ax}$, br, s), 38.1 ($SF_{2\,eq}$, br, s); Me_3SiF: –156.9 (decet).

The ^{19}F NMR spectra suggested that $SF_3C_2F_5$ is adducted to pyridine, causing the coalescence of sulfur-bound fluorine signals, discussed further in Chapter 3.

Attempted Fractional Distillation: The pentafluoroethylation of SF_4 was performed according to the procedure described in 2.7.2.2. The sample was fractionally distilled using dynamic vacuum with the sample cooled to –40 °C using traps at –60 °C, –78 °C, and –197 °C; each fraction was characterized by ^{19}F NMR spectroscopy. The –78 °C trap contained primarily $SF_2(C_2F_5)_2$ and $SOFC_2F_5$, while the –60 °C trap contained primarily $SOFC_2F_5$ and likely NC_5H_5. Finally, the –197 °C trap contained SF_4, SF_6, Me_3SiF, $SF_3C_2F_5$, and $SF_2(C_2F_5)_2$.

2.7.4 Attempted Isolation of $SF_3C_2F_5$ using BF_3

Pentafluoroethylsulfur trifluoride was synthesized according to the procedure described in 2.7.2.2 and separated according to the procedure described in 2.7.3. The fraction containing $SF_3C_2F_5$ was redissolved in $CFCl_3$ and an excess of BF_3 was added to the solution by distillation. Upon warming to 0 °C, a white solid formed and slowly (*ca.* 5 minutes) developed a yellow colour. Volatiles were condensed into a liquid-nitrogen-cooled trap and the remaining yellow solid was dissolved in $CFCl_3$ and characterized by ^{19}F NMR spectroscopy.

^{19}F NMR (ppm from $CFCl_3$, $CFCl_3$, 293 K, $\omega_o(^{19}F)$ = 282 MHz): $[SF_2C_2F_5]^+$: 72 (s, SF_2), –77.9 (s, CF_3), –106.5 (s, CF_2); $[BF_4]^-$: –142.8 (s, br)

2.8 Preparation of Pentafluoroethyl Derivatives of SOF_2

2.8.1 Pentafluoroethylation of SOF_2 by $Me_3SiC_2F_5$

Excess SOF_2: A ¼ inch o.d. reactor was loaded with 0.224 g (1.17 mmol) of $Me_3SiC_2F_5$ by distillation on a glass vacuum line. Thionyl fluoride (0.747 g, 8.68 mmol) was distilled onto the sample at –197 °C, followed by pyridine (0.277 g, 3.50 mmol). The clear and colourless solution was reacted at room temperature for *ca.* 16 hours, at which time the sample became dark yellow/red. Volatiles were removed by dynamic vacuum at room temperature and condensed into a glass trap at –197 °C, appearing colourless. The trap was warmed to –60 °C and volatiles were distilled into a 4 mm FEP tube that was heat sealed and the contents were characterized by ^{19}F NMR spectroscopy, containing primarily $SOFC_2F_5$ and smaller amounts of $SO(C_2F_5)_2$.

^{19}F NMR (ppm from $CFCl_3$,$CDCl_3$, 293 K, $\omega_o(^{19}F)$ = 282 MHz)

Major component – SOF_2: 76.1 (SF_2, s); $SOFC_2F_5$: –17.9 (SF, m), –79.4 (CF_3, d), –124.1 (CF, m), –125.4 (CF, m); Me_3SiF: –157.5 (decet).

Minor component – $SO(C_2F_5)_2$: –112.3 to –118.9 (CF_2, AB pattern), –80.4 (CF_2, s); C_2F_5H: –138.4 (CF_2, d), –86.5 (CF_3, s).

Excess Pyridine: The pyridine activator is used as solvent, which allows easy separation of $SOFC_2F_5$ and $SO(C_2F_5)_2$ from the SOF_2 substrate and favors the formation of $SO(C_2F_5)_2$. This reaction also forms side-products and impurities from the reaction between $Me_3SiC_2F_5$ and NC_5H_5, evidenced by the formation of C_2F_5H. For these reactions, $Me_3SiC_2F_5$ was distilled into a ¼ inch o.d. FEP reactor (0.224 g, 1.17 mmol) followed by 0.052 g (0.604 mmol) of SOF_2. The two liquids were mixed at –50 °C, followed by the addition of *ca.* 0.75 g (9.5 mmol) of NC_5H_5 by distillation. Upon melting the sample at –40 °C, the reaction immediately evolved gas and developed a yellow colour that remained upon removal of volatiles at –50 °C. The colourless volatiles were characterized by ^{19}F NMR spectroscopy, containing mostly $SO(C_2F_5)_2$, small quantities of $SOFC_2F_5$, and larger quantities of C_2F_5H and Me_3SiF.

^{19}F NMR (ppm from $CFCl_3$,$CDCl_3$, 293 K, $\omega_o(^{19}F)$ = 282 MHz)

Major component – $Me_3SiC_2F_5$: –81.8 (CF_3, s), –131.3 (CF_2, s); $SO(C_2F_5)_2$: –112.1 to –117.5 (CF_2, AB pattern), –79.8 (CF_2, s); $SOFC_2F_5$: –17.6 (SF, m), –123.1 (CF, m), –124.6 (CF, m); Me_3SiF: –157.5 (decet).

Minor component – C_2F_5H: –138.2 (CF_2, d), –85.9 (CF_3, s).

2.9 Preparation of DABCO-SF_4 Adducts

2.9.1 Preparation of DABCO•2SF_4

A ¼ inch o.d. FEP reactor was prepared and loaded with 0.015 g of DABCO (0.13 mmol). To this white solid, 0.545 g (5.1 mmol) of SF_4 was added by distillation at –197 °C using the metal vacuum line. Upon warming to –40 °C in an ethanol cold bath, the sample melted and formed a suspension of solid DABCO in clear colourless liquid SF_4. Brief warming to room temperature (*ca.* 1-2 minutes) with gentle mixing dissolved the solid, forming a clear colourless solution. Cooling to –20 °C immediately precipitated a white solid that sank to the bottom of the reactor. Crystals of $C_6H_{12}N_2$•2SF_4 were grown at –20 °C, followed by removal of volatiles by dynamic vacuum at *ca.* –75 °C. The crystals were harvested from the solid sample at *ca.* –80 °C for X-ray crystallography.

2.9.2 Crystal Growth of [$C_6H_{12}N_2H$]F[SF_5]•6SF_4

A ¼ inch o.d. FEP reactor was loaded with 0.012 g (0.107 mmol) of DABCO in the dry box. A large excess (*ca.* 0.6 g, 5.6 mmol) of SF_4 was distilled upon the white solid using the metal vacuum line, forming a suspension at –50 °C. The sample, a clear colourless liquid below white solid, was cooled to –80 °C in an ethanol cold bath, at which temperature volatiles were removed under dynamic vacuum. The resulting fine white solid was stored at –80 °C for approximately two months, after which the solid appeared to form crystals above the white solid. Raman spectra were recorded of this solid and crystals of [$C_6H_{12}N_2H$]F[SF_5]•6SF_4 were harvested for X-ray crystallography.

2.9.3 Variable-Temperature Evacuation of the DABCO-SF_4 System

In a ¼ inch o.d. FEP reactor, 0.025 g (0.22 mmol) of DABCO was reacted with *ca.* 0.5 g (5 mmol) of SF_4. The sample was warmed to room temperature, at which point they reacted vigorously producing a clear-colourless liquid. Upon rapid cooling to –70 °C, a white solid precipitated from the solution. Volatiles were removed under dynamic vacuum over four hours while warming from –70 °C to –65 °C, until volatiles ceased condensing in the –197 °C trap. Raman spectra were recorded at –100°C. The white solid was evacuated under dynamic vacuum for 3 hours at –25 °C, with volatiles visibly condensing in the liquid nitrogen-cooled trap. Raman spectra were recorded at –100 °C. Evacuation at room temperature caused the white solid to release volatiles, evidenced by the effervescence of the solid under dynamic vacuum. After approximately three hours evacuating, the final Raman spectra were recorded at –100 °C.

References

[1] J. M. Winfield, *J. Fluorine Chem.* **1984**, *25*, 91–98.

[2] K. O. Christe, W. W. Wilson, R. D. Wilson, R. Bau, J. A. Feng, *J. Am. Chem. Soc.* **1990**, *112*, 7619–7625.

[3] Seppelt, K. (**2012**) *Preparation of Highly Active Cesium Fluoride, in Efficient Preparations of Fluorine Compounds Chapter 2* (ed H. W. Roesky), John Wiley & Sons, Inc., Hoboken, NJ, USA.

[4] *CrysAlisPRO*, Oxford Diffraction /Agilent Technologies UK Ltd, Yarnton, England.

[5] *Saint-plus*. Bruker AXS Inc.: Madison, W., USA, **2006**.

[6] G. Sheldrick, *Acta Crystallogr., Sect. A: Found. Adv.* **2014**, *70*, C1437–C1437.

[7] G. M. Sheldrick, *Acta Crystallogr. Section B* **2015**, *71*, 3–8.

[8] G. M. Sheldrick, *Acta Crystallogr. Section A* **2008**, *64*, 112–122.

[9] a) *SCALE3 ABSPACK*, Oxford Diffraction /Agilent Technologies UK Ltd, Yarnton, England. b) E. Spedicato, E. Bodon, A. Popolo, N. Mahdavi-Amiri, *Quarterly Journal of the Belgian, French and Italian Operations Research Societies* **2003**, *1*, DOI 10.1007/s10288-002-0004-0.

[10] O. V. Dolomanov, L. J. Bourhis, R. J. Gildea, J. A. K. Howard, H. Puschmann, *J. Appl. Crystallogr.* **2009**, *42*, 339–341

[11] *Apex2*. Bruker AXS Inc.: Madison, W., USA, **2006**.

[12] Sheldrick, G. M. 6.14 ed.; Bruker AXS INC.: Madison, Wisconsin, USA, **2003**

[13] *OPUS 4.2*, Bruker Instruments, Inc.: Billerica, Massachusetts, USA

[14] *Topspin 3.5*, Bruker Instruments, Inc.: Billerica, Massachusetts, USA

[15] *Topshim*, Bruker Instruments, Inc.: Billerica, Massachusetts, USA

[16] *SpinWorks 4*, Kirk Marat: Winnipeg, Manitoba, CAN

[17] *MestreNova,* Mestrelabs Research R.L.: Santiago de Compostela, A Coruña, ES

[18] Frisch, M. J.; Trucks, G. W.; Schlegel, H. B.; Scuseria, G. E.; Robb, M. A.; Cheeseman, J. R.; Scalmani, G.; Barone, V.; Petersson, G. A.; Nakatsuji, H., et al. *Gaussian 09, Revision D.01;* Gaussian, Inc., Wallingford, CT, 2016.

[19] *GaussView*, version 5.0; Gaussian, Inc., Wallingford, CT, 2016.

[20] P. Chaudhary, J. T. Goettel, H. P. A. Mercier, S. Sowlati-Hashjin, P. Hazendonk, M. Gerken, *Chem. - Eur. J.* **2015**, *21*, 6247–6256.

[21] S. A. Hayes, R. J. F. Berger, B. Neumann, N. W. Mitzel, J. Badera, B. Hoge, *Dalton Trans.*, **2010**, *39*, 5630-5636.

3. Pentafluoroethyl Derivatives of SF_4

3.1 Introduction

In their 1971 study, Shreeve and Sauer synthesized $SF_2(C_2F_5)_2$ through the high-temperature reaction (150–180 °C) of SF_4 with C_2F_4 and CsF, (Equation 3.1).[1] In addition to this product, many other mixed perfluoroalkyl sulfides, sulfoxides, and disulfides were synthesized. Due to the high temperature of the reaction, some products underwent pyrolysis, forming $SF_3C_2F_5$. Shreeve and Sauer used fractional distillation to separate products and characterized them by mass spectrometry, infrared, and NMR spectroscopy. In this study, it was determined that $SF_2(C_2F_5)_2$ is hydrolytically stable at room temperature for at least one week in the presence of water vapour while the presence of HCl facilitates the formation of $SO(C_2F_5)_2$ via hydrolysis.

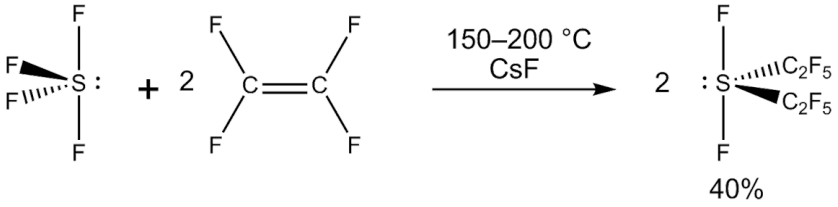

(3.1)

Unlike Shreeve and Sauer who used SF_4 as a substrate for pentafluoroethylation, Mews and coworkers used bis(pentafluoroethyl)disulfide as a starting material and fluorinated the disulfide bond using AgF_2 forming $SF_3C_2F_5$ (Equation 3.2), besides $SF_5C_2F_5$, and $SOFC_2F_5$.[2] These products were separated by fractional distillation. If elemental fluorine was used for the disulfide fluorination, only $SF_5C_2F_5$ was isolated. Pentafluoroethylsulfur trifluoride was characterized by ^{19}F NMR spectroscopy. Fluoride-ion abstraction using

AsF_5 yielded $[SF_2C_2F_5][AsF_6]$ which was identified by X-ray crystallography, Raman, and ^{19}F NMR spectroscopy. This synthetic route relies on the $S_2(C_2F_5)$ starting material, synthesized primarily by the reaction between $Hg_2(C_2F_5)_2$ and sulfur at 250 °C. The $SOFC_2F_5$ impurity observed in this reaction is likely formed by hydrolysis of $SF_3C_2F_5$.

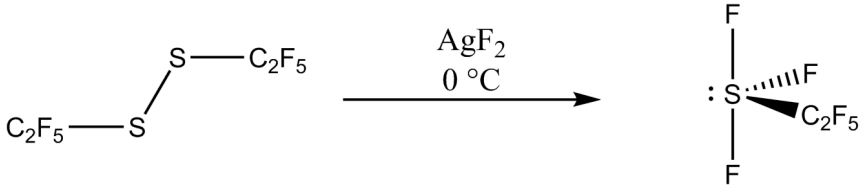

(3.2)

3.2 Results and Discussion

3.2.1 Synthesis

Pentafluoroethyltrimethyl silane, $Me_3SiC_2F_5$, will transfer a pentafluoroethyl group but requires an activator such as fluoride or a nitrogen base, shown in Equation 3.3.

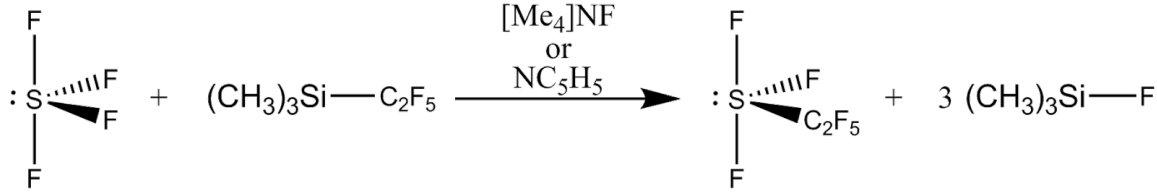

(3.3)

For pentafluoroethyl derivatization of SF_4, pyridine was found to be a preferable activator. Before the introduction of pyridine as an activator, $Me_3SiC_2F_5$ was mixed with SF_4 which do not react at room temperature. Upon addition of catalytic NC_5H_5 (*ca.* 15 mol % with

respect to $Me_3SiC_2F_5$), the reaction proceeds immediately at room temperature. This reaction results in a mixture of Me_3SiF, $SF_3C_2F_5$, $SF_2(C_2F_5)_2$, $SO(C_2F_5)_2$, and $SOFC_2F_5$. The latter two are minor products resulting from hydrolysis due to trace amounts of moisture. By using SF_4 as solvent, the reaction will favour the formation of $SF_3C_2F_5$; however, $SF_2(C_2F_5)$ is always formed in this reaction in small quantities.

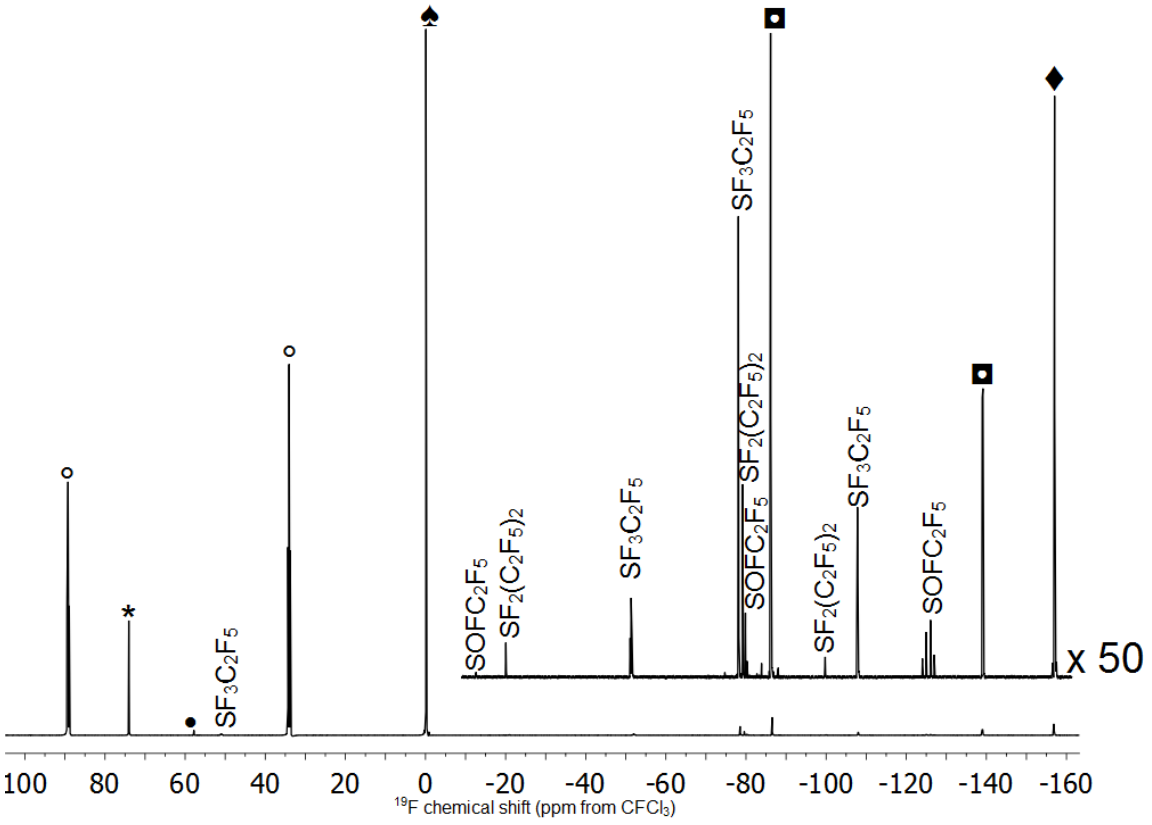

Figure 3.1 - Fluorine-19 NMR spectrum of the reaction between SF_4 and $Me_3SiC_2F_5$ in SF_4 with NC_5H_5 (*ca.* 15% with respect to $Me_3SiC_2F_5$) after condensation of volatiles at –50 °C and redissolution in $CFCl_3$. ○SF_4; *SOF_2; •SF_6; ◘$Me_3SiC_2F_5$; ♠$CFCl_3$; ♦ Me_3SiF

A ^{19}F NMR spectrum of the mixture formed in the reaction between SF_4 and $Me_3SiC_2F_5$ using NC_5H_5 as an activator and SF_4 as solvent is shown in Figure 3.1. After being

formed, $SF_3C_2F_5$ was separated from pyridine by first condensing volatiles at –50 °C into a liquid-nitrogen-cooled U-trap under dynamic vacuum; this traps $SF_3C_2F_5$, Me_3SiF, SF_4, and any traces of $SF_2(C_2F_5)_2$, $SOFC_2F_5$, $SO(C_2F_5)_2$, SOF_2, and SF_6 from pyridine. Afterwards, $SF_3C_2F_5$ was isolated from this mixture by removing excess SF_4 and Me_3SiF along with $SF_2(C_2F_5)_2$, $SOFC_2F_5$, $SO(C_2F_5)_2$, SOF_2, and SF_6 under dynamic vacuum at –80 °C. Since $SF_3C_2F_5$ likely forms an adduct with pyridine, small amounts of pyridine will cause the coalescence of sulfur-bound fluorine resonances in the ^{19}F NMR spectrum. Pyridine could not be removed completely from $SF_3C_2F_5$ since small quantities of pyridine were still transferred during the distillation, even after two fractional vacuum distillations. The presence of thionyl derivatives $SOFC_2F_5$, $SO(C_2F_5)_2$ in the reaction mixture were due to reaction of $Me_3SiC_2F_5$ with SOF_2, present in SF_4 because of hydrolysis from trace amounts of moisture, shown in Equation 3.4.

$$SF_4 + H_2O \longrightarrow SOF_2 + 2\,HF \tag{3.4}$$

When CsF or $[N(CH_3)_4]F$ was used to activate the $Me_3SiC_2F_5$ pentafluoroethyl transfer reagent, a similar mixture of products was formed, shown in Figure 3.2, along with traces of unidentified side-products. The advantage of using fluorides is that pentafluoroethyl derivatives are easily separated from fluoride salts by vacuum distillation, allowing characterization in the absence of fluorides that could cause the broadening of NMR signals. The reaction between fluoride and $Me_3SiC_2F_5$ is fast, likely forming the unstable

$[Me_3Si(F)C_2F_5]^-$ intermediate anion. This reaction occurs faster than the pentafluoroethyl transfer reaction to SF_4, leading to decomposition of $[Me_3Si(F)C_2F_5]^-$ in solution. Some fluoride salts such as $[N(CH_3)_4]F$ are insoluble in most solvents, requiring the use of CH_3CN to dissolve. Tetramethylammonium fluoride reacts with CH_3CN, CH_2Cl_2, and CH_3Cl at room temperature via deprotonation.[3] Using a fluoride source as $Me_3SiC_2F_5$ activator is only optimal when SF_4 is used as solvent because a large excess of substrate limits side-reactions and favours the formation of $SF_3C_2F_5$ over higher substituted $SF_2(C_2F_5)_2$. However, reactions performed in SF_4 are difficult due to the high vapour pressure of the solvent, which can be avoided by reducing the temperature that, in turn, lowers the solubility of fluoride in SF_4 and reduces the rate of reaction.

If a nitrogen base with a lower vapour pressure such as 1,4-diazabicyclo[2.2.2]octane, DABCO, is used side reactions are minimized and products are easily separated from excess base, however, non-adducted $SF_3C_2F_5$ becomes difficult to separate from SF_4 solvent due to their similar vapour pressures at –80 °C. By using DABCO as $Me_3SiC_2F_5$ activator, $SF_3C_2F_5$ can be produced near-quantitatively, however, attempts to separate the product from SF_4 solution were unsuccessful.

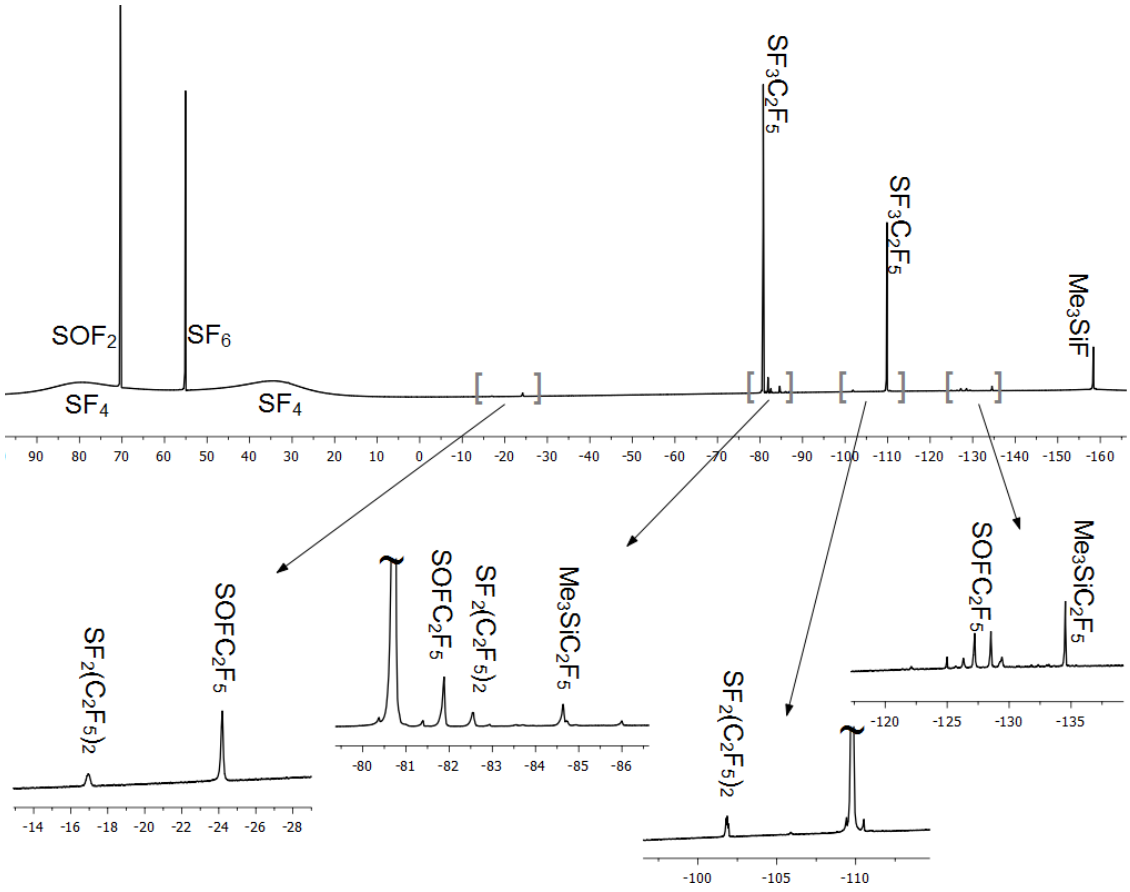

Figure 3.2 - Fluorine-19 NMR spectrum of the crude mixture formed by the reaction of $Me_3SiC_2F_5$ with TMAF in SF_4. The spectrum was acquired at –40 °C in SF_4 with ~10 % TMAF (with respect to $Me_3SiC_2F_5$) and is referenced to $CFCl_3$ external standard. Sulfur-bound fluorine shifts of $SF_3C_2F_5$ are not observed due to rapid exchange with fluoride in solution.

In their 1997 study, Mews and coworkers synthesized the $[SF_2C_2F_5][AsF_6]$ salt, demonstrating the fluorobacisity of the sulfur-bound fluorines of $SF_3C_2F_5$. A separation of $SF_3C_2F_5$ was attempted using BF_3 as a Lewis acid to abstract a fluoride from $SF_3C_2F_5$. Pentafluoroethylsulfur trifluoride was produced by the reaction between SF_4 and $Me_3SiC_2F_5$ using catalytic amounts of pyridine as activator and employing an excess of SF_4 in order to favor the formation of $SF_3C_2F_5$. Upon separating the $SF_3C_2F_5$ from other pentafluoroethyl-containing species, the $SF_3C_2F_5$ was dissolved in $CFCl_3$ and reacted with

an excess of BF_3. A white solid formed, which slowly turned yellow was isolated by removal of volatiles under dynamic vacuum at 0 °C. The yellow solid was redissolved in $CFCl_3$ and was characterized by ^{19}F NMR spectroscopy, showing the characteristic resonances for the $[SF_2C_2F_5][BF_4]$ salt: 72 (s, SF_2), –77.9 (s, CF_3), –106.5 (s, CF_2) ($CFCl_3$, ppm from $CFCl_3$). These chemical shifts are in agreement with those found by Mews and coworkers who acquired the ^{19}F NMR spectrum of $[SF_2C_2F_5^+][AsF_6^-]$: 57.7 (s, SF_2), –76.0 (s, CF_3), –94.7 (s, CF_2) (SO_2, CD_2Cl_2, $CFCl_3$, ppm from $CFCl_3$).[2] Similarly, Mews and coworkers observed that SF_2, CF_2, and CF_3 resonate as singlets upon abstraction of the fluoride from $SF_3C_2F_5$.

The use of LiC_2F_5 was investigated for the pentafluoroethylation of SF_4 since this has been the method of choice for silicate, germane, bismuth, and stannic substrates.[4–12] These reactions require the deprotonation of C_2F_5H by t-BuLi or n-BuLi in diethylether at low temperature with subsequent mixing with SF_4 and slow warming, shown in Equation 3.5.

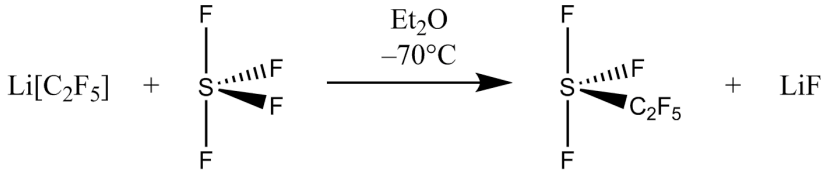

(3.5)

The vigorous reaction forms a mixture of many pentafluoroethyl compounds including $SF_3C_2F_5$, $SF_2(C_2F_5)_2$, and $SO(C_2F_5)_2$. A ^{19}F NMR spectrum of this mixture is shown in Figure 3.3.

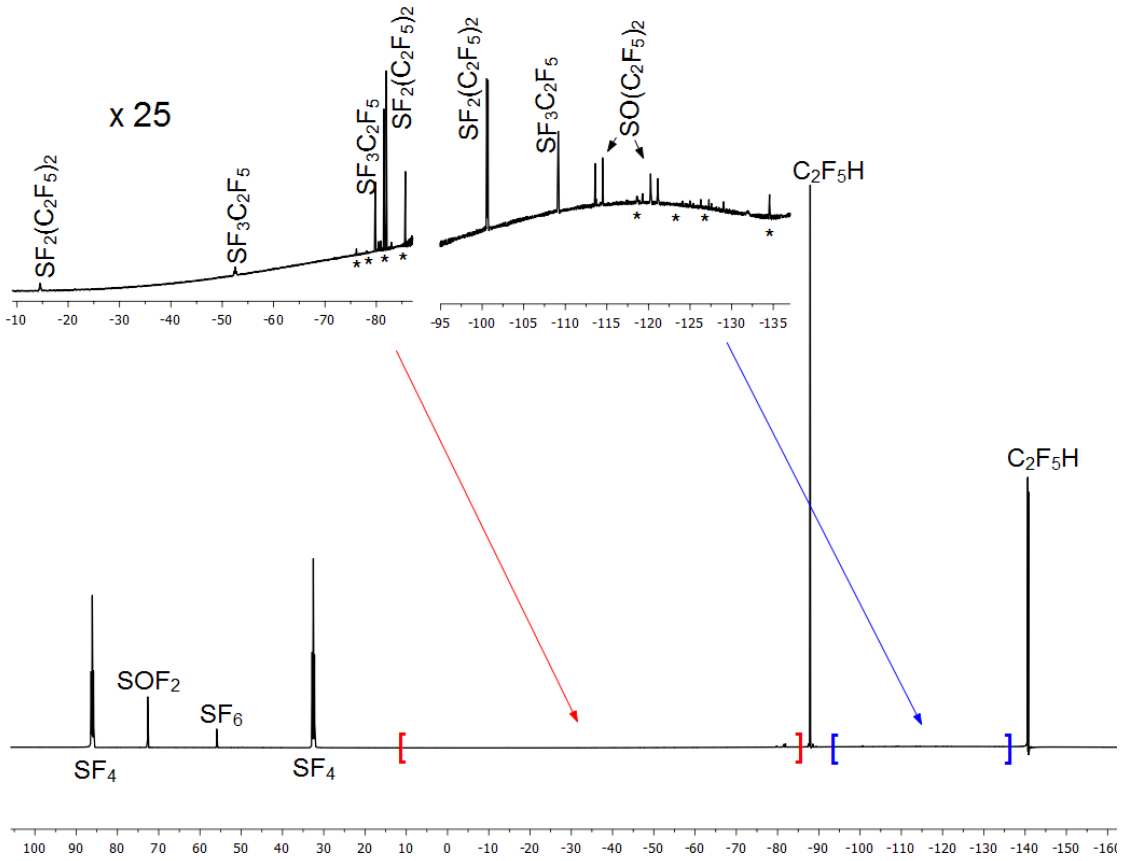

Figure 3.3 - Fluorine-19 NMR spectrum of the mixture formed by reaction of SF_4 with LiC_2F_5 in ether acquired at –40 °C. Asterisks denote signals belonging to unknown products.

The ^{19}F NMR spectrum of this reaction shows the major component of this reaction mixture is unreacted starting materials C_2F_5H and SF_4. The desired products are produced in very small quantities and are not easily separated from the mixture. During the reaction, the solution becomes yellow likely due to reduction of SF_4. The reaction between LiC_2F_5 and SF_4 causes the ethereal solution to become viscous due to polymerization of C_2F_4, formed by the decomposition of LiC_2F_5, which complicates mixing and causes non-uniform heating by the polymerization of C_2F_4. While the desired products were formed in the reaction between SF_4 and LiC_2F_5 in very small quantities,

$Me_3SiC_2F_5$ was found to be the superior pentafluoroethyl source in terms of yield, purity of products, and simplicity due to milder reaction conditions.

3.2.2 Pentafluoroethylsulfur Trifluoride, $SF_3C_2F_5$

3.2.2.1 Optimized Geometry of $SF_3C_2F_5$

The gas-phase geometry of $SF_3C_2F_5$ was optimized using B3LYP/aug-cc-pVTZ and the global minimum-energy geometry is shown in Figure 3.4, selected bond angles and distances are tabulated in Table 3.1.

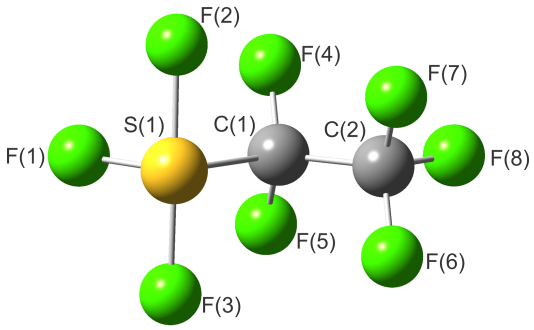

Figure 3.4 - Gas-phase geometry of $SF_3C_2F_5$ optimized using B3LYP/aug-cc-pVTZ

Table 3.1 - Selected bond lengths (Å) and angles (°) from the B3LYP/aug-cc-pVTZ optimized geometry of $SF_3C_2F_5$.

Atoms	Distance (Å)	Atoms	Distance (Å)
S(1)–F(1)	1.592	C(1)–F(4)	1.327
S(1)–F(2)	1.698	C(1)–F(5)	1.327
S(1)–F(3)	1.698	C(2)–F(6)	1.334
S(1)–C(1)	1.959	C(2)–F(7)	1.333
C(1)–C(2)	1.556	C(2)–F(8)	1.334
Atoms	**Angle (°)**	**Atoms**	**Angle (°)**
F(1)–S(1)–F(2)	87.9	F(1)–S(1)–C(1)	98.6
F(1)–S(1)–F(3)	87.9	S(1)–C(1)–C(2)	109.7
F(2)–S(1)–F(3)	173.9	F(4)–C(1)–F(5)	109.2

Due to the larger size of the pentafluoroethyl group, VSEPR rules predict it to be in an equatorial position. By constraining the $–C_2F_5$ to an axial position of the molecule followed by geometry optimization, the energy rises by 57.4 kJ $mol^{–1}$. Comparing the sulfur-centre geometries of $SF_3C_2F_5$ and SF_4 (Table 3.2), S–F bonds are elongated slightly by pentafluoroethyl incorporation. This bond extension is expected since fluorine is more electron withdrawing than the pentafluoroethyl group, resulting in more covalent S–F bonds in SF_4. The angle between equatorial substituents of $SF_3C_2F_5$ (98.6°) is slightly smaller compared to SF_4 (101.2°). Both differ greatly from the ideal 120° bond angle expected for a trigonal bipyramidal geometry because of lone-pair-ligand repulsion.

Table 3.2 - Comparison of sulfur-centre geometry of SF_4 and $SF_3C_2F_5$ calculated using B3LYP/aug-cc-pVTZ

	Distance (Å) or angle (°)	
	$SF_3C_2F_5$	SF_4
F_{ax}–S	1.698	1.682
F_{eq}–S	1.592	1.575
F_{ax}–S–F_{ax}	173.9	172.8
F_{eq}–S–F_{eq}		101.2
F_{eq}–S–C	98.6	

A relaxed potential energy surface scan was performed, rotating the pentafluoroethyl group about the C–S bond in 9° steps and performing a geometry optimization at each point (Figure 3.5). This scan shows three minima, with two local minima at a F_{eq}–S–C–C dihedral angle of 0°, 90°, and the global minimum at 180°.

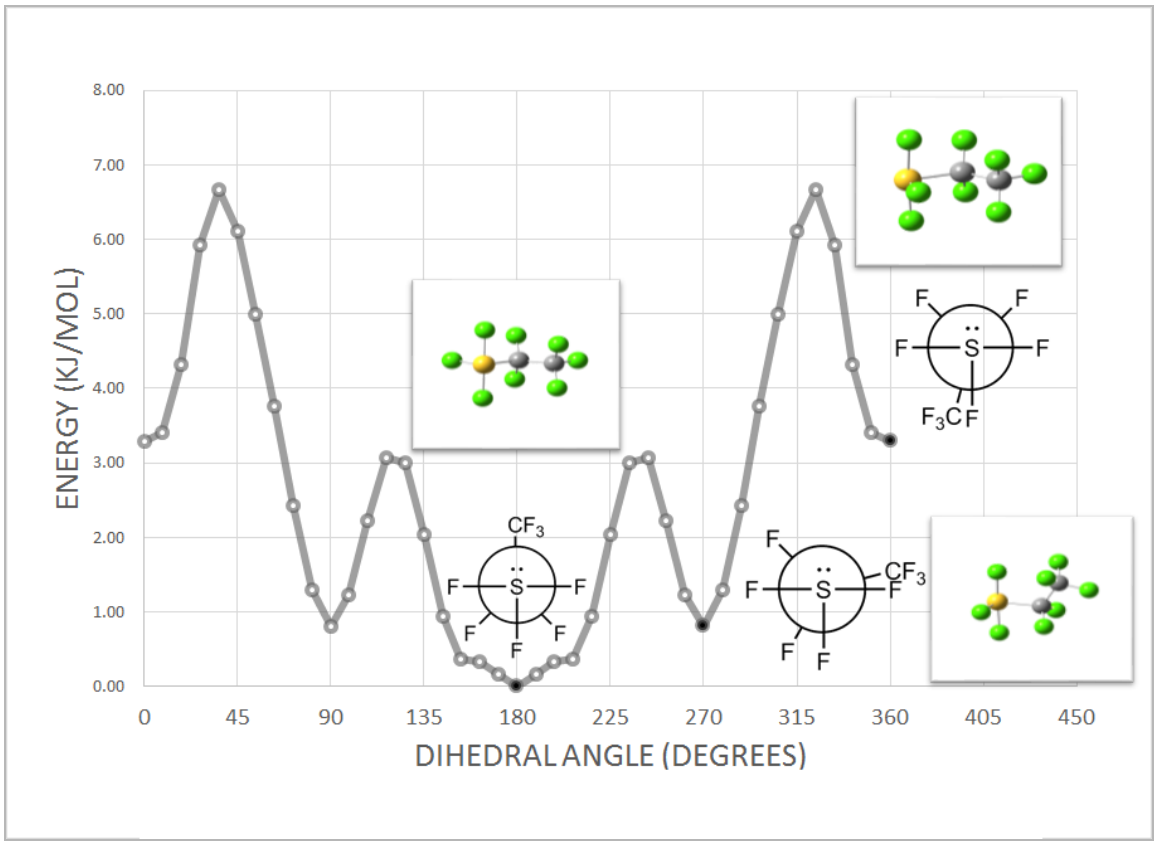

Figure 3.5 - Relaxed potential energy surface scan using B3LYP/aug-cc-pVTZ of the F_{eq}–S–C–C dihedral angle of $SF_3C_2F_5$. Minima geometries are shown with Newman projections. Energies are normalized to the global minimum at a F_{eq}–S–C–C dihedral angle of 180°.

Geometries of the minimum-energy conformers are compared in Table 3.3. Some geometric parameters remain essentially unchanged among rotamer minima, such as the angle between axial fluorines. The most dramatic change is observed for the S(1)–C(1)–C(2) angle that varies from 109.7 to 118.0°. This angle increases due to the trifluoromethyl group being brought to close proximity to the axial sulfur-bound fluorines. In the case of rotamer B that has the pentafluoroethyl group eclipsed to the

axial positions on sulfur, the S–C–C angle is distorted to 118°. Other bond lengths and angles are unsurprisingly very similar between the three rotamers, since their energies are very similar differing by only 3.29 kJ mol^{-1}. The energy barriers between rotamers A–B and B–C are 1.74 and 5.75 kJ mol^{-1}, respectively. The small energy barriers separating rotamers and the similarities of conformer energies calculated by these methods suggest rapid exchange at room temperature at the NMR timescale.

Table 3.3 - Comparison of calculated minimum-energy geometries of $SF_3C_2F_5$ rotamers calculated using B3LYP/aug-cc-pVTZ

	Rotamer		
	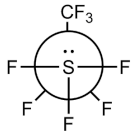	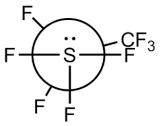	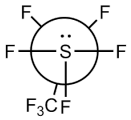
	A	B	C
Relative Energy	0 kJ mol^{-1}	0.81 kJ mol^{-1}	3.29 kJ mol^{-1}
Angle			
F(1)–S(1)–C(1)–C(2)	180°	90°	0°
F(2)–S(1)–F(3)	173.9°	172.9°	171.4°
F(1)–S(1)–C(1)	98.6°	101.0°	103.9°
F(4)–C(1)–F(5)	109.2°	110.3°	108.8°
S(1)–C(1)–C(2)	109.7°	118.0°	114.1°
Bond length			
F(ax.)–S(1)	1.698 Å	1.703/1.700 Å	1.697 Å
F(eq.)–S(1)	1.592 Å	1.589 Å	1.593 Å
S(1)–C(1)	1.959 Å	1.937 Å	1.951 Å

3.2.2.2 Fluorine-19 NMR Spectroscopy of $SF_3C_2F_5$

Table 3.4 -Fluorine-19 NMR chemical shifts of $SF_3C_2F_5$ in various solvents including those reported in literature

	^{19}F NMR[a]			
Conditions	SF_2	SF	CF_2,	CF_3
NC_5H_5, 298 K, ppm			–105.04 (s)	–76.88 (s)
CH_3CN, 298 K, ppm	51.64 (m)	–51.42 (m)	–108.30 (m)	–79.13 (td)
SF_4, ~1M TMAF, 208 K, ppm			–110.05 (s)	–81.07 (s)
$O(C_2H_5)_2$, 233 K, ppm	49.70 (m)	–52.49 (m)	–109.14 (m)	–79.78 (td)
$CDCl_3/CFCl_3$, 243 K, ppm[2]	53 (br)	–51 (br)	–108.3 (s)	–79.8 (s)

[a](s) singlet; (br) broad; (m) multiplet; (td) triplet of doublets

Fluorine-19 chemical shifts of $SF_3C_2F_5$ observed in this study are given in Table 3.4. Upon condensing off $SF_3C_2F_5$ from the fluoride activator into CH_3CN solvent, the ^{19}F NMR spectrum reveals an AA′DMM′X_3 spin system (Figures 3.6 and 3.7), recorded at room temperature. Previous studies[2] reporting NMR data for $SF_3C_2F_5$ did not observe the second order multiplicity of the NMR signals, presumably due to the low resolution of the spectra and/or the presence of fluoride or some other donor in the reaction that causes increased fluxionality of the sulfur-bound fluorines as well as the broadening of that signal.

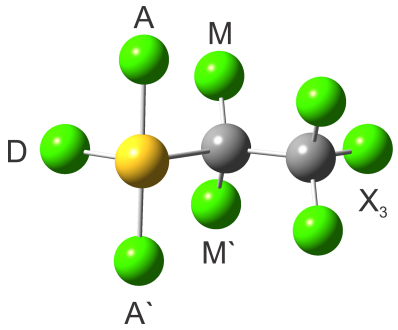

Figure 3.6 - Labelling scheme for the AA′DMM′X_3 spin system of $SF_3C_2F_5$

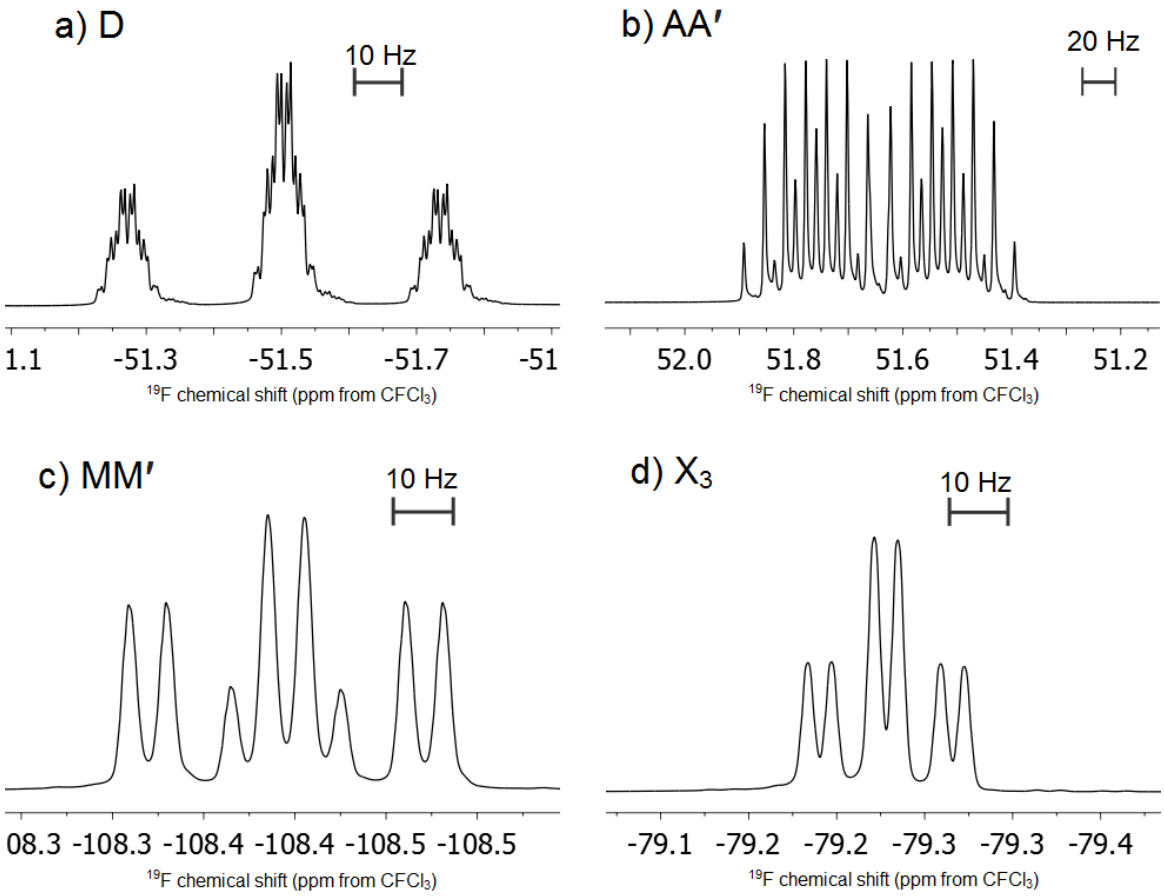

Figure 3.7 - Fluorine-19 NMR multiplets for $SF_3C_2F_5$ synthesized by the reaction between $Me_3SiC_2F_5$ and SF_4 in the presence of TMAF activator. Spectrum recorded at room temperature in CH_3CN after removal of fluoride. a) SF signal, b) SF_2 signal, c) CF_2 signal, and d) CF_3 signal.

Due to the fast exchange regime suggested by the small energy barriers calculated in section 3.2.2.1, the observed NMR data are the result of an average geometry caused by the rapid rotation of pentafluoroethyl groups about the C–S bond. The AA′DMM′X_3 spin system contains four chemically equivalent environments, while the A and M environments exhibit magnetic inequivalence due to their inequivalent coupling pathways. Using resolution enhancement by Gaussian multiplication, additional multiplet structure was extracted. Resolution-enhanced multiplets are shown in Figure 3.8,

revealing the extensive coupling observed in $SF_3C_2F_5$. Attempts to simulate the multiplets shown in Figure 3.7 and 3.8 were undertaken, but were unsuccessful using one spin system.

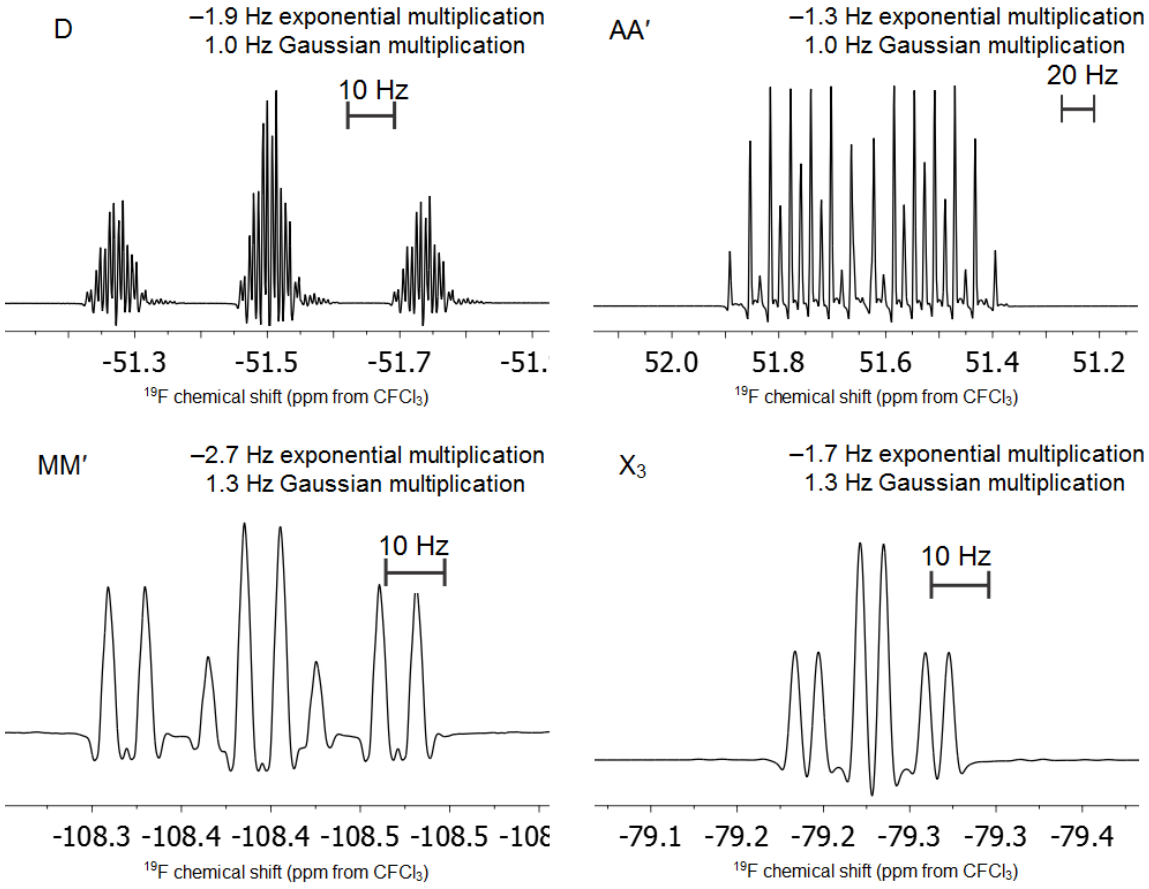

Figure 3.8 - Resolution enhanced multiplets for the ^{19}F NMR spectrum of $SF_3C_2F_5$ acquired at room temperature in CH_3CN.

Preliminary results show that overlap of at least three spin systems had to be used to obtain a satisfactory fit with the experimental spectra. The physical explanation of the existence of three subspectra is currently not understood and further investigation is needed. Some preliminary coupling constants were easily extracted from the multiplets, specifically, $J_{DA=DA'}$ and J_{AX} were found to be –65.5 and 10.8 Hz, respectively.

3.2.3 Bis(pentafluoroethyl)sulfur Difluoride, $SF_2(C_2F_5)_2$

3.2.3.1 OptimizedGeometry of $SF_2(C_2F_5)_2$

The gas-phase geometry of $SF_2(C_2F_5)_2$ was optimized using B3LYP/aug-cc-pVTZ and is shown in Figure 3.9 with bond lengths and angles listed in Table 3.5. The two pentafluoroethyl groups are positioned in equatorial positions on the sulfur centre. Other rotamers were optimized by rotating the pentafluoroethyl groups about the C–S bond, shown in Figure 3.10. Compared to the minimum-energy geometry, these two minima have relative energies of 10.6 and 3.0 kJ mol^{-1}. Table 3.6 compares selected geometric parameters of these rotamers.

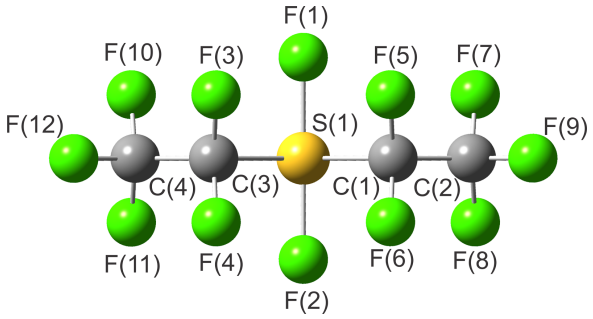

Figure 3.9 - Minimum-energy gas-phase geometry of $SF_2(C_2F_5)_2$ optimized using B3LYP/aug-cc-pVTZ.

Table 3.5 - Selected bond angles and distances for the B3LYP/aug-cc-pVTZ optimized geometry of $SF_2(C_2F_5)_2$.

Atoms	distance (Å)	Atoms	Angle (°)
F(1)–S(1)	1.723	F(1)–S(1)–F(2)	174.1
S(1)–C(1)	1.949	C(3)–S(1)–C(1)	101.6
F(5)–C(1)	1.327	F(5)–C(1)–F(6)	109.3
C(1)–C(2)	1.560	S(1)–C(1)–C(2)	108.7
C(2)–F(9)	1.334		

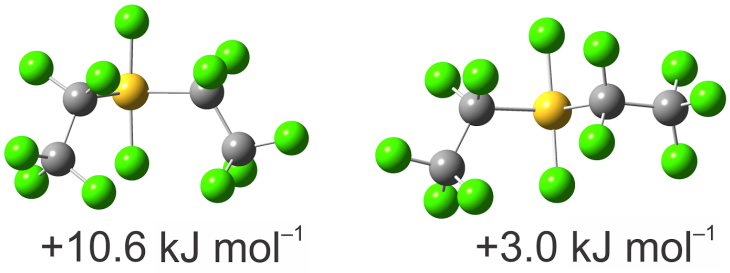

Figure 3.10 - Gas-phase local minimum-energy geometries for $SF_2(C_2F_5)_2$ optimized using B3LYP/aug-cc-pVTZ. Energies shown are normalized to global minimum geometry.

Table 3.6 - Comparison of calculated minimum-energy geometries of $SF_2(C_2F_5)_2$ rotamers calculated using B3LYP/aug-cc-pVTZ

	Rotamer		
	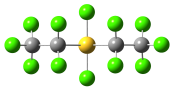		
	A	B	C
Energy	0 kJ mol^{-1}	3.0 kJ mol^{-1}	10.6 kJ mol^{-1}
Point Group	C_{2V}	C_1	C_S
Angle			
F(1)–S(1)–F(2)	174.1°	173.0°	171.2°
F(3/5)–C(3/1)–F(4/6)	109.3°	109.5/109.4°	109.6°
C(1)–S(1)–C(3)	101.6°	103.8°	110.3°
S(1)–C(1/3)–C(2/4)	108.7°	108.6/117.2°	117.5°
C(3)–S(1)–C(1)–C(2)	180°	175.4°	95.9°
C(1)–S(1)–C(3)–C(4)	180°	96.8°	95.9°
Bond Length			
F_{ax}–S(1)	1.723/1.722 Å	1.721/1.729 Å	1.727/1.729 Å
C(1/3)–S(1)	1.949 Å	1.952/1.930 Å	1.937 Å
C(1/3)–C(2/4)	1.560 Å	1.561/1.567 Å	1.567 Å
F(5/3)–C(1/3)	1.327 Å	1.325/1.334 Å	1.337/1.328 Å

The predicted angles between axial fluorines of the three rotamers of $SF_2(C_2F_5)_2$ are similar, ranging from 172.8 to 174.1°, and compare well with that of SF_4. By rotating both pentafluoroethyl groups about the C–S bond (rotamer C) the C–S–C angle becomes larger, expanding from 101.6° to 110.3°. This can be explained by the steric interaction

between difluoromethylene groups that are brought closer to one another by bond rotation. In the case of rotamer B, one of these bonds is rotated while the other is not, allowing enough space for one difluoromethylene, and therefore the C–S–C increases only slightly from 101.6 to 103.8°. Similar to the case of $SF_3C_2F_5$, steric interactions of the trifluoromethyl groups with the axial fluorine atoms increase the S–C–C angle to 117° due to. When only one pentafluoroethyl group is rotated (in the case of rotamer B), the S–C–C angle of only that pentafluoroethyl group is distorted. In rotamers of both $SF_3C_2F_5$ and $SF_2(C_2F_5)_2$, the C–S bond is predicted to be shorter when the pentafluoroethyl group is eclipsed by an axial fluorine. For $SF_2(C_2F_5)_2$, rotation to this eclipsed rotamer causes the C–S bond to contract from 1.949/1.952 Å to 1.930/1.937 Å.

3.2.3.2 Fluorine-19 NMR Spectroscopy of $SF_2(C_2F_5)_2$

In their 1971 study, Sauer and Shreeve noted that the ^{19}F NMR spectra of $SF_2(C_2F_5)_2$ are complicated due to the AA′XX′-type coupling created by magnetic inequivalence of the sulfur-bound fluorine atoms and the fluorine atoms of the difluoromethylene moiety.[1] The shifts reported by Shreeve and Sauer contain a caveat that more analysis is required. In this study, ^{19}F NMR spectra were acquired for $SF_2(C_2F_5)_2$ in mixtures containing $SF_3C_2F_5$, $SO(C_2F_5)_2$, and $SOFC_2F_5$. Chemical shifts are summarized in Table 3.7 and multiplets are shown in Figure 3.12. Unlike $SF_3C_2F_5$, the presence of fluoride or base does not cause ^{19}F NMR signals of $SF_2(C_2F_5)_2$ to broaden or lose multiplicity.

Table 3.7 - Fluorine-19 NMR chemical shifts of $SF_2(C_2F_5)_2$ in various solvents including those reported in literature

$SF_2(C_2F_5)_2$	SF_2	CF_2	CF_3
CH_3CN, 298 K, ppm	–13.70	–99.55	–80.79
NC_5H_5, 298 K, ppm	–14.78	–98.56	–79.59
$CFCl_3$, 203 K, ppm	–13.53	–99.96	–80.26
$CFCl_3$, ppm[1]	–11.2	–98.9	–80.5

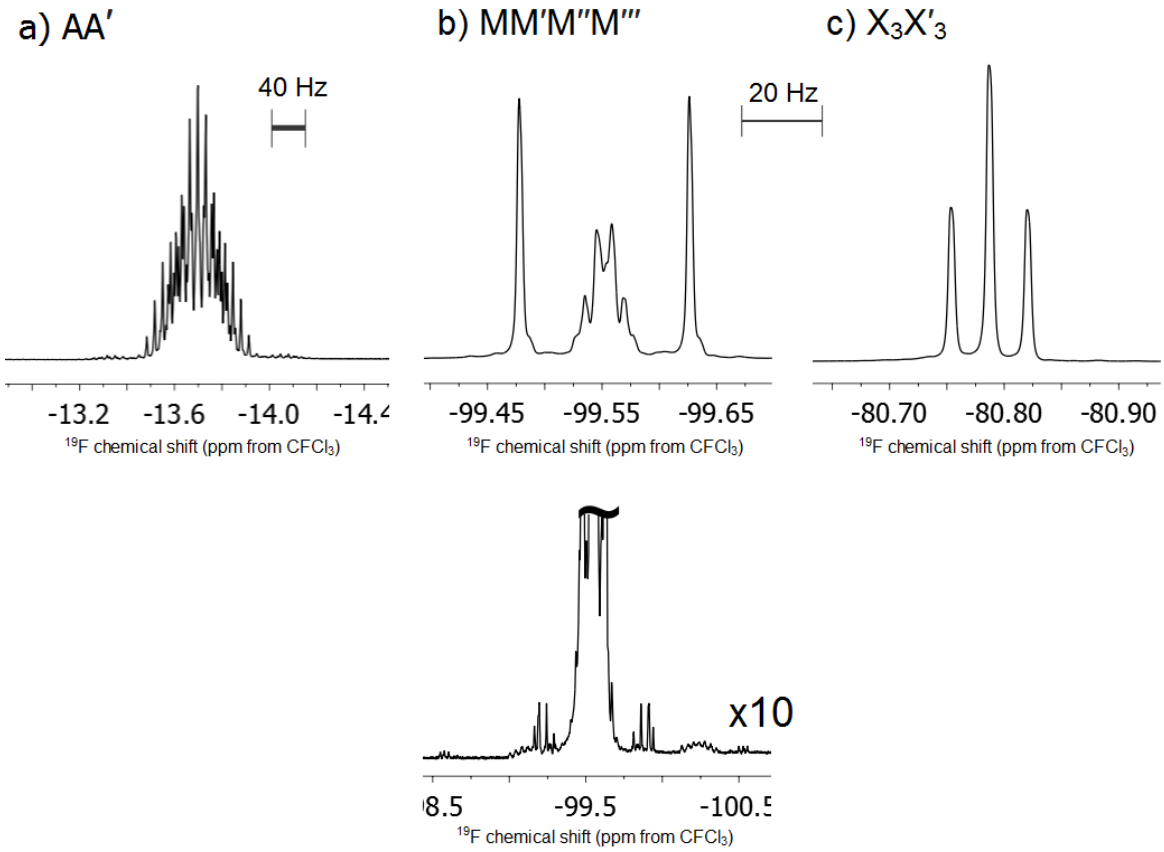

Figure 3.11 - Fluorine-19 NMR multiplets for $SF_3C_2F_5$ recorded at room temperature in CH_3CN. a) SF_2 signal, b) CF_2 signal (expanded baseline below), and c) CF_3 signal.

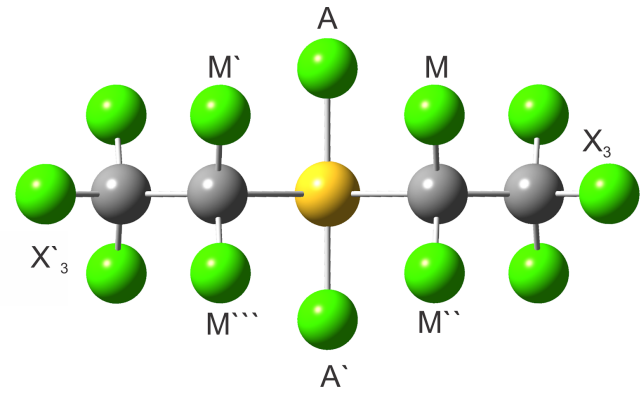

Figure 3.12 - Labelling scheme for the AA′MM′M″M‴$X_3X'_3$ spin system of $SF_2(C_2F_5)_2$.

The ^{19}F NMR spectrum of $SF_2(C_2F_5)_2$ exhibits an AA′MM′M″M‴$X_3X'_3$ spin system due to the magnetic inequivalence of each sulfur-bound and methylene fluorine atom (Figure 3.12). The triplet signal, Figure 3.11c representing the trifluoromethyl signals X_3 and X'_3 appears to be first-order due to the small (< 1 Hz) $^3J_{F–F}$ coupling to methylene fluorines. Simulation of this NMR spectrum using Spinworks and MestreNova allowed the determination of *J*-coupling constants and chemical shifts. The simulated multiplets are shown in Figure 3.13 and the determined *J*-constants are reported in Table 3.8. The coupling constants determined by simulation show strong $^2J_{FF}$ coupling between geminal difluoromethylene fluorines of –182 Hz. Additionally, the geminal coupling between axial sulfur-bound fluorines is also strong and negative (–92 Hz). The negative sign of the geminal CF_2 coupling is surprising since geminal difluoromethylene couplings have generally been thought to be positive.[13,14] The spin system presented below is sensitive to the sign of the *J*-coupling constants and using positive geminal coupling constants did not produce a sufficient fit with experimental spectra.

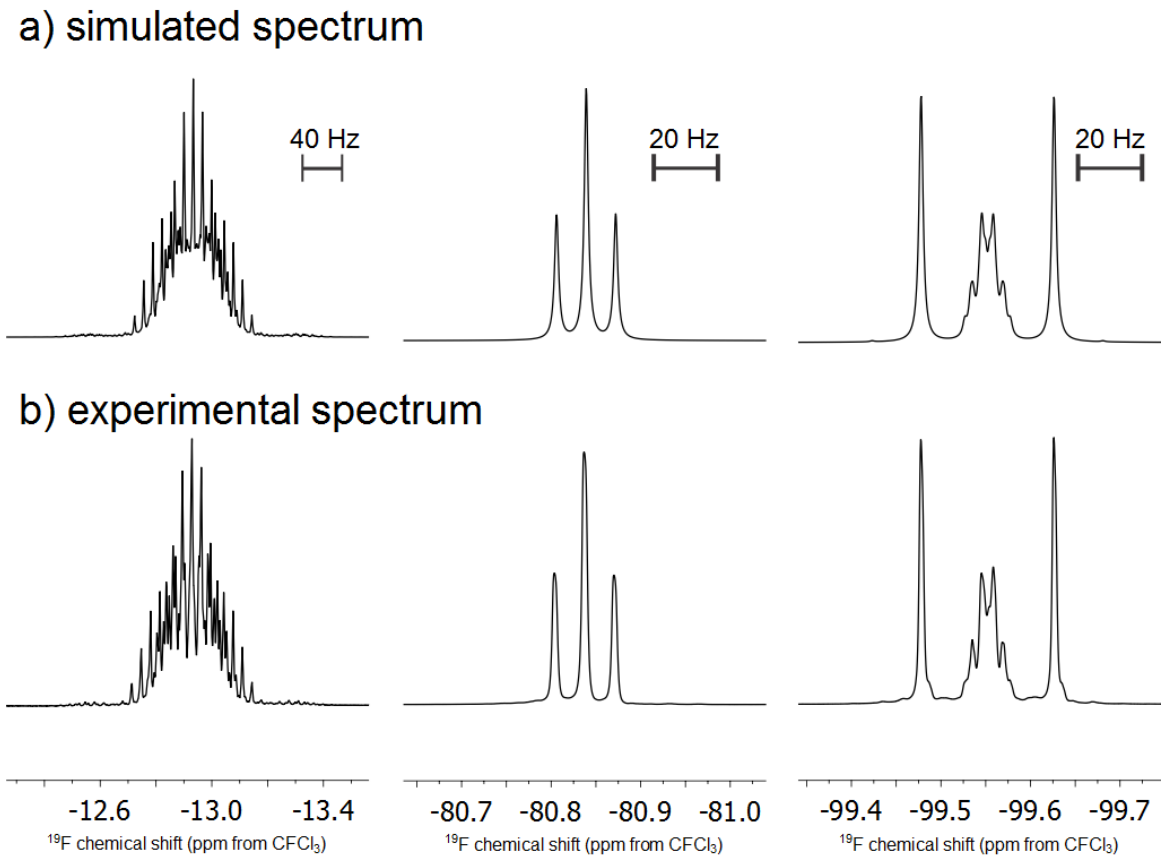

Figure 3.13 - Comparison of a) simulated and b) experimental ^{19}F NMR spectrum of $SF_2(C_2F_5)_2$. Simulation was performed using MestreNova and experimental spectra were acquired at room temperature in CH_3CN.

Table 3.8 - Coupling constants for the AA′MM′M″M‴$X_3X'_3$ spin system of $SF_2(C_2F_5)_2$

Coupling constant	Value (Hz)	Coupling constant	Value (Hz)
$^2J_{A–A'}$	–92	$^4J_{M–M' = M''–M'''}$	–16
$^3J_{A–M = A–M' = A'–M'' = A'M''}$	42.62	$^4J_{M–M''' = M'–M''}$	–8
$^3J_{A–M'' = A–M''' = A'–M = A'–M'}$	–0.65	$^4J_{A–X = A'–X = A–Y = A'–Y}$	9.3
$^2J_{M–M'' = M'–M'''}$	–182		

Coupling between trifluoromethyl and difluoromethylene environments ($^3J_{FF}$) are expected to be small, and tend to have magnitudes less than 5 Hz.[15] This small $^3J_{MX}$ coupling constant in $SF_2(C_2F_5)_2$ is non-zero and less than 1 Hz. The $X_3X'_3$ signal shown in

Figure 3.11c is broadened by this coupling, which could not be precisely measured. Long range coupling is observed between sulfur-bound fluorine environments (A spins) and trifluoromethyl fluorines (X_3 and X'_3) at 9.3 Hz, which splits the trifluoromethyl signal to a first order triplet. Since difluoromethylene fluorine atoms are magnetically inequivalent, M multiplets are complicated by introducing additional 3- and 4-bond coupling to sulfur-bound fluorines and opposite methylene fluorines, respectively. Each methylene fluorine atom couples to 5 magnetically inequivalent fluorine atoms. For example, the atom labelled M couples to five atoms with the following constants: $^2J_{MM'} = -182$ Hz, $^3J_{MA} = 42.62$ Hz, $^3J_{MA'} = -0.65$ Hz, $^4J_{MM'} = -16$ Hz, and $^4J_{MM''} = -8$ Hz.

Considerations for outer transitions, shown in Figure 3.14, were paramount in the simulation of the "M" multiplet. A spin flip is the changing of quantum number, *m*, from –½ to ½ in the case of $I = ½$ nuclei. NMR selection rules only allow lines to be observed in one-dimensional experiments when the transition results in a spin flip that changes the total magnetic quantum number by one unit. For first-order spectra, these transitions occur when only one nucleus undergoes a spin-flip and change in total *m* remains one ($\Delta m_{total} = 1$), called a single-quantum transition. When the magnitude of coupling is similar to the chemical shift frequency as is the case in second-order multiplets, selection rules allow the observation of transitions when multiple spin-flips occur as long as $\Delta m_{total} = 1$. Since the position of these low-intensity lines are highly sensitive to changes in coupling constant or chemical shift, they were used to refine the simulated ^{19}F NMR spectrum.

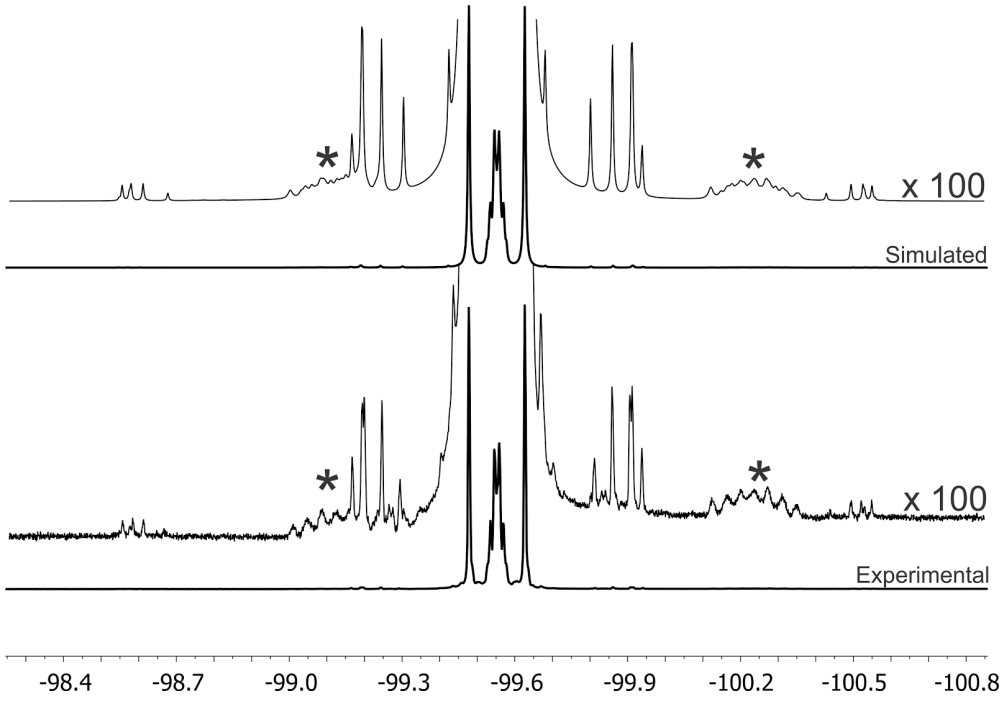

Figure 3.14 - Fluorine-19 NMR spectrum of the CF_2 signal of $SF_2(C_2F_5)_2$ showing combination bands that allowed the simulation of this multiplet. ^{13}C satellites are denoted by *.

Additionally, the multiplicity of ^{13}C satellites for the CF_2 signal, shown in Figure 3.14, arising from the $(CF_3CF_2)SF_2(^{13}CF_2CF_3)$ isotopologue changing the spin system to a $AA'MM'M'M'''QX_3X'_3$. This perturbation of the spin system allows the verification of other coupling constants and is strong evidence for the correct assignment of the coupling constants presented. Additionally, this allowed the determination of the $^1J_{C-F}$ coupling constant for the difluoromethylene moiety of 317.26 Hz.

3.3 Trisethoxysulfonium Trihydrogen Tetrafluoride, $[S(OC_2H_5)_3][H_3F_4]$

Attempts to crystallize $SF_3C_2F_5$ were unsuccessful using SF_4 as solvent. In these attempts, SF_4 was slowly removed by dynamic vacuum while cooling the reactor vessel in an ethanol bath cooled by liquid nitrogen. The reactor was cooled to –80 °C while solvent

was removed; at that temperature, ethanol became viscous and sticky due to moisture. Apparently, while transferring the cut-off piece of FEP tubing that contained the crystals, some attached ethanol was also transferred to the nitrogen-cooled aluminium trough used for crystal manipulation (described in Chapter 2). The ethanol then reacted with some sulfur containing species forming $[S(OC_2H_5)_3][H_3F_4]$ inside the trough. Possible species that could have reacted with the ethanol are SF_4, $[HNC_5H_5]F{\bullet}SF_4$, $SF_3C_2F_5$, SOF_2, or $SOFC_2F_5$ with HF formation. The $FS(OC_2H_5)_3$ then donated fluoride to the excess HF forming as a crystalline salt. The crystal structure of $[S(OC_2H_5)_3][H_3F_4]$ was acquired and is shown in Figure 3.15, data collection parameters and crystallographic information are shown in Table 3.10, and some bond angles and lengths are tabulated in Table 3.9. This crystal structure features a $H_3F_4^-$ anion that has previously been reported in 11 salts: $Ba[H_3F_4]_2$,[16] $Ba[H_3F_4][H_2F_3]_3$, $Cs[H_3F_4]{\bullet}IF_5$,[17] $Cs[H_3F_4]$,[18] $[NH_4][H_3F_4]$,[19] $Ag[H_3F_4]$,[20] $Na[H_3F_4]$,[21] $Tl[H_3F_4]$,[22] $Rb[H_3F_4]$,[18] $[HNC_5H_2(CH_3)_3][H_3F_4]$,[23] and $K[H_3F_4]$.[24] Of these reports, the crystal structures of $K[H_3F_4]$,[25] and $Ba[H_3F_4]_2$ are known.[16] In the $[H_3F_4]^-$ anion, three HF molecules are hydrogen bonded to a central fluoride ion. Two of the three F---(H)F distances of $[S(OC_2H_5)_3][H_3F_4]$ (2.391(2) and 2.389(2)) Å are similar to within 3σ of those reported in the 1986 study by Mootz and Boenigk in their report of $K[H_3F_4]$ (2.401(4) Å).[25] On the other hand, F(4)---(H)F(1) (2.362(2) Å) is shorter than those previously reported by 0.039 Å likely due to the close contact between F(4) and the central sulfur atom of the $[S(OC_2H_5)_3]^+$ cation. Two structures featuring this anion contain close contacts with metal atoms. In the case of $Ba[H_3F_4]_2$, the D_{3h} symmetry is distorted due to HF coordinating to the Ba centre. This causes the F---H–F distance to become

shorter (2.323(4) Å), and bond angles between HF molecules and the central fluoride were distorted up to 14° from the idealized 120° angle. [16,26]

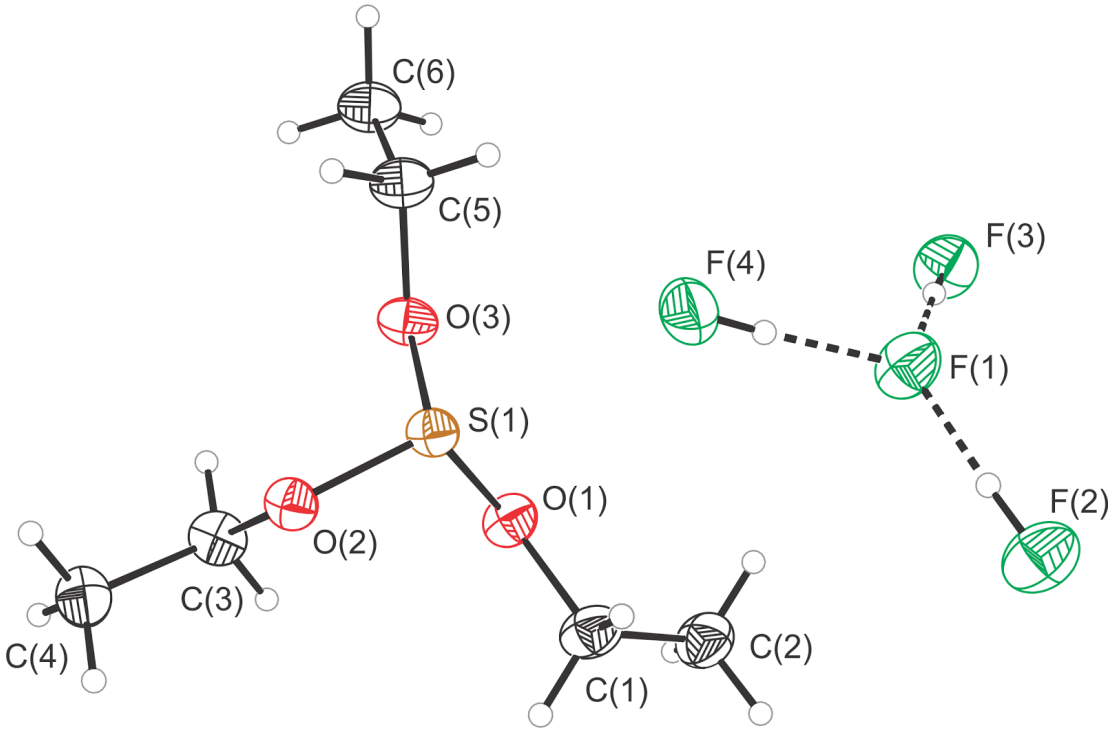

Figure 3.15 - Thermal ellipsoid plot of $[S(OC_2H_5)_3][H_3F_4]$; Thermal ellipsoids are drawn to 50% probability.

Table 3.9 - Selected bond distances and angles for the crystal structure of $[S(OC_2H_5)_3][H_3F_4]$

Atoms	Distance (Å)	Atoms	Distance (Å)
S(1)–O(1)	1.5626(16)	F(1)---H–F(2)	2.391(2)
S(1)–O(2)	1.5545(16)	F(1)---H–F(3)	2.389(2)
S(1)–O(3)	1.5587(16)	F(1)---H–F(4)	2.362(2)
O(1)–C(1)	1.492(3)	O(2)–C(3)	1.500(3)
O(3)–C(5)	1.494(3)		
Atoms	**Angle (°)**	**Atoms**	**Angle (°)**
O(1)–S(1)–O(2)	104.84(9)	F(2)–F(1)–F(3)	125.35(9)
O(2)–S(1)–O(3)	104.56(9)	F(3)–F(1)–F(4)	112.97(9)
O(3)–S(1)–O(1)	95.29(9)	F(4)–F(1)–F(2)	119.98(9)
S(1)–O(1)–C(1)	115.49(14)	O(1)–C(1)–C(2)	106.79(19)
S(1)–O(2)–C(3)	121.45(13)	O(2)–C(3)–C(4)	106.88(17)
S(1)–O(3)–C(5)	114.85(13)	O(3)–C(5)–C(6)	106.20(18)

Table 3.10 - Crystal data collection parameters and results of the crystal structure of $[S(OC_2H_5)_3][H_3F_4]$.

Parameter	Value
Identification code	MG17007_1
Empirical formula	$C_6H_{18}F_4O_3S$
Formula weight (g mol^{-1})	246.26
Temperature (K)	100.00(19)
Crystal system	triclinic
Space group	*P-1*
Unit cell dimensions (Å / °)	a = 8.3199(7) α = 63.394(8) b = 8.9895(7) β = 86.735(7) c = 9.5917(8) γ = 72.510(8)
Volume ($Å^3$)	609.22(10)
Z	2
ρ_{calc}g cm^{-3}	1.342
μ (mm^{-1})	2.766
F(000)	260.0
Crystal size (mm^3)	0.2 × 0.18 × 0.16
Radiation	CuKα (λ = 1.54184)
2Θ range for data collection (°)	10.358 to 159.666
Index ranges	$-9 \leq h \leq 10$, $-11 \leq k \leq 11$, $-10 \leq l \leq 12$
Reflections collected	13241
Independent reflections	2625 [R_{int} = 0.0807, R_{sigma} = 0.0468]
Data/restraints/parameters	2625/0/143
Goodness-of-fit on F^2	1.104
Final R indexes[a] I>=2σ (I)	R_1 = 0.0486 wR_2 = 0.1299
Largest diff. peak/hole (e $Å^{-3}$)	0.52/-0.48

[a] $R_1 = \Sigma||F_o| - |F_c||/\Sigma|F_o|$ and $wR_2 = [\Sigma w(F_o^2 - F_c^2)^2/\Sigma w(F_o^4)]^{1/2}$

Other instances of trisalkoxysulfonium compounds exist in literature, such as $[S(OCH_3)_3]^+$,[27] and $[S(OCH(CF_3)_2)_3]^+$,[28] and $[S(OCH_2CF_3)_3]^+$ in patent literature.[29]

None of these trisalkoxysulfonium compounds were characterized by X-ray crystallography. The $[S(OC_2H_5)_3]^+$ cation adopts a trigonal pyramidal structure about the sulfur centre with S–O distances of 1.5626(16), 1.5545(16), and 1.5587(16) Å. The O–S–O angles between ethoxy groups are 104.84(9), 104.56(9), and 95.29(9)°. Two of the ethoxy groups have similar S–O–C–C dihedral angles at 175.70(16) and 176.34(15)°, while the third has a lower dihedral angle of 145.26(17)° that causes the cation to lose its 3-fold symmetry about the sulfur centre. This difference in S–O–C–C means one of the ethoxy groups is pointed downward compared to the other two groups.

The geometry of $[S(OC_2H_5)_3]^+$ can be compared to that of $[SF_3]^+$ that also adopts a trigonal pyramidal structure (see Table 3.11). The O–S–O angles of $[S(OC_2H_5)_3]^+$ are larger than the F–S–F angles of $[SF_3]^+$ meaning the sulfur centre of $[S(OC_2H_5)_3]^+$ sits closer to the O–O–O plane, making it less pyramidal. This could be due to the extra steric bulk caused by the size of the ethoxy groups compared to fluoro substituents and the longer S–O bond length compared to the S–F bonds of $[SF_3]^+$.

Table 3.11 - Comparison of some sulfur-centre bond angle and distances of $[S(OC_2H_5)_3][H_3F_4]$ and $[SF_3][BF_4]$ from literature.

	$[SF_3]^+$ [a]	$[S(OC_2H_5)_3]^+$
Bond distance, Å		
S–F[30]	1.499/1.495/1.495	
S–O		1.5626(16)/1.5545(16)/1.5587(16)
Bond Angle		
F–S–F[22]	97.4/97.6/97.4	
O–S–O		104.84(9)/104.56(9)/95.29(9)

[a]M.-J. Boinon, G. Coffy, A. Tranquard, *Bull. Soc. Chim. Fr.* **1975**, *11-12 (pt.1)*, 2380–2382.

3.4 Crystal Structure of $Me_3SiC_2F_5$

The reaction between SF_4 and $Me_3SiC_2F_5$ forming pentafluoroethyl derivatives of SF_4 is fast at room temperature, while it remains slow at low temperature. In an FEP reactor, $Me_3SiC_2F_5$ was dissolved in an excess of SF_4, followed by the addition of a catalytic amount of pyridine. In order to avoid overpressurization of the reactor, it was kept at approximately –80 °C while mixing occurred. The mixture was evacuated by dynamic vacuum using a glass vacuum line at –100 °C, and clear colourless crystals of $Me_3SiC_2F_5$ formed. Due to the low temperature, pyridine (melting point: –35 °C) presumably remained solid, preventing proper mixing and bulk activation of $Me_3SiC_2F_5$. Crystals of $Me_3SiC_2F_5$ were harvested from the contents of this reactor and the crystal structure of $Me_3SiC_2F_5$ is shown in Figure 3.16 with bond angles and distances shown in Table 3.12. Crystal structure parameters are shown in Table 3.13.

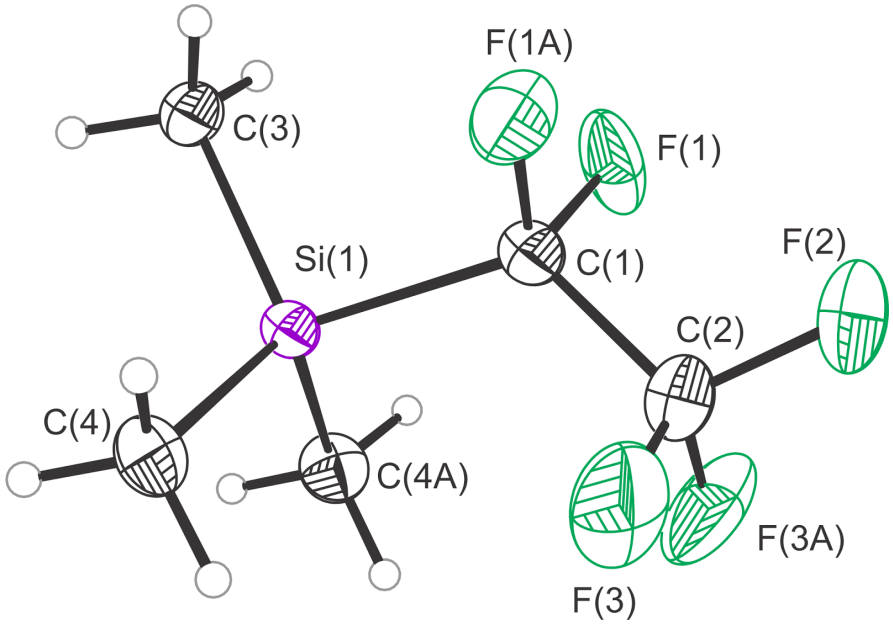

Figure 3.16 - Thermal ellipsoid plot of $Me_3SiC_2F_5$; thermal ellipsoids are drawn to 50% probability. Disorder of the $C(3)H_3$ protons is omitted.

Table 3.12 - Selected bond distances and angles for the crystal structure of $Me_3SiC_2F_5$

Atoms	Distance (Å)	Atoms	Distance (Å)
C(1)–F(1)	1.370(3)	Si(1)–C(1)	1.953(5)
C(2)–F(2)	1.328(7)	Si(1)–C(3)	1.861(5)
C(2)–F(3)	1.318(4)	Si(1)–C(4)	1.856(3)
C(1)–C(2)	1.518(7)		
Atoms	**Angle (°)**	**Atoms**	**Angle (°)**
F(1)–C(1)–F(1A)	105.0(4)	C(3)–Si(1)–C(1)	102.0(2)
Si(1)–C(1)–C(2)	121.2(4)	C(4)–Si(1)–C(1)	107.68(14)
F(2)–C(2)–F(3)	107.3(3)	C(3)–Si(1)–C(4)	113.08(13)

Trimethylpentafluoroethyl silane crystallizes in the *Cmc2₁* space group. The $Me_3SiC_2F_5$ molecule is bisected by a mirror plane perpendicular to the c-axis coplanar to C(3)–Si(1)–C(1)–C(2)–F(2). For this reason, the asymmetric unit contains half of a molecule, and causes slight rotational disorder of the $C(3)H_3$ group. The Si–C–C angle of the pentafluoroethyl group is 121.2(4)°, showing that the $–CF_3$ group is pushed away by the sterically large $–Si(CH_3)_3$ moiety. The Si(1)–C(1) bond linking the pentafluoroethyl group is 1.953(5) Å.

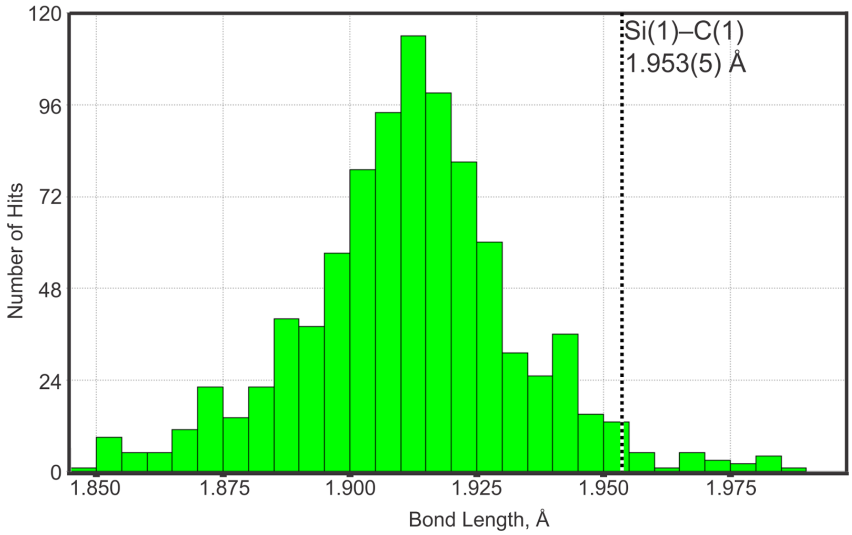

Figure 3.17 - *Mogul* histogram of Si–C bond lengths of 961 systems comparable to $Me_3SiC_2F_5$. The Si(1)–C(1) crystal structure bond length is shown by a dashed line at a z-score of 1.947.

The Si–C bond length is shown as a dashed line in Figure 3.17, a histogram of relevant Cambridge Structural Database structures produced using *Mogul 1.7.2*. The Si(1)–C(1) bond is reasonably within the distribution of usual bond lengths with a z-score of 1.947, measuring the absolute difference between the mean and the measured bond distance (Equation 3.6).

$$\frac{\left|r_{C-Si} - \overline{r_{C-Si}}\right|}{\sigma_{C-Si}} \qquad (3.6)$$

The Si(1)–C(1) bond is significantly longer than the mean length of 1.912 Å, likely due to the steric effects of the $Si(CH_3)_3$ group. This is consistent with the reactivity of $Me_3SiC_2F_5$ as a pentafluoroethyl transfer reagent since electron donation to the silicon center by some activator would extend this bond. The high-pressure-freezing crystal structure of Me_3SiCF_3, the Ruppert-Prakash reagent, features a Si–C bond length of 1.943(12) Å.[31] This bond is shorter than the analogous bond distance in $Me_3SiC_2F_5$ due to the increased steric bulk of the $–C_2F_5$ group compared to $–CF_3$.

Table 3.13 - Crystal data collection parameters and results of the crystal structure of $[S(OC_2H_5)_3][H_3F_4]$

Parameter	Value
Identification code	MG16033
Empirical formula	$C_5H_9F_5Si$
Formula weight (g mol^{-1})	215.35
Temperature (K)	100.00(19)
Crystal system	orthorhombic
Space group	$Cmc2_1$
Unit cell dimensions (Å / °)	a = 9.72944(18) α = 90 b = 8.10011(16) β = 90 c = 10.9645(2) γ = 90
Volume ($Å^3$)	864.11(3)
Z	4
ρ_{calc}g cm^{-3}	1.655
μ (mm^{-1})	4.572
F(000)	415.0
Crystal size (mm^3)	0.2 × 0.18 × 0.16
Radiation	CuKα (λ = 1.54184)
2Θ range for data collection (°)	14.228 to 158.37
Index ranges	$-12 \leq h \leq 12$, $-10 \leq k \leq 8$, $-13 \leq l \leq 13$
Reflections collected	4698
Independent reflections	965 [R_{int} = 0.0566, R_{sigma} = 0.0356]
Data/restraints/parameters	965/1/60
Goodness-of-fit on F^2	1.119
Final R indexes[a] I>=2σ (I)	R_1 = 0.0368 wR_2 = 0.0995
Largest diff. peak/hole (e $Å^{-3}$)	0.27/-0.25
Flack parameter	-0.01(4)

[a] $R_1 = \Sigma||F_o| - |F_c||/\Sigma|F_o|$ and $wR_2 = [\Sigma w(F_o^2 - F_c^2)^2/\Sigma w(F_o^4)]^{1/2}$

3.5 Summary and Conclusion

An alternative and convenient method for the synthesis of $SF_3C_2F_5$ and $SF_2(C_2F_5)_2$ is presented using SF_4 as a substrate for pentafluoroethyl transfer by $Me_3SiC_2F_5$ using some base as activator. By using different activators for $Me_3SiC_2F_5$, such as fluoride, pyridine, or other nitrogen bases, different product distributions and purities are achieved. The reaction occurs at or below room temperature and the use of excess SF_4 as solvent causes the reaction to favour the formation of $SF_3C_2F_5$. Upon separation from donor species, high-resolution ^{19}F NMR spectra were acquired showing multiplets with significant second-order character and long-range coupling. A simulated spin system was presented for the $SF_2(C_2F_5)_2$ species that shows excellent agreement with experimental spectra. Both compounds studied were modelled using B3LYP/aug-cc-pVTZ and minimum-energy geometries were presented. The crystal structure of $[S(OC_2H_5)_3][H_3F_4]$ was presented, being only the fourth reported trisalkoxysulfonium compounds and one of 11 salts observed containing the $[H_3F_4]^-$ anion and one of three crystal structures of such salt obtained. Additionally, the crystal structure of the $Me_3SiC_2F_5$ reagent was acquired for the first time.

References

[1] D. T. Sauer, J. M. Shreeve, *J. Fluorine Chem.* **1971**, *1*, 1–11.

[2] D. Viets, E. Lork, R. Mews, U. Behrens, *Z. Anorg. Allg. Chem.* **1997**, *623*, 1892–1896.

[3] K. O. Christe, W. W. Wilson, *J. Fluorine Chem.* **1990**, *47*, 117–120.

[4] M. Wiesemann, J. Klösener, M. Niemann, B. Neumann, H.-G. Stammler, B. Hoge, *Chem. - Eur. J.* **2017**, *23,* 14476–14484.

[5] S. Solyntjes, J. Bader, B. Neumann, H.-G. Stammler, N. Ignat'ev, B. Hoge, *Chem. - Eur. J.* **2017**, *23*, 1557–1567.

[6] N. Schwarze, B. Kurscheid, S. Steinhauer, B. Neumann, H.-G. Stammler, N. Ignat'ev, B. Hoge, *Chem. - Eur. J.* **2016**, *22*, 17460–17467.

[7] N. Schwarze, S. Steinhauer, B. Neumann, H.-G. Stammler, B. Hoge, *Angew. Chem. Int. Ed Engl.* **2016**, *55*, 16156–16160.

[8] B. Hoge, S. Pelzer, B. Neumann, H.-G. Stammler, N. Ignat'ev, R. Eujen, *Synthesis* **2017**, *49*, 2389–2393.

[9] S. Steinhauer, J. Bader, H.-G. Stammler, N. Ignat'ev, B. Hoge, *Angew. Chem. Int. Ed Engl.* **2014**, *53*, 5206–5209.

[10] S. Pelzer, B. Neumann, H.-G. Stammler, N. Ignat'ev, B. Hoge, *Chem. - Eur. J.* **2016**, *22*, 4758–4763.

[11] S. A. Hayes, R. J. F. Berger, B. Neumann, N. W. Mitzel, J. Bader, B. Hoge, *Dalton Trans.* **2010**, *39*, 5630-5636.

[12] S. Steinhauer, H.-G. Stammler, B. Neumann, N. Ignat'ev, B. Hoge, *Angew. Chem. Int. Ed.* **2013**, *53*, 562–564.

[13] K. G. Sharp, K. L. Servis, *J. Magn. Reson.* **1977**, *28*, 295–297.

[14] D. F. Evans, S. L. Manatt, D. D. Elleman, *J. Am. Chem. Soc.* **1963**, *85*, 238–239.

[15] J. W. Emsley, L. Phillips, V. Wray, *Prog. Nucl. Magn. Reson. Spectrosc.* **1976**, *10*, 83–752.

[16] T. Bunič, M. Tramšek, E. Goreshnik, B. Žemva, *Solid State Sci.* **2006**, *8*, 927–931.

[17] A. R. Mahjoub, D. Leopold, K. Seppelt, *Eur. J. Solid State Inorg. Chem.* **1992**, *29*, 635–647.

[18] A. A. Opalovskii, T. D. Fedotova, *Izv. Sib. Otd. Akad. Nauk SSSR, Ser. Khim. Nauk*

1967, 50–55.

[19] T. L. Higgins, E. F. Westrum, *J. Phys. Chem.* **1961**, *65*, 830–836.

[20] H. J. Thomas, A. W. Jache, *J. Inorg. Nucl. Chem.* **1960**, *13*, 54–57.

[21] J. S. Morrison, A. W. Jache, *J. Am. Chem. Soc.* **1959**, *81*, 1821–1823.

[22] M.-J. Boinon, G. Coffy, A. Tranquard, *Bull. Soc. Chim. Fr.* **1975**, *11-12 (pt.1)*, 2380–2382.

[23] I. G. Shenderovich, P. M. Tolstoy, N. S. Golubev, S. N. Smirnov, G. S. Denisov, H.-H. Limbach, *J. Am. Chem. Soc.* **2003**, *125*, 11710–11720.

[24] D. D. Ikrami, *Izv. Akad. Nauk Tadzh. SSR, Otd. Fiz.-Mat. Geol.-Khim. Nauk* **1971**, 40–46.

[25] D. Mootz, D. Boenigk, *J. Am. Chem. Soc.* **1986**, *108*, 6634–6636.

[26] M. Tramšek, E. Goreshnik, M. Lozinšek, B. Žemva, *J. Fluorine Chem.* **2009**, *130*, 1093–1098.

[27] H. Minato, K. Yamaguchi, M. Kobayashi, *Chem. Lett.* **1975**, *4*, 307–310.

[28] H. Hacklin, G.-V. Roeschenthaler, *Chem.-Ztg.* **1984**, *108*, 291.

[29] A. Palomo Coll, *Improvements in the Object of Patent 9,102,594 for a Process for the Preparation of Pyridine Derivatives* **1994**, ES 2058027.

[30] D. D. Gibler, C. J. Adams, M. Fischer, A. Zalkin, N. Bartlett, *Inorg. Chem.* **1972**, *11*, 2325–2329.

[31] A. Olejniczak, K. Andrzej, V. Ashwani, *J. Fluorine Chem.* **2008**, *129*, 1090–1095.

4. Pentafluoroethyl Derivatives of SOF_2

4.1 Introduction

In their 1968 study, Ratcliffe and Shreeve synthesized $SOFC_2F_5$ by the reaction between SOF_2 and C_2F_4 at high temperature and pressure (150–180 °C and 18–20 atm) in the presence of CsF.[1] The product was isolated by fractional distillation and vapour phase chromatography in good yield (*ca.* 80%). Compared to the analogous reaction using the SF_4 substrate (see Chapter 3), this reaction proceeds more predictably and with higher yields likely due to the stability of products at 150 °C (the temperature this reaction proceeds). Some disproportionation of $SOFC_2F_5$ was noted to $C_2F_5SSC_2F_5$ and $SO_2FC_2F_5$, but no evidence for the expected FSC_2F_5 intermediate was found. The ^{19}F NMR analysis of $SOFC_2F_5$ was subsequently reported in a 1973 by Shreeve and DeMarco as an $AMNX_3$ spin system.[2]

A 1971 study by Shreeve and Sauer reported the synthesis of $SF_2(C_2F_5)_2$ and $SF_3C_2F_5$ (discussed in detail in Chapter 3). The latter was shown to hydrolyse to $SOFC_2F_5$.[3] While bis(pentafluoroethyl)sulfur difluoride does not react with water vapour at room temperature, hydrolysis can be achieved using HCl to form $SO(C_2F_5)_2$. Shreeve and Sauer noted that the ^{19}F NMR spectrum is complicated by magnetic inequivalence of the difluoromethylene nuclei.

4.2 Results and Discussion

4.2.1 Synthesis

Pentafluoroethylsulfinyl fluoride, $SOFC_2F_5$, and bis(pentafluoroethyl) sulfoxide, $SO(C_2F_5)_2$, were synthesized by the reaction of $Me_3SiC_2F_5$ with SOF_2 using an activator base such as NC_5H_5 (Equation 4.1).

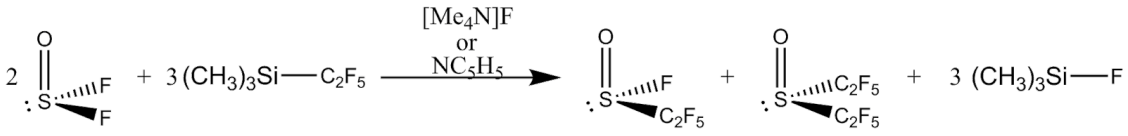

(4.1)

At room temperature, the reaction proceeded very quickly and the two products were formed in admixture if a molar deficiency of SOF_2 was used. First, SOF_2 is mixed with $Me_3SiC_2F_5$ in the desired ratios; the two species do not react at room temperature without an activator present. Upon addition of small quantities of pyridine (~1:12 mole ratio between pyridine and $Me_3SiC_2F_5$), the reaction proceeded rapidly at room temperature. The reaction can also be performed at –45 °C, which is below the boiling point of SOF_2 (boiling point *ca.* –44 °C), allowing the use of excess SOF_2. In SOF_2 solvent, the product distribution can favor the formation of $SOFC_2F_5$, forming only trace amounts of $SO(C_2F_5)_2$. If pyridine is used as solvent, the reaction proceeds normally but develops a yellow colour caused by an uncharacterized oil that does not have an appreciable vapour pressure at room temperature. By using excess pyridine as solvent, $SOFC_2F_5$ and $SO(C_2F_5)_2$ can be separated from the reaction mixture at –50 °C by condensation into a U-trap at –196°C under dynamic vacuum. With pyridine as the solvent, however, C_2F_5H was observed by ^{19}F NMR spectroscopy, indicating some reaction causing the protonation

of the pentafluoroethyl group of $[Me_3Si(F)C_2F_5]^-$ or by decomposition of $Me_3SiC_2F_5 \bullet NC_5H_5$. The latter species is expected to be unstable due to the polarized Si–C_f bond caused by pyridine coordination. Attempts to isolate $SO(C_2F_5)_2$ were unsuccessful, although crystallization followed by filtration at low temperature may allow $SO(C_2F_5)_2$ to be separated from the reaction mixture. The formation of $SO(C_2F_5)_2$ can be favoured by using excess $Me_3SiC_2F_5$ with respect to SOF_2 substrate, although $SOFC_2F_5$ is also formed in the reaction in small quantities.

Pentafluoroethylsulfinyl fluoride and bis(pentafluoroethyl) sulfoxide are formed by the reaction between SF_4 and $Me_3SiC_2F_5$ (discussed in Chapter 3), partially due to the presence of SOF_2 as an impurity in SF_4, formed by the hydrolysis shown in Equation 4.2.

$$SF_4 + H_2O \longrightarrow SOF_2 + 2\,HF \qquad (4.2)$$

Some $SOFC_2F_5$ also originates from the production of $SF_3C_2F_5$ that can be hydrolysed by trace amounts of moisture introduced to the reaction vessel.[3] Small amounts of $SOFC_2F_5$ were detected by ^{19}F NMR spectroscopy for the reaction between SF_4 and LiC_2F_5 in Et_2O, discussed and shown in Chapter 3. It is unclear whether this product resulted from the reaction between SOF_2 and LiC_2F_5 or the hydrolysis of $SF_3C_2F_5$. It is likely that hydrolysis is the dominant source since some $SO(C_2F_5)_2$ would be expected if LiC_2F_5 was reacting with SOF_2. Bis(pentafluoroethyl) sulfoxide was not observed in the reaction between SF_4 and LiC_2F_5, likely because $SF_2(C_2F_5)_2$ does not easily hydrolyse, requiring acidic solution to facilitate such a reaction.[3]

4.2.2 Pentafluoroethylsulfinyl Fluoride, $SOFC_2F_5$

4.2.2.1 Optimized Geometry

The geometry of $SOF(C_2F_5)$ was calculated using B3LYP/aug-cc-PVTZ generating a minimum-energy geometry shown in Figure 4.1.

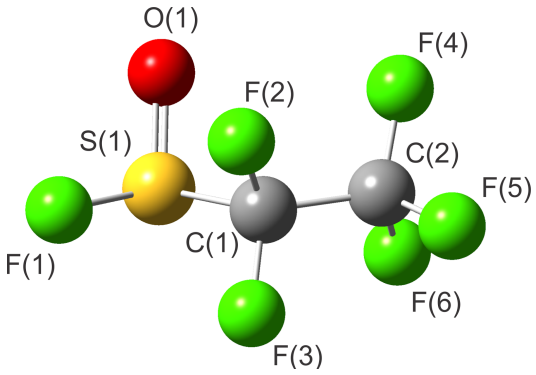

Figure 4.1 - Minimum-energy gas-phase geometry for $SOFC_2F_5$ calculated at the B3LYP/aug-cc-PVTZ Level of theory

Table 4.1 - Selected bond lengths and angles from the B3LYP/aug-cc-pVTZ optimized geometry of $SOFC_2F_5$.

Atoms	Distance (Å)	Atoms	Distance (Å)
S(1)–F(1)	1.639	C(1)–C(2)	1.548
S(1)–O(1)	1.456	C(1)–F(2)	1.334
S(1)–C(1)	1.944	C(1)–F(3)	1.345
Atoms	**Angle (°)**	**Atoms**	**Angle (°)**
F(1)–S(1)–O(1)	107.8	S(1)–C(1)–C(2)	111.8
F(1)–S(1)–C(1)	90.0	O(1)–S(1)–C(1)–C(2)	69.2
F(2)–C(1)–F(3)	109.9	F(1)–S(1)–C(1)–C(2)	177.7
O(1)–S(1)–C(1)	105.7		

Selected bond angles and distances from the calculated geometry are presented in Table 4.1. The sulfur centre of $SOFC_2F_5$ adopts a trigonal pyramidal geometry with bonds to fluorine (1.639 Å), oxygen (1.456 Å), and the carbon of a pentafluoroethyl group (1.944 Å). The pentafluoroethyl group adopts a conformation with a F(1)–S(1)–C(1)–C(2)

dihedral angle of 177.7°. This conformation minimizes the steric crowding around the sulfur atom that is exacerbated by the S=O double bond (1.456 Å). A comparison of the gas-phase geometries of SOF_2 and $SOFC_2F_5$ optimized at the same level of theory is shown in Table 4.2. Angles between sulfur-bound groups are not changed substantially by pentafluoroethyl substitution. Compared to thionyl fluoride, $SOFC_2F_5$ has longer predicted S=O and S–F bond lengths due to the smaller electronegativity of the pentafluoroethyl group compared to the fluoro group. This has also been found for the SF_4 derivatives discussed in Chapter 3, with predicted S–F distances of $SF_3C_2F_5$ and $SF_2(C_2F_5)_2$ being longer than those of SF_4.

Table 4.2 - Selected bond lengths and angles for the $SOFC_2F_5$ and SOF_2 gas-phase structures optimized using B3LYP/aug-cc-PVTZ.

	$SOFC_2F_5$	SOF_2
Bond Length (Å)		
S–F	1.639	1.618
S=O	1.456	1.433
S–C	1.944	
Bond Angle (°)		
F–S–O	107.8	106.4
F–S–F		93.0
F–S–C	90.0	
O–S–C	105.7	

4.2.2.2 Fluorine-19 NMR Spectroscopy of $SOFC_2F_5$

A ^{19}F NMR spectrum of the reaction mixture containing $SOFC_2F_5$ is shown in Figure 4.2 showing the reaction between $Me_3SiC_2F_5$ and SOF_2 after being separated by condensation at –50 °C. Pentafluoroethylsulfinyl fluoride is chiral about the sulfur centre

creating chemical inequivalence between the methylene fluorines, giving rise to an $AMNX_3$ spin system. The chemical shift difference between the CF_2 fluorine environments (–125.0 and –124.7 ppm) is small and second-order effects cause significant roofing that complicates the NMR spectroscopic characterization of this M/N region of the spectrum.

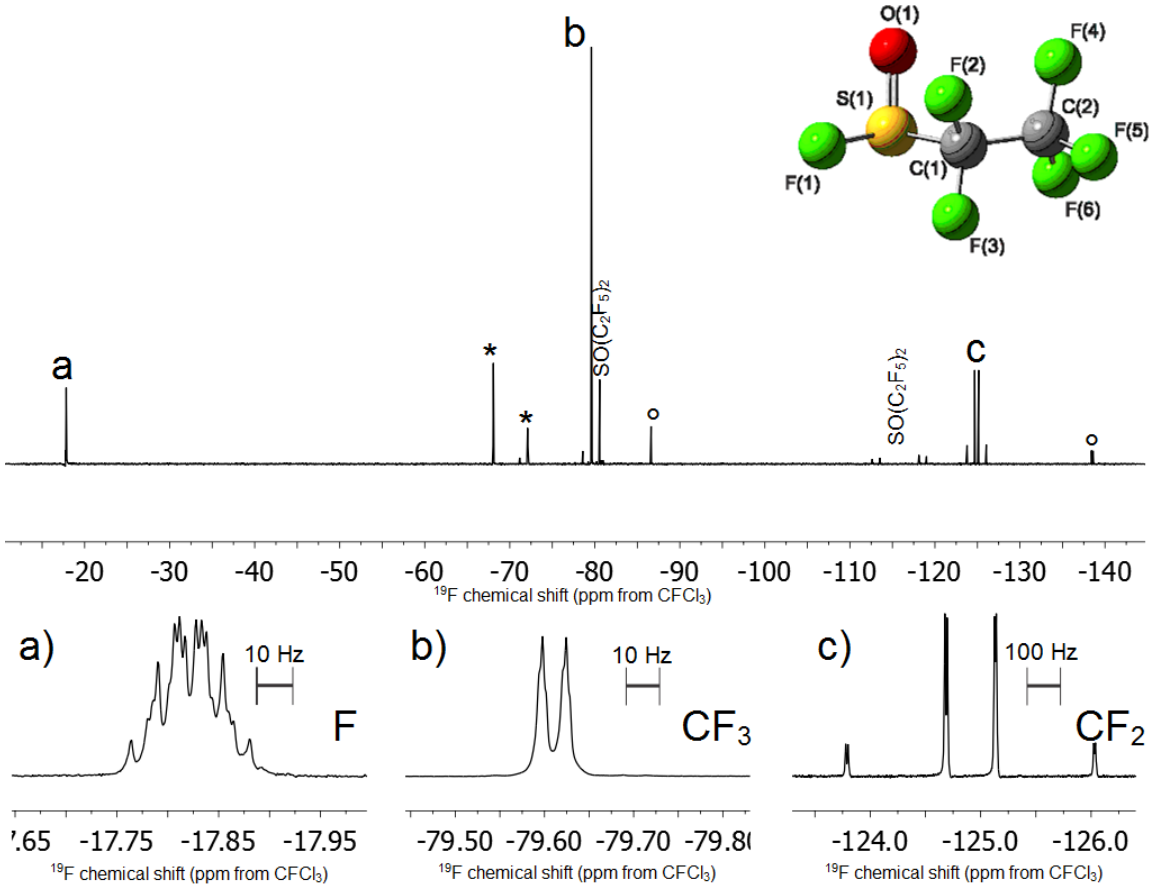

Figure 4.2 - Fluorine-19 NMR spectrum of the reaction between $Me_3SiC_2F_5$ and excess SOF_2 in NC_5H_5 after being separated and redissolved in $CFCl_3$ at room temperature. *denotes uncharacterized side-products and °denotes signals belonging to C_2F_5H.

Additional information is extracted from these multiplets by resolution enhancement using Gaussian multiplication (see Figure 4.3).

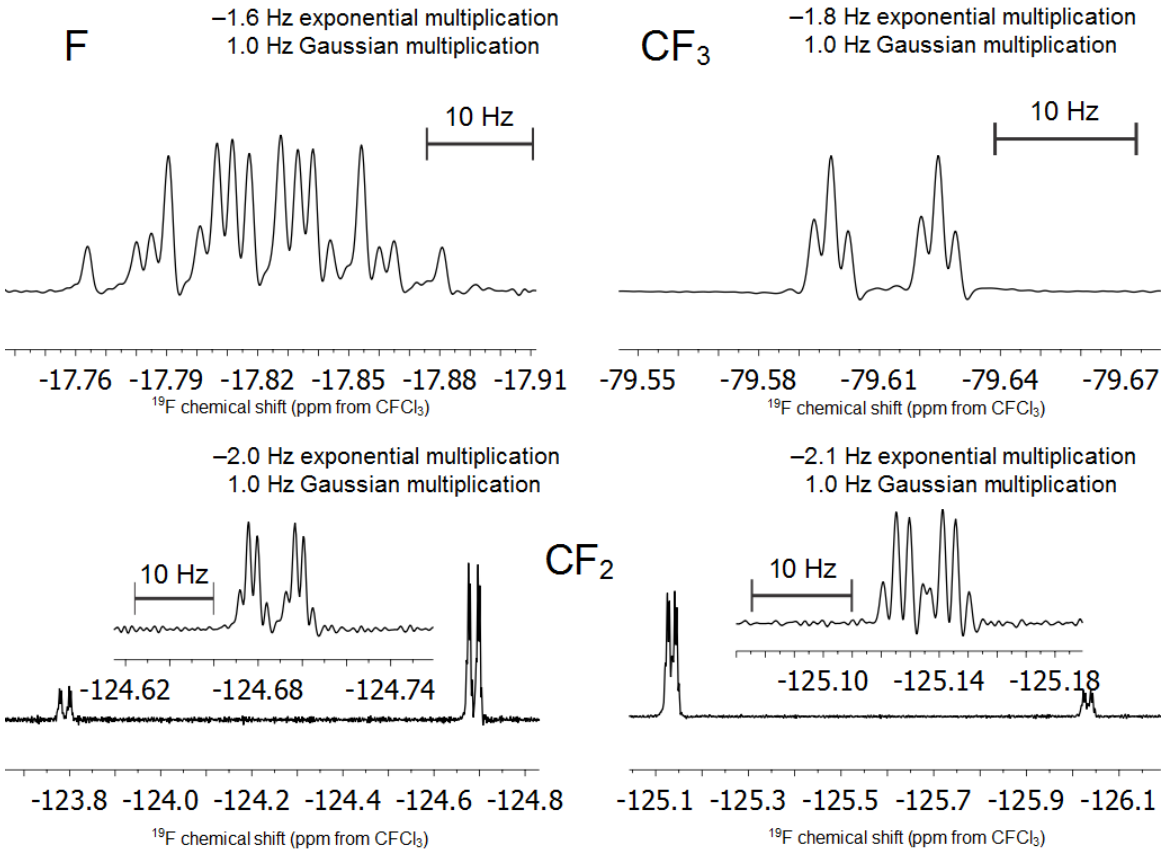

Figure 4.3 - Resolution enhanced ^{19}F NMR multiplets for $SOFC_2F_5$ by exponential and Gaussian multiplication.

Resolution enhancement reveals a pseudo-triplet splitting in the CF_3 signal (X_3) from $^3J_{X(M/N)}$. The two methylene fluorine signals are further split into quartets by $^3J_{X(M/N)}$. The M and N signals of the difluoromethylene moiety differ slightly due to the inequivalence of $^3J_{AN}$ and $^3J_{AM}$ (6.2 and 5.1 Hz, respectively). The second-order effect caused by the proximity of these two signals and the large $^2J_{NM}$ coupling causes the outermost transitions of the MN multiplet arising from the $^3J_{A(N/M)}$ splitting to become low intensity.

4.2.2.2.1 Spectral Simulation

The ^{19}F NMR spectrum of $SOFC_2F_5$ was simulated using SpinWorks and MestreNova achieving an excellent fit to experimental data, shown in Figure 4.4.

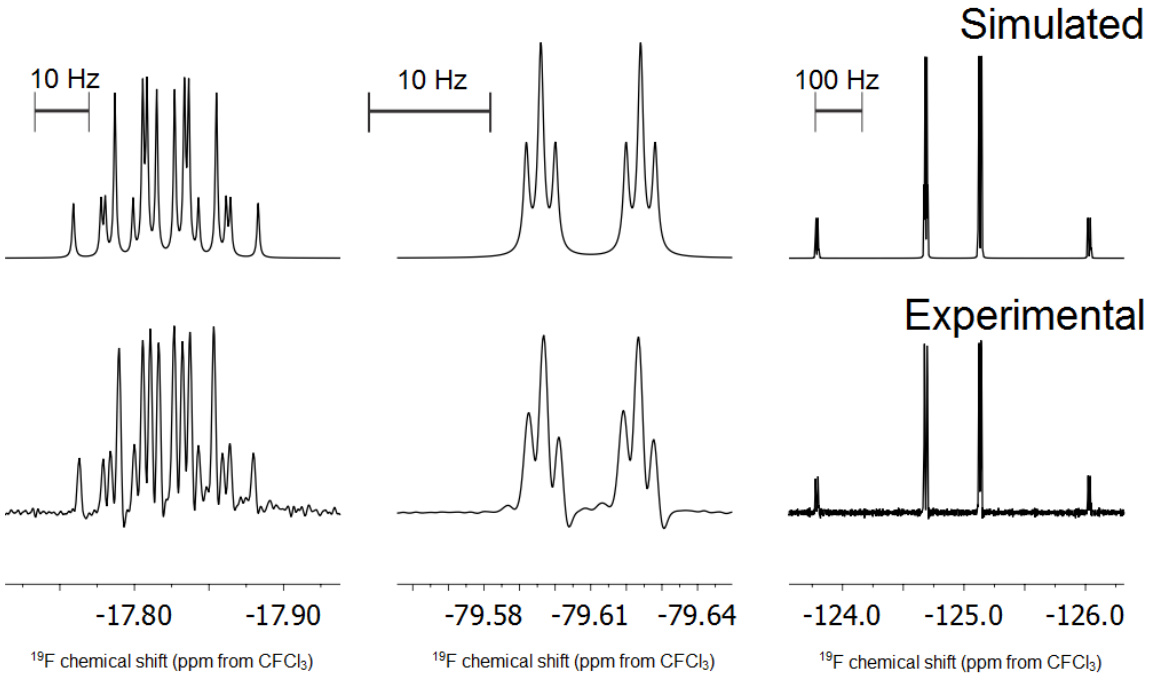

Figure 4.4 - Simulated and experimental ^{19}F NMR spectra for the multiplets of $SOFC_2F_5$. Experimental multiplets are resolution enhanced with –1.8 Hz exponential multiplication and 1 Hz Gaussian multiplication. Simulated multiplets were generated using MestreNova and optimized using Spinworks.

The spin system was confirmed to be $AMNX_3$ with two chemical shifts for methylene fluorines (Figure 4.5). The ^{19}F coupling constants and chemical shifts used in the final simulation are shown in Table 4.3 and are mostly different than the ones determined by DeMarco and Shreeve in their 1973 study.[2]

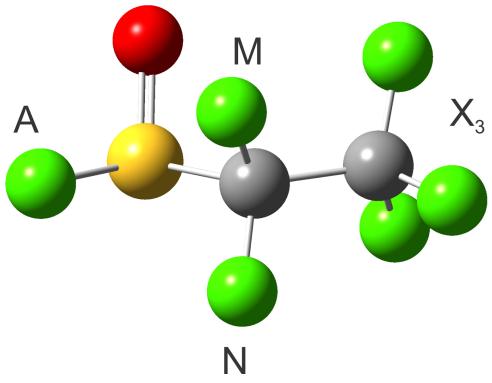

Figure 4.5 - Gas-phase structure of $SOFC_2F_5$ as calculated using B3LYP/aug-cc-PVTZ labelled with the $AMNX_3$ system used for the simulation herein.

Table 4.3 - Fluorine-19 NMR chemical shifts and coupling constants determined by simulation using *SpinWorks* and *MestreNova* for $SOFC_2F_5$ at room temperature in $CFCl_3$ including a comparison to those chemical shifts and coupling constants reported by DeMarco and Shreeve.

	Experimental	Literature[a]
^{19}F NMR chemical shift (ppm from $CFCl_3$)		
A	–17.8	–19.4
M	–124.4	–124.7
N	–125.4	–125.0
X_3	–79.6	–79.6
Coupling constants (Hz)		
$^3J_{AM}$	5.1	5.8
$^3J_{AN}$	6.2	5.8
$^2J_{MN}$	253.5	5.2
$^3J_{NX}$	1.1	1.1
$^3J_{MX}$	1.2	1.0
$^4J_{AX}$	7.9	7.7

[a]R. A. De Marco, J. M. Shreeve, *Inorg. Chem.* **1973**, *12*, 1896–1899.

The most dramatic difference is that of the geminal $^2J_{FF}$ coupling constant of the CF_2 group. DeMarco and Shreeve reported this coupling constant surprisingly small as 5.2 Hz while our work shows the coupling to be 253.5 Hz. This large difference in coupling

constants can be attributed to the low-field NMR spectrometer being used in their study (94.7 MHz) compared to those used in the present study (248 MHz and 658.97 MHz). A comparison of simulations following the coupling proposed by DeMarco and Shreeve, as well as those presented in this study, is shown in Figure 4.6 including simulations at varied magnetic field strength.

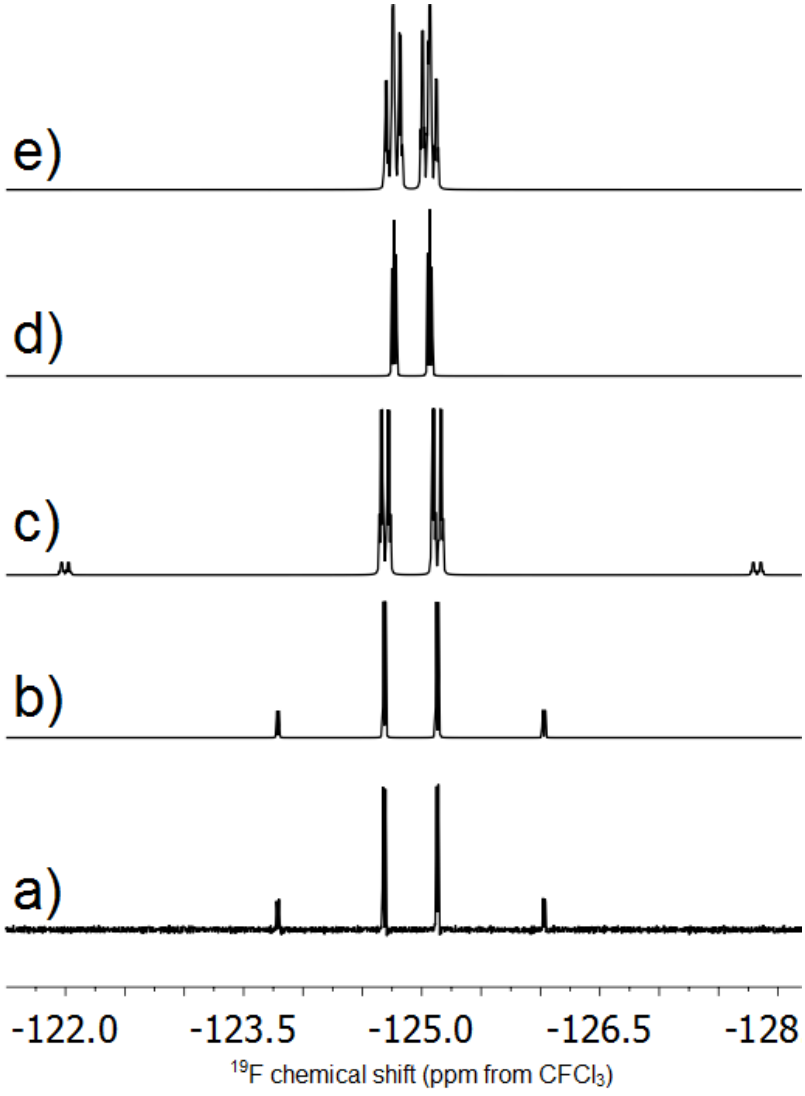

Figure 4.6 - Comparison of ^{19}F NMR spectra: **a)** experimental ^{19}F NMR spectrum of the reaction between $Me_3SiC_2F_5$ and SOF_2 in pyridine **b)** simulation presented in this work featured in Table 4.3 at 282.38 MHz field strength and **c)** this work's simulation at 94.1 MHz field strength **d)** simulation of the spin system presented by DeMarco and Shreeve[2] at 282.38 MHz **e)** DeMarco and Shreeve simulation at 94.1 MHz.

By simulating the spin system determined in this study at a lower magnetic field (Figure 4.6c), we observe the outermost doublets split by $^{3}J_{A(N/M)}$ of very low intensity and are spread to a far higher and lower ppm value than those in the simulation run at higher field, as a consequence of more severe second-order effects. With a low signal-to-noise ratio, these peaks could be lost in the baseline which would not allow the measurement of the $^{2}J_{MN}$ that we determined to be 253.5 Hz.

The sign of the geminal coupling constant, $^{2}J_{MN}$, is reported as positive; however, the multiplicity of the ^{19}F NMR signals does not seem to be sensitive to the sign of geminal coupling like those discussed in Chapter 3. The magnitudes of $^{3}J_{NX}$ and $^{3}J_{MX}$ are slightly different (1.1 and 1.2 Hz, respectively) as expected for this spin system along with the $^{3}J_{AM}$ and $^{3}J_{AN}$ coupling constants that are also slightly different (5.1 and 6.2, respectively).

4.2.3 Bis(pentafluoroethyl) Sulfoxide, $SO(C_2F_5)_2$

4.2.3.1 Optimized Geometry of $SO(C_2F_5)_2$

The minimum-energy gas-phase geometry of $SO(C_2F_5)_2$ was optimized using B3LYP/aug-cc-PVTZ to the model shown in Figure 4.7. Selected bond lengths and angles are reported in Table 4.4.

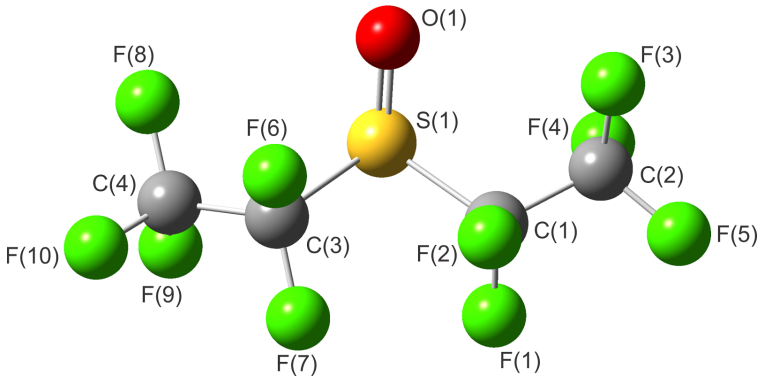

Figure 4.7 - Calculated gas-phase minimum geometry of $SO(C_2F_5)_2$ determined using B3LYP/aug-cc-PVTZ.

The model suggests the pentafluoroethyl groups are twisted to different C–S–C–C dihedral angles (158.8 and 165.3°). This C–S–C–C dihedral angle was predicted to be 180° in the computational geometry of $SF_2(C_2F_5)_2$ discussed in Section 3.2.3. The C–S–C angle of $SO(C_2F_5)_2$ is smaller (94.0°) compared that in $SF_2(C_2F_5)_2$ (101.6°), meaning the difluoromethylene groups of flanking pentafluoroethyl groups are drawn closer to each other in $SO(C_2F_5)_2$ causing this twisted conformation due to steric interactions. The F–C–F angles of both difluoromethylene groups are essentially the same on both pentafluoroethyl groups (109.8 and 110.2°). Additionally, the S–C–C angles of both pentafluoroethyl groups remain similar at 110.0 and 109.2° which are comparable to the analogous angle in $SOFC_2F_5$ (111.8°).

4.2.3.2 Crystal Structure of $SO(C_2F_5)_2$

Crystals of $SO(C_2F_5)_2$ were harvested from SF_4 solvent containing a mixture of primarily $SF_2(C_2F_5)_2$, $SF_3C_2F_5$, $SOFC_2F_5$, and $SO(C_2F_5)_2$. Cooling to –85 °C and condensing off volatiles by dynamic vacuum removed SF_4, and formed small colourless

rectangular prisms. These crystals were separated from other solid materials in an aluminium trough cooled by dry nitrogen to –85 °C (setup described in Chapter 2) and the crystal structure was obtained, shown in Figure 4.8. Selected bond lengths and angles are reported in Table 4.4 and crystal structure parameters in Table 4.5.

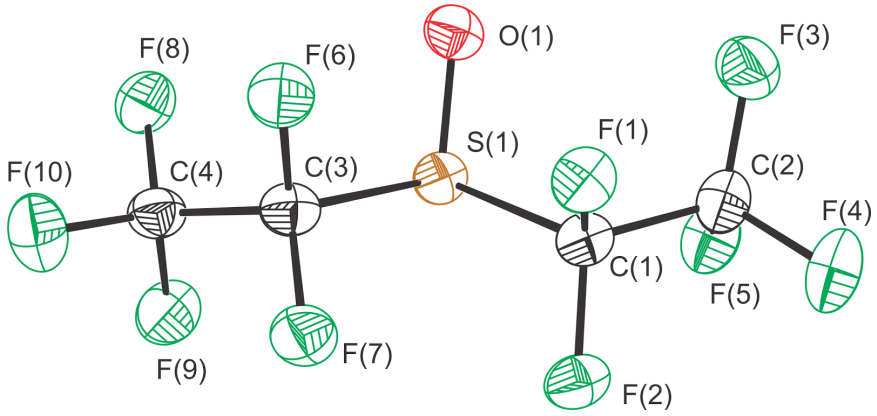

Figure 4.8 - Thermal ellipsoid plot of $SO(C_2F_5)_2$; thermal ellipsoids are drawn to 50% probability.

Bispentafluoroethyl sulfoxide crystallizes in the *P-1* space group with a dimeric motif containing weak S---O contacts at 3.0262(2) Å. This contact is below the sum of the van der Waals radii of sulfur and oxygen (3.32 Å),[4] shown in Figure 4.9. The dimerization of $SO(C_2F_5)_2$ is caused by the polar S–O bond and creates an energetically favored crystal packing. The unit cell of the presented crystal structure has been obtained multiple times while attempting to crystallize other compounds because the bispentafluoroethyl sulfoxide packs nicely in the solid state, likely as a consequence of the S---O contacts.

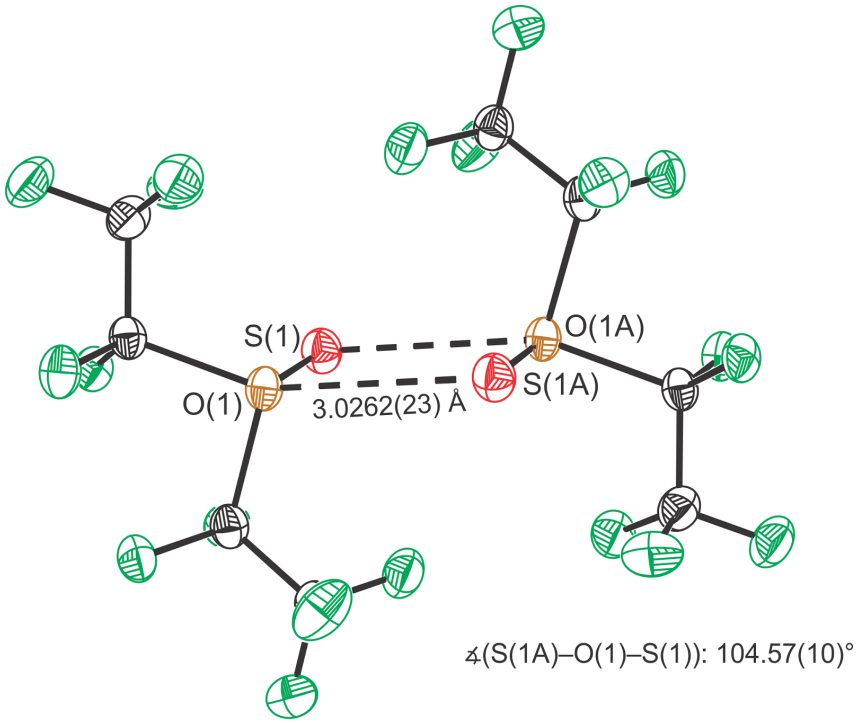

Figure 4.9 - Thermal ellipsoid plot showing the dimerization in the crystal structure $SO(C_2F_5)_2$; thermal ellipsoids are drawn to 50% probability.

The crystal structure of $SO(C_2F_5)_2$ adopts a similar geometry to the predicted gas-phase geometry at the B3LYP/aug-cc-PVTZ level of theory discussed in Section 4.2.3.1, Table 4.4 and Figure 4.10 compare some geometrical parameters between the experimental $SO(C_2F_5)_2$ crystal structure, SOF_2 gas-phase electron diffraction, and calculated geometries of $SO(C_2F_5)_2$ and SOF_2. The crystal structure of $SO(C_2F_5)_2$ has similarly twisted pentafluoroethyl groups predicted in the optimized gas-phase geometry, shown by C–S–C–C dihedral angles of 162.37(16) and 169.04(19)°, meaning the two pentafluoroethyl groups point in different directions with respect to the sulfur centre. The twisting of pentafluoroethyl groups is likely caused by crowding of the difluoromethylene

groups in close proximity to the sulfur centre. The angle between fluorines of SOF_2 (F–S–F: 92.2(3)°) is similar to the angle between carbons of $SO(C_2F_5)_2$ (C–S–C: 94.26(12)°), indicating that the geometry about the sulfur is not distorted greatly by pentafluoroethyl substitution. The S=O distances of $SO(C_2F_5)_2$ and SOF_2 are 1.470(2) and 1.420(3) Å, respectively, showing the small elongation of the S–O bond caused by pentafluoroethyl substituents being less electron-withdrawing than fluorine. The bond lengths of the optimized gas-phase model are expectedly longer than those measured in the crystal structure.

The crystal structures of $SOCl_2$ and $SOBr_2$ do not adopt dimeric motifs in the solid state, however, they do feature S---O contacts of 3.1761(11)/3.0915(10) and 3.18(1)/3.12(2) Å, respectively,[6] forming a layered chain-like structure. The crystal structure of dimethyl sulfoxide features no S---O contacts shorter than the sum of van der Waals radii.[7] This lack of oxygen to sulfur coordination is likely due to less electron-poor sulfur centre caused by electron-donating methyl groups. Sulfoxides with halogen substituents have a Lewis acidic sulfur centre that favours coordination. In the solid state, $SO(C_2F_5)_2$ adopts a dimeric structure likely because of a combination of electron withdrawing and the size of the pentafluoroethyl group substituents.

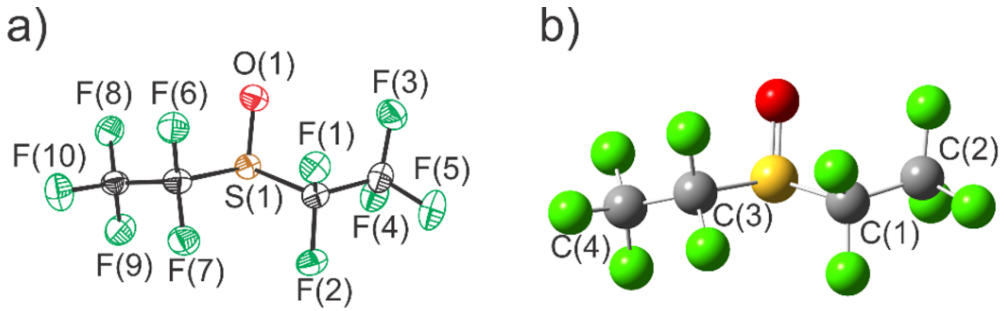

Figure 4.10 – a) Crystal structure of $SO(C_2F_5)_2$ thermal ellipsoid plot drawn at 50% probability and b)optimized gas-phase minimum geometry determined with B3LYP/aug-ccPVTZ geometry

Table 4.4 - Comparison of geometric parameters of $SO(C_2F_5)_2$, SOF_2 using B3LYP/aug-ccPVTZ optimized geometries, the crystal structure of $SO(C_2F_5)_2$ and the electron diffraction geometry of SOF_2

	$SO(C_2F_5)_2$		SOF_2	
Atoms	Crystal structure geometry	B3LYP/aug-ccPVTZ geometry	Electron diffraction geometry[5]	B3LYP/aug-ccPVTZ geometry
		Bond distance (Å)		
S=O	1.470(2)	1.482	1.420(3)	1.433
S–(C/F)	1.886(3)/1.913(3)	1.942/1.961	1.583(3)	1.618
C(1/3)–C(2/4)	1.546(4)/1.538(4)	1.556/1.551		
C(1)–F(1/2)	1.341(3)/1.340(3)	1.345/1.338		
C(2)–F(3/4/5)	1.318(4)/1.327(4)/1.328(4)	1.328/1.340/1.336		
C(3)–F(6/7)	1.340(3)/1.329(3)	1.332/1.343		
C(4)–F(8/9/10)	1.314(4)/1.325(3)/1.326(4)	1.334/1.338/1.334		
		Bond angle (°)		
O–S–R	105.43(12)/104.46(12)	107.5/105.4	106.2(2)	106.4
R–S–R	94.26(12)	94.0	92.2(3)	93.0
S–C–C	105.43(12)/109.6(2)	110.0/109.2		
F–C–F	109.2(2)/109.9(2)	109.8/110.2		
C(1/3)–S(1)–C(3/1)–C(4/2)	162.37(16)/169.04(19)	158.8/165.3		
O–S–C–C	62.8(2)/90.48(17)	57.7/91.7		

Table 4.5 - Crystal data collection parameters and results of the crystal structure of $SO(C_2F_5)_2$

Parameter	Value
Identification code	MG16017
Empirical formula	$C_4OF_{11}S$
Formula weight (g mol^{-1})	305.10
Temperature (K)	100.00(19)
Crystal system	triclinic
Space group	P-1
Unit cell dimensions (Å / °)	a = 4.9343(2) α = 62.377(3) b = 9.6146(3) β = 83.540(3) c = 10.1797(3) γ = 86.211(3)
Volume ($Å^3$)	425.12(3)
Z	2
ρ_{calc}g cm^{-3}	2.383
μ (mm^{-1})	5.227
F(000)	294.0
Crystal size (mm^3)	0.4 x 0.5 x 0.8
Radiation	CuKα (λ = 1.54178)
2Θ range for data collection (°)	9.848 to 155.298
Index ranges	$-6 \leq h \leq 6$, $-12 \leq k \leq 12$, $-12 \leq l \leq 12$
Reflections collected	8081
Independent reflections	1742 [$R_{int} = 0.0570$, $R_{sigma} = 0.0386$]
Data/restraints/parameters	1742/0/146
Goodness-of-fit on F^2	1.146
Final R indexes[a] I>=2σ (I)	$R_1 = 0.0407$ $wR_2 = 0.1141$
Largest diff. peak/hole (e $Å^{-3}$)	0.51/-0.49

[a] $R_1 = \Sigma||F_o| - |F_c||/\Sigma|F_o|$ and $wR_2 = [\Sigma w(F_o^2 - F_c^2)^2/\Sigma w(F_o^4)]^{½}$

4.2.3.3 Fluorine-19 NMR Spectroscopy of $SO(C_2F_5)_2$

Bispentafluoroethyl sulfoxide was observed by ^{19}F NMR spectroscopy in reactions between $Me_3SiC_2F_5$ and SOF_2 in the presence of pyridine, shown in Figure 4.11. If an excess of $Me_3SiC_2F_5$ is used, the reaction tends to favour $SO(C_2F_5)_2$ over $SOFC_2F_5$.

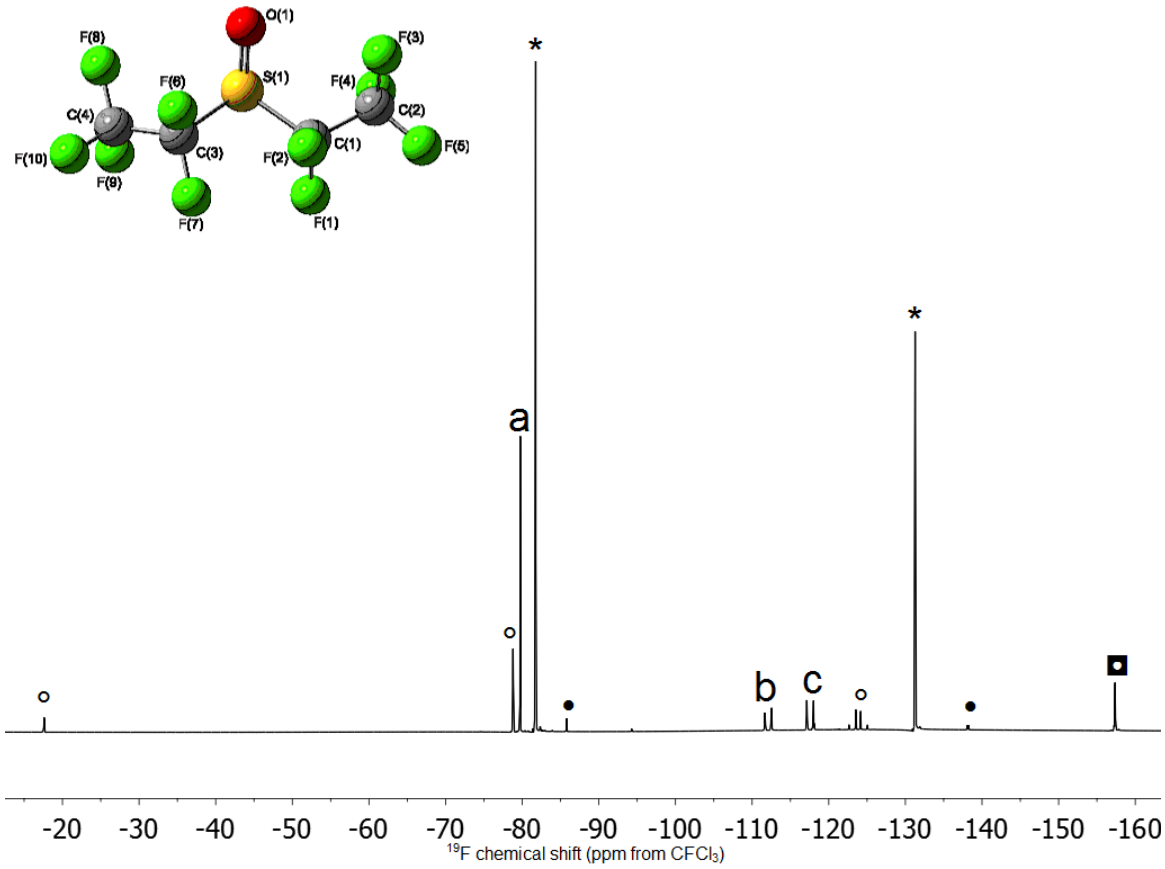

Figure 4.11 - Fluorine-19 NMR spectrum of the reaction between excess $Me_3SiC_2F_5$ and SOF_2 in NC_5H_5 after being condensed off at –50 °C and redissolved in $CFCl_3$ at room temperature. $^{abc}SO(C_2F_5)_2$; °$SOFC_2F_5$; *$Me_3SiC_2F_5$; ˙C_2F_5H; ▫Me_3SiF

The multiplicity of signals belonging to $SO(C_2F_5)_2$ is shown in Figure 4.12. Similar to $SOFC_2F_5$, the CF_2 groups exhibit magnetic and chemical inequivalence causing the molecule to exhibit an AA′BB′$X_3X'_3$ spin system as labelled in Figure 4.13.

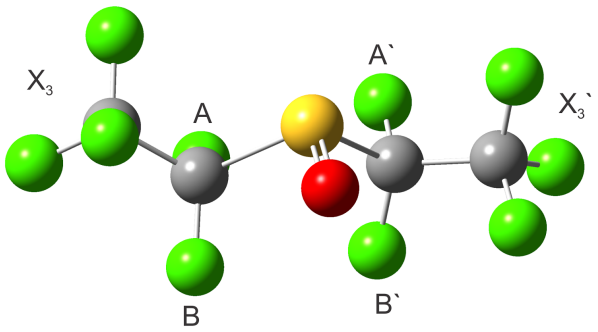

Figure 4.13 - Gas-phase geometry of $SO(C_2F_5)_2$ optimized using B3LYP/aug-cc-PVTZ labelled according to the preliminary $AA'BB'X_3X'_3$ spin system

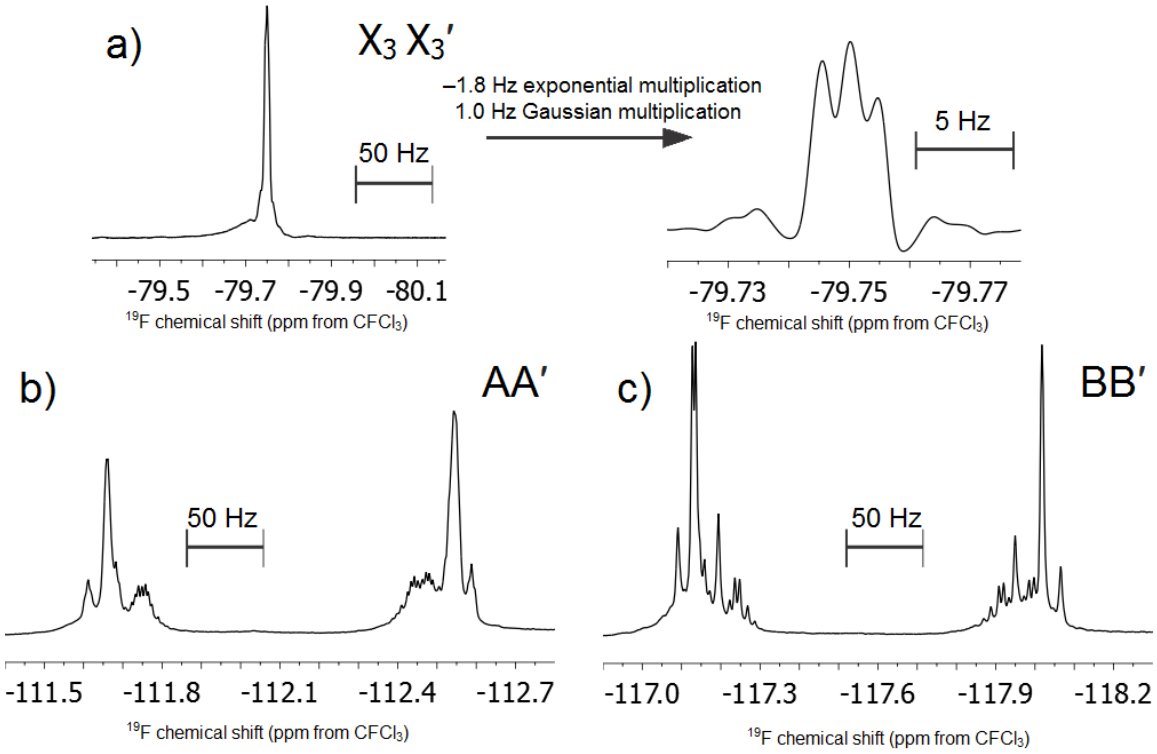

Figure 4.12 - Fluorine-19 NMR spectrum of $SO(C_2F_5)_2$ showing the $AA'BB'X_3X'_3$ spin system.

Resolution enhancement by Gaussian multiplication reveals a triplet splitting of the trifluoromethyl signal (–79.75 ppm) by 1.28 Hz presumably from $^3J_{X(A/B)}$. The CF_2 signals labelled A and B are distorted due to second-order effects caused by the proximity of

chemical shifts and strong $^2J_{AB}$ coupling similar to $SF_3C_2F_5$, $SF_2(C_2F_5)_2$, and $SOFC_2F_5$. Attempts to simulate difluoromethylene signals have yet to attain sufficient fit. Preliminary attempts treat the system as an AA′BB′ system that is complicated by additional coupling to the trifluoromethyl fluorines. The low-intensity features of the AA′BB′ multiplet are part of the signal, but a sufficient fit has not yet been achieved by spectral simulation.

4.3 Summary and Conclusion

Bispentafluoroethyl sulfoxide and pentafluoroethylsulfinyl fluoride were synthesized by the reaction between SOF_2 and $Me_3SiC_2F_5$. Pentafluoroethylsulfinyl fluoride was also synthesized in small quantities by the hydrolysis of $SF_3C_2F_5$ during the reaction of SF_4 and LiC_2F_5. Both products, $SO(C_2F_5)_2$ and $SOFC_2F_5$, were characterized by ^{19}F NMR spectroscopy and the spin system of $SOFC_2F_5$ was determined by spectral simulation. The determination of this spin system allows the correction of the geminal coupling constants that were previously reported.[2] The crystal structure of $SO(C_2F_5)_2$ was determined by crystallization from SF_4 solvent and adopts a dimeric structure, coordinating oxygen to sulfur at a distance of 3.026(2) Å. The geometry of $SO(C_2F_5)_2$ in the solid state is similar to the gas-phase geometry optimized at the B3LYP/aug-cc-PVTZ level of theory. Pentafluoroethylsulfinyl fluoride was also optimized by B3LYP/aug-cc-PVTZ to a minimum-energy geometry that is consistent with the spin-system determined by ^{19}F NMR spectroscopy.

References

[1] C. T. Ratcliffe, J. M. Shreeve, *J. Am. Chem. Soc.* **1968**, *90*, 5403–5408.

[2] R. A. De Marco, J. M. Shreeve, *Inorg. Chem.* **1973**, *12*, 1896–1899.

[3] D. T. Sauer, J. M. Shreeve, *J. Fluorine Chem.* **1971**, *1*, 1–11.

[4] A. Bondi, *J. Phys. Chem.* **1964**, *68*, 441–451.

[5] I. Hargittai, F. C. Mijlhoff, *J. Mol. Struct.* **1973**, *16*, 69–77.

[6] D. Mootz, A. Merschenz-Quack, *Acta Crystallogr., Sect. C: Cryst. Struct. Commun.* **1988**, *44*, 926–927.

[7] R. Thomas, C. B. Shoemaker, K. Eriks, *Acta Crystallogr.* **1966**, *21*, 12–20.

5 DABCO-SF_4 Lewis-Acid-Base System

5.1 Introduction

Sulfur tetrafluoride forms Lewis-acid-base adducts with nitrogen bases including triethylamine,[1] pyridine and pyridine derivatives.[2] The first Lewis-acid-base adduct containing SF_4 was claimed by Muetterties in his 1960 study of metal tetrafluoride reactions and some non-metal tetrafluorides with organic bases.[3] Upon reaction of SF_4 with Me_3N, Et_3N, and NC_5H_5, Muetterties observed ^{19}F NMR evidence for adduct formation and crude tensiometric results indicated a 1:1 adduct with pyridine and Et_3N. Studies by Gerken and coworkers conclusively characterized such adducts by X-ray crystallography, Raman spectroscopy, and DFT calculations.[1,2] The solvolysis of SF_4•NC_5H_5, SF_4•$NC_5H_4(CH_3)$, SF_4•$NC_5H_3(CH_3)_2$, and SF_4•$NC_5H_4N(CH_3)_2$ adducts by HF, generated by the hydrolysis of SF_4 using stoichiometric amounts of water, gave the salts $[HNC_5H_5]F$•SF_4, $[HNC_5H_5]F[HF]$•$2SF_4$, $[HNC_5H_4(CH_3)]F$•SF_4, $[NC_5H_4N(CH_3)_2][HF_2]$•$2SF_4$, $[NH_4C_5$–$C_5H_4NH]F$•$2SF_4$, $[HNH_4C_5$–$C_5H_4NH_2]2F$•$4SF_4$, $[HNC_5H_4N(CH_3)_2]_2F[SF_5]$•$CH_2Cl_2$, $[HNC_5H_4N(CH_3)_2]_2F[SF_5]$•$CH_2Cl_2$, and $[HNC_5H_3(CH_3)_2]_2F[SF_5]$•$nSF_4$ (n=1,4), which were characterized by X-ray crystallography and Raman spectroscopy.[4] Four of these structures are particularly interesting because they contain $[SF_5]^-$ anions. The pentafluorosulfate ion is formed when a sufficiently "naked" fluoride reacts with SF_4, first synthesized by Seppelt and coworkers in their 1988 study of $Rb[SF_5]$ and $Cs_6[SF_5]_4[HF_2]_2$.[5] Other salts containing $[SF_5]^-$ have been synthesized, including $[Cs(18\text{-crown-}6)][SF_5]$,[6] and $[(Me_2N)_3S][SF_5]$,[7] although structures containing this anion remain rare.

Diazabicyclo[2.2.2]octane (DABCO), $N_2(C_2H_4)_3$, is a simple bicyclic dibasic cage amine primarily used as catalyst and reagent in polymer applications.[8] Specifically, DABCO is used as catalyst in a polyurethane synthesis, accounting for the majority of its industrial use. The structure of the DABCO-SF_4 adduct is particularly interesting since DABCO contains two basic sites where SF_4 could coordinate. This study aims to expand the study of Lewis-acid-base interactions between SF_4 and nitrogen bases beyond pyridine derivatives.

5.2 Results and Discussion

5.2.1 Synthesis

Diazabicyclo[2.2.2]octane is very soluble in SF_4 close to room temperature and reacts with excess SF_4 yielding the 1:2 adduct $C_6H_{12}N_2 \bullet 2SF_4$ (Equation 5.1), in which both amine groups of one DABCO molecule form chalcogen bonds to separate SF_4 molecules. At low temperature, DABCO floats on top of liquid SF_4. Upon warming to room temperature, SF_4 dissolves the DABCO forming a clear colourless solution. Upon cooling below −20 °C a fine and dense white solid immediately precipitated and sank to the bottom of the reactor. The density allows the differentiation of $C_6H_{12}N_2 \bullet 2SF_4$ from any unreacted DABCO at low temperature. By slowly precipitating this solid at –20 °C, followed by pumping at *ca.* –80 °C, crystals of $C_6H_{12}N_2 \bullet 2SF_4$ were grown that were suitable for X-ray crystallography.

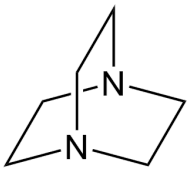

DABCO + 2 SF_4 $\xrightarrow{SF_4}$ DABCO•2SF_4 (5.1)

At low temperature, white solids were obtained upon removal of volatiles at −78 °C that incorporate additional SF_4, as evidenced by Raman spectroscopy and mass balance. The amount of SF_4 in DABCO•nSF_4 varies and depend on the duration and temperature that the sample is kept under dynamic vacuum. Attempts to produce pure $C_6H_{12}N_2$•SF_4 were undertaken by removal of SF_4 from the DABCO-SF_4 system at various temperatures. Removal of volatiles under dynamic vacuum at –75 °C produced a solid that contains SF_4 in addition to the SF_4 coordinated to DABCO. This additional SF_4 is weakly bound and is removed by pumping at elevated temperature. Pumping on the $C_6H_{12}N_2$•2SF_4 adduct at –25 °C produced a solid containing strongly adducted SF_4, as indicated by Raman spectroscopy (*vide infra*), (Equation 5.2). This solid is tentatively assigned to the DABCO•SF_4 adduct.

DABCO•2SF_4 $\xrightarrow[-(2-m)\ SF_4]{\text{pumping at } -25°C}$ DABCO•mSF_4 $(0 < m < 2)$ (5.2)

By pumping at room temperature for long periods (*ca.* 4 hours) DABCO was recovered, although trace moisture introduced throughout the reaction (and pumping cycles) can

cause the formation of HF from the hydrolysis of SF_4 (Equation 5.3). As consequence DABCO is protonated by HF, producing $[C_6H_{12}N_2H]^+$ or even $[C_6H_{12}N_2H_2]^{2+}$ if sufficient HF is produced.

$$SF_4 + H_2O \longrightarrow SOF_2 + 2\,HF \tag{5.3}$$

Similar to the pyridine derivative systems,[4] the chalcogen bond in the $C_6H_{12}N_2 \bullet 2SF_4$ adduct can be solvolysed by HF, shown in Equation 5.4. The formation of this solvolysis product was accidental and occured after long-term storage of $C_6H_{12}N_2 \bullet 2SF_4$ in an ethanol cold-bath (*ca.* –80 °C). The reaction proceeded with trace moisture that likely diffused through the FEP walls of the reactor over the course of two months, yielding $[C_6H_{12}N_2H]_2F[SF_5] \bullet 6SF_4$, which was characterized by X-ray crystallography and Raman spectroscopy.

$$DABCO \bullet 2SF_4 + 2\,HF \xrightarrow[-75°C]{SF_4} [C_6H_{12}N_2H^+]_2F^-[SF_5^-] \bullet 6SF_4 \tag{5.4}$$

A conclusive mass balance could not be obtained for the DABCO-SF_4 system due to SF_4 absorption into the FEP walls of the reactor. Unlike previously characterized nitrogen-base adducts, DABCO/SF_4 samples required warming to room temperature for

reaction to occur. The boiling point of SF_4 is –35 °C and therefore the sample is highly pressurized at room temperature, forcing SF_4 into the FEP walls.

5.2.2 X-Ray Crystallography

5.2.2.1 $C_6H_{12}N_2$•2SF_4

The $C_6H_{12}N_2$•2SF_4 adduct crystallizes in the monoclinic space group $P2_1/c$ with one entire adduct molecule in the asymmetric unit shown in Figure 5.1. Selected bond lengths and angles are shown in Table 5.1. Crystal structure parameters are tabulated in Table 5.2. Crystals of $C_6H_{12}N_2$•2SF_4 grew from excess SF_4 solvent upon pumping at –20 °C. Sulfur tetrafluoride is not as readily lost from this adduct under dynamic vacuum as observed for previously studied SF_4 adducts,[1,2] for which the complete loss of SF_4 was observed above −40 °C.

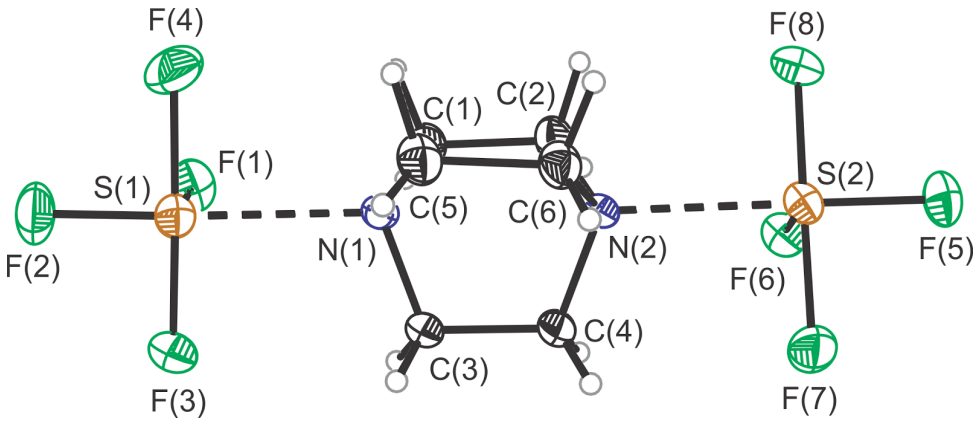

Figure 5.1 - Thermal ellipsoid plot of the $C_6H_{12}N_2$•2SF_4 adduct; Thermal ellipsoids are drawn to 50% probability.

Table 5.1 - Selected bond lengths and angles for the crystal structure of $C_6H_{12}N_2$•$2SF_4$

Bond length (Å)			
S(1)−F(1)/S(2)−F(5)	1.561(3)/1.574(3)	N(1)–C(1)/N(2)–C(2)	1.478(4)/1.477(4)
S(1)−F(2)/S(2)−F(6)	1.596(3)/1.595(3)	N(1)–C(3)/N(2)–C(4)	1.474(4)/1.478(4)
S(1)−F(3)/S(2)−F(7)	1.685(3)/1.684(3)	N(1)–C(5)/N(2)–C(6)	1.483(4)/1.483(4)
S(1)−F(4)/S(2)−F(8)	1.685(3)/1.697(3)	C(1)–C(2)	1.557(4)
S(1)---N(1)/S(2)---N(2)	2.362(4)/2.337(4)	C(3)–C(4)	1.548(4)
		C(5)–C(6)	1.553(4)
Bond Angle (°)			
F(1)−S(1)−F(2)/ F(5)−S(2)−F(6)	92.66(11)/92.27(9)	C(2)–N(2)–C(4)/ C(2)–N(2)–C(6)/ C(4)–N(2)–C(6)	108.7(2)/109.2(2)/108.45(19)
F(3)−S(1)−F(4)/ F(7)−S(2)−F(8)	171.01(11)/170.86(10)	C(3)–N(1)–C(1)/ C(3)–N(1)–C(5)/ C(1)–N(1)–C(5)	109.2(2)/108.7(2)/108.7(2)
F(1)−S(1)−N(1)/ F(5)−S(2)−N(2)	82.22(9)/81.07(8)	N(1)–C(1)–C(2)/ N(1)–C(3)–C(4)/ N(1)–C(5)–C(6)	110.0(2)/110.0(2)/110.1(2)
F(2)−S(1)---N(1)/ F(5)−S(2)---N(2)	174.80(9)/173.26(9)	N(2)–C(2)–C(1)/ N(2)–C(4)–C(3)/ N(2)–C(6)–C(5)	110.0(2)/110.4(2)/109.9(2)

Both nitrogen atoms of DABCO form chalcogen bonds to two different SF_4 with similar S---N distances (2.362(4) and 2.337(4) Å), which are comparable to that in SF_4•NEt_3 (2.3844(19) Å).[1] The geometry of the N---SF_4 moiety is square pyramidal, and the metric parameters of the SF_4 moieties in the DABCO adduct are similar to that of the NEt_3 adduct,[1] with the S−F bonds *cis* to the S---N chalcogen bond and *trans* to the lone pair being the shortest (S(1)−F(1): 1.561(3) and S(2)−F(5): 1.574(3) Å), followed by the S−F bonds *trans* to the S---N chalcogen bond (S(1)−F(2): 1.596(3) and S(2)−F(6): 1.595(3) Å). The two S−F bonds *trans* to each other, which correspond to the axial bonds in free SF_4, are substantially longer (1.684(3) to 1.697(3) Å), in agreement with the other structurally characterized SF_4-Lewis base adducts.[2] The DABCO moiety exhibits a small

distortion from D_{3h} symmetry with a slight twisting (N−C−C−N torsion angles: 4.2(3), 4.9(3), and 5.1(3)°). Such twisting has been observed for other DABCO compounds, such as DABCO·2H_2O_2.[9] The crystal structure of neat DABCO, on the other hand, showed a non-twisted conformation, based on neutron diffraction data.[10]

5.2.2.2 $[C_6H_{12}N_2H]_2[F][SF_5]$•6$SF_4$

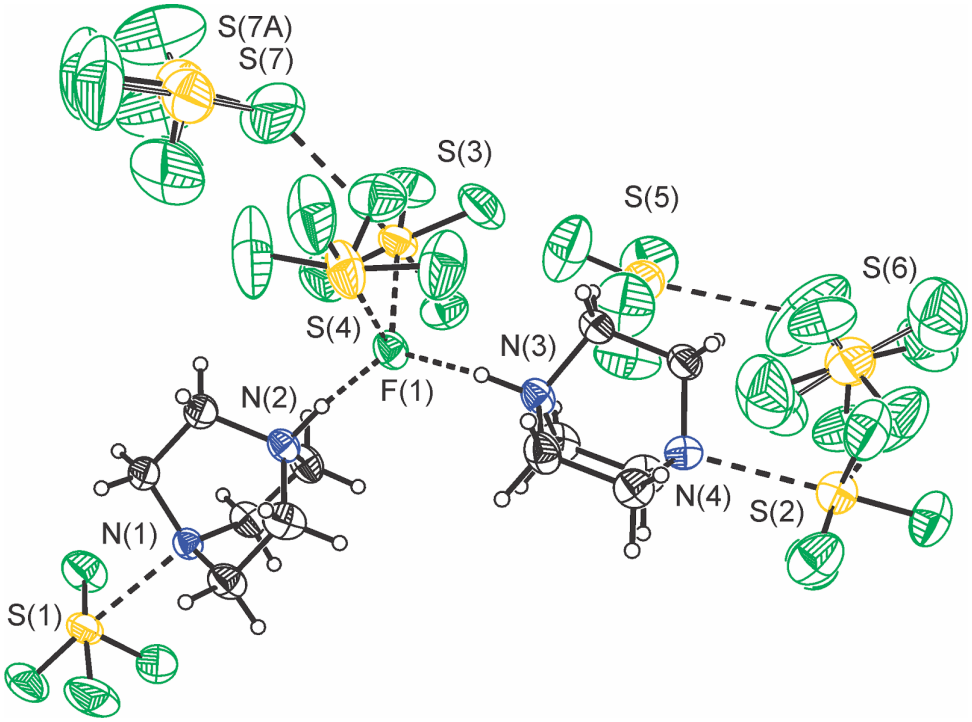

Figure 5.2 - Thermal ellipsoid plot of the $[C_6H_{12}N_2H]_2F[SF_5]$•6SF_4 crystal structure. Thermal ellipsoids are drawn at the 50% probability level. Sulfur tetrafluoride molecule containing S(7) is shown exhibiting positional disorder and $[SF_5]^-$ is depicted exhibiting rotational disorder.

The solvolysis product of $C_6H_{12}N_2$•2SF_4, $[C_6H_{12}N_2H]_2F[SF_5]$•6SF_4, crystallizes from excess SF_4 in the orthorhombic *Pbca* space group and contains two crystallographically unique, singly protonated DABCO molecules with the unprotonated nitrogens coordinated to SF_4, shown in Figure 5.2. Selected bond lengths and angles are

shown in Table 5.3, and crystal structure parameters are tabulated in Table 5.2. These two singly protonated DABCO molecules hydrogen-bond to one fluoride anion, which in turn forms F---S chalcogen bonds to two SF_4 molecules, forming the $[(F_4S\text{---}NC_6H_{12}NH)_2F(SF_4)_2]^+$ cationic moiety, shown in Figure 5.3.

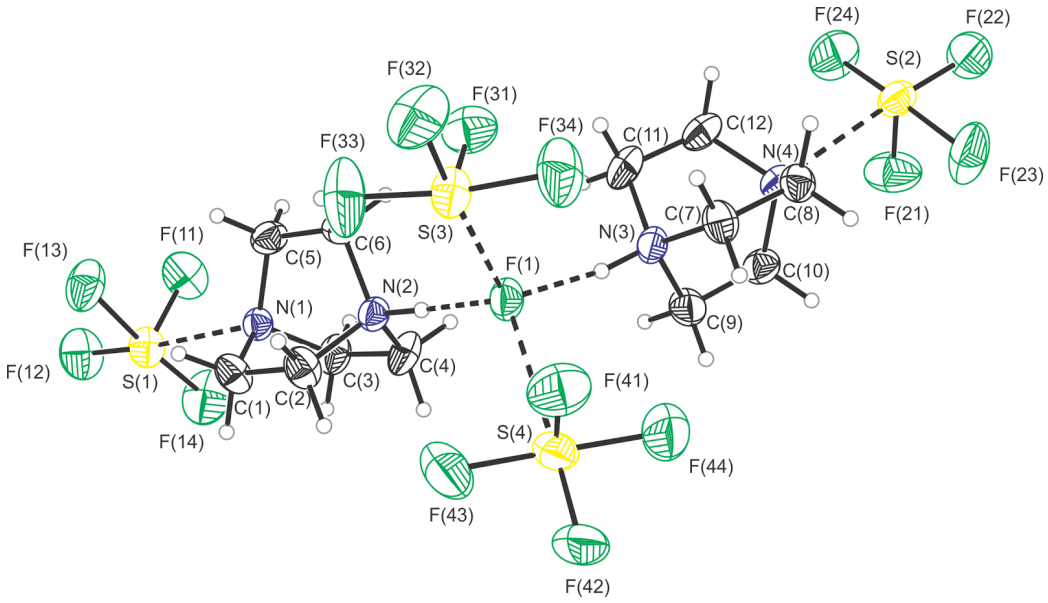

Figure 5.3 - Thermal ellipsoid plot of the $[(F_4S\text{---}NC_6H_{12}NH)_2F(SF_4)_2]^+$ cationic moiety of the $[C_6H_{12}N_2H]_2F[SF_5]\bullet 6SF_4$ crystal structure. Thermal ellipsoids are drawn at the 50% probability level.

Table 5.2 - Crystal structure parameters for $[C_6H_{12}N_2H]_2F[SF_5]\cdot 6SF_4$ and $C_6H_{12}N_2\cdot 2SF_4$

Compound	$[C_6H_{12}N_2H]_2F[SF_5]\cdot 6SF_4$	$C_6H_{12}N_2\cdot 2SF_4$
Empirical Formula	$C_{12}H_{26}F_{30}N_4S_7$	$C_6H_{12}F_8N_2S_2$
Formula weight, g mol^{-1}	1020.79	328.30
Temperature, K	163	153
Wavelength, Å	0.71073	0.71073
Crystal System	Orthorhombic	Monoclinic
Space Group	*Pbca*	$P2_1/c$
Unit Cell	a = 22.75(5) Å b = 12.51(3) Å c = 25.65(5) Å	*a* = 13.87(2) Å *b* = 7.859(14) Å *c* = 11.33(2) Å *β* = 101.572(19)°
Volume, $Å^3$	7300(25)	1210(4)
Z	8	4
μ (mm^{-1})	0.60	0.53
ρ_{calc}g cm^{-3}	1.858	1.802
F(000)	4064	664
Crystal Size, mm^3	0.35 × 0.20 × 0.10	0.33 × 0.12 × 0.09
Reflections Collected	77262	12237
Independent Reflections	8007	2753
Data/Restraints/ Parameters	8007/22/501	2753/0/163
Goodness-of-fit on F^2	1.04	1.13
$\Delta\rho_{max}$ (e $Å^{-3}$)	0.85	0.38
$\Delta\rho_{min}$ (e $Å^{-3}$)	−0.67	−0.43
R_1, $I > 2\sigma(I)$ [a]	0.0670	0.0469
wR_2 (F^2) [a]	0.1717	0.0832

[a] $R_1 = \Sigma||F_o| - |F_c||/ \Sigma|F_o|$; $wR_2 = [\Sigma w(F_o^2 - Fc^2)^2/ \Sigma w(F_o^4)]^{1/2}$.

Table 5.3 - Selected bond lengths and angles for the crystal structure of $C_6H_{12}N_2$•$2SF_4$

Bond length (Å)

S(1)–F(11)/S(2)–F(21)	1.539(4)/1.551(4)	F(1)---S(3)/S(4)	2.662(5)/2.641(4)
S(1)–F(12)/S(2)–F(22)	1.584(3)/1.577(4)	F(1)---H–N(2)/N(3)	2.598(5)/2.613(6)
S(1)–F(13)/S(2)–F(23)	1.692(4)/1.690(4)	N(1)–C(1)/C(3)/C(5)	1.490(6)/1.487(5)/1.492(6)
S(1)–F(14)/S(2)–F(24)	1.693(4)/1.669(4)	N(2)–C(2)/C(4)/C(6)	1.515(5)/1.503(5)/1.512(5)
S(1)–N(1)/S(2)–N(4)	2.514(5)/2.594(5)	N(3)–C(7)/C(9)/C(11)	1.503(5)/1.504(5)/1.507(6)
S(3)–F(31)/S(4)–F(41)	1.545(4)/1.547(4)	N(4)–C(8)/C(10)/C(12)	1.484(6)/1.487(6)/1.491(5)
S(3)–F(32)/S(4)–F(42)	1.561(4)/1.553(4)	C(1)–C(2)/C(7)–C(8)	1.553(6)/1.552(6)
S(3)–F(33)/S(4)–F(43)	1.667(4)/1.686(5)	C(3)–C(4)/C(9)–C(10)	1.557(6)/1.559(6)
S(3)–F(34)/S(4)–F(44)	1.669(4)/1.669(5)	C(5)–C(6)/C(11)–C(12)	1.552(6)/1.550(7)

Bond Angle (°)

F(11)–S(1)–F(12)	95.4(2)	C(1)–N(1)–C(3)	109.5(3)/108.7(3)/109.0(3)
F(21)–S(2)–F(22)	96.08(19)	C(1)–N(1)–C(5)	
		C(3)–N(1)–C(5)	
F(13)–S(1)–F(14)	172.76(19)	C(2)–N(2)–C(4)	109.1(3)
F(23)–S(2)–F(24)	171.2(2)	C(2)–N(2)–C(6)	109.2(3)
		C(4)–N(2)–C(6)	110.0(3)
F(12)–S(1)---N(1)	175.23(16)	C(7)–N(3)–C(9)	109.8(3)
F(22)–S(2)---N(4)	176.38(15)	C(7)–N(3)–C(11)	109.8(3)
		C(9)–N(3)–C(11)	110.2(3)
F(31)–S(3)–F(32)	98.5(2)	C(8)–N(4)–C(10)	109.3(3)
F(41)–S(4)–F(42)	99.0(3)	C(8)–N(4)–C(12)	109.0(3)
		C(10)–N(4)–C(12)	108.3(3)
F(33)–S(3)–F(34)	172.6(2)	N(1)–C(1)–C(2)	110.4(3)
F(43)–S(4)–F(44)	168.4(3)	N(1)–C(3)–C(4)	110.9(3)
		N(1)–C(5)–C(6)	110.6(3)
F(32)–S(3)---F(1)	174.88(17)	N(2)–C(2)–C(1)	108.9(3)
F(42)–S(4)---F(1)	176.5(2)	N(2)–C(4)–C(3)	108.4(3)
		N(2)–C(6)–C(5)	108.7(3)
S(4)---F(1)---S(3)	105.24(17)	N(3)–C(7)–C(8)	108.2(3)
		N(3)–C(9)–C(10)	108.2(3)
		N(3)–C(11)–C(12)	107.8(3)
		N(4)–C(8)–C(7)	111.0(3)
		N(4)–C(10)–C(9)	110.6(3)
		N(4)–C(12)–C(11)	111.4(4)

A similar motif has been observed in the protonated 2,6-dimethylpyridine structure $[HNC_5H_3(CH_3)_2]_2[SF_5]F{\cdot}SF_4$.[11] In contrast to the 2,6-dimethylpyridinium structure, the hydrogen-bonded fluoride anion in the $DABCOH^+$ structure coordinates towards two SF_4 molecules (2.662(5) and 2.641(4) Å), versus one in the 2,6-dimethylpyridinium structure (F---S: 2.5116(12) Å). As in the 2,6-dimethylpyridinium structure, the remaining fluoride anion is left sufficiently 'naked' to combine with SF_4 to form the $[SF_5]^-$ anion. Two equatorial fluorine atoms of the $[SF_5]^-$ anion form very weak S---F contacts to two additional adjacent SF_4 molecules, i.e., $S(5)F_4$ (3.119(8) Å) and $S(7)F_4$ (3.168(11)/3.398(9) Å), which are close to the limit of the sum of the van der Waals radii (3.27 Å). These two contacts keep the two equatorial fluorines that are *trans* to each other fixed, allowing for a rotational disorder of the $[SF_5]^-$ anion about this F−S−F axis, shown in Figure 5.4.

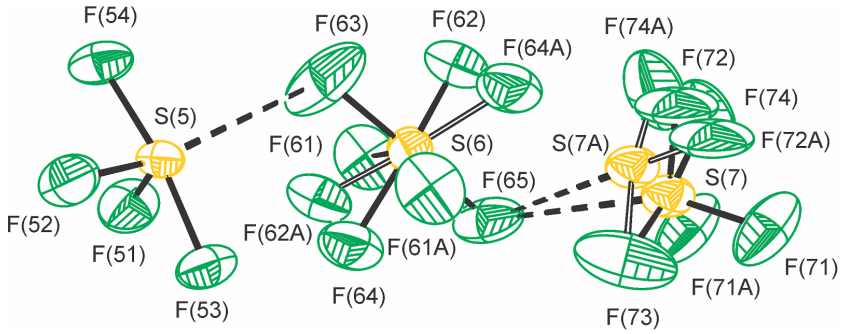

Figure 5.4 - Thermal ellipsoid plot of the $[F_4S{\bullet}SF_5{\bullet}SF_4]^-$ anion moiety of the $[C_6H_{12}N_2H]_2F[SF_5]{\bullet}6SF_4$ crystal structure. Thermal ellipsoids are drawn at 50% probability. Rotational disorder about S(6) and positional disorder of $S(7)F_4$ are shown.

The $S(7)F_4$ molecules exhibit a positional disorder with one axial fluorine atom (F73) acting as the pivot point; this axial fluorine atom is held in place by a very weak S---F contact (3.110(7) Å) to the $S(3)F_4$ molecule.

The S---N distances (2.514(5) and 2.594(5) Å) in $[C_6H_{12}N_2H]_2F[SF_5]\cdot 6SF_4$ are significantly longer than those in $C_6H_{12}N_2\cdot 2SF_4$ adduct, as a consequence of the reduced Lewis basicity upon protonation of one amine group of DABCO. The S---N length is closer to that in the pyridine adduct of SF_4 (2.514(2) Å) than that in the triethylamine adduct (2.3844(19) Å). The structure contains one disordered SF_4 molecule that does not have any contacts to DABCO or fluoride. The metric parameters of this SF_4 molecule are within the range of the values for solid SF_4, with a $F_{eq}{-}S{-}F_{eq}$ of 101.2(3)°,[11] which is not contracted by any contact as in the other adducted SF_4 molecules (N---SF_4: 95.4(2) and 96.08(19)°; F^----SF_4, 98.5(2) and 99.0(3)°). Similar incorporation of additional SF_4 molecules has been observed in the 2,6-dimethylpyridinium structure $[HNC_5H_3(CH_3)_2]_2[SF_5]F\cdot 4SF_4$.[11] The present structure exemplifies how easily SF_4 can be incorporated into the solid state at low temperature via chalcogen bonds and corroborates the Raman spectroscopic finding of facile incorporation of SF_4 into $C_6H_{12}N_2\bullet 2SF_4$ at low temperature.

5.2.3 Raman Spectroscopy

Raman spectra were obtained for $C_6H_{12}N_2$•$2SF_4$ and the solvolysed $[C_6H_{12}N_2H]_2F[SF_5]$•$6SF_4$ adduct; they are shown in Figures 5.5 and 5.6, respectively. The Raman frequencies for $C_6H_{12}N_2$•$2SF_4$ and $[C_6H_{12}N_2H]_2F[SF_5]$•$6SF_4$ are listed in Tables 5.4 and 5.5, respectively, along with comparison to SF_4 and DABCO Raman bands and tentative assignments.

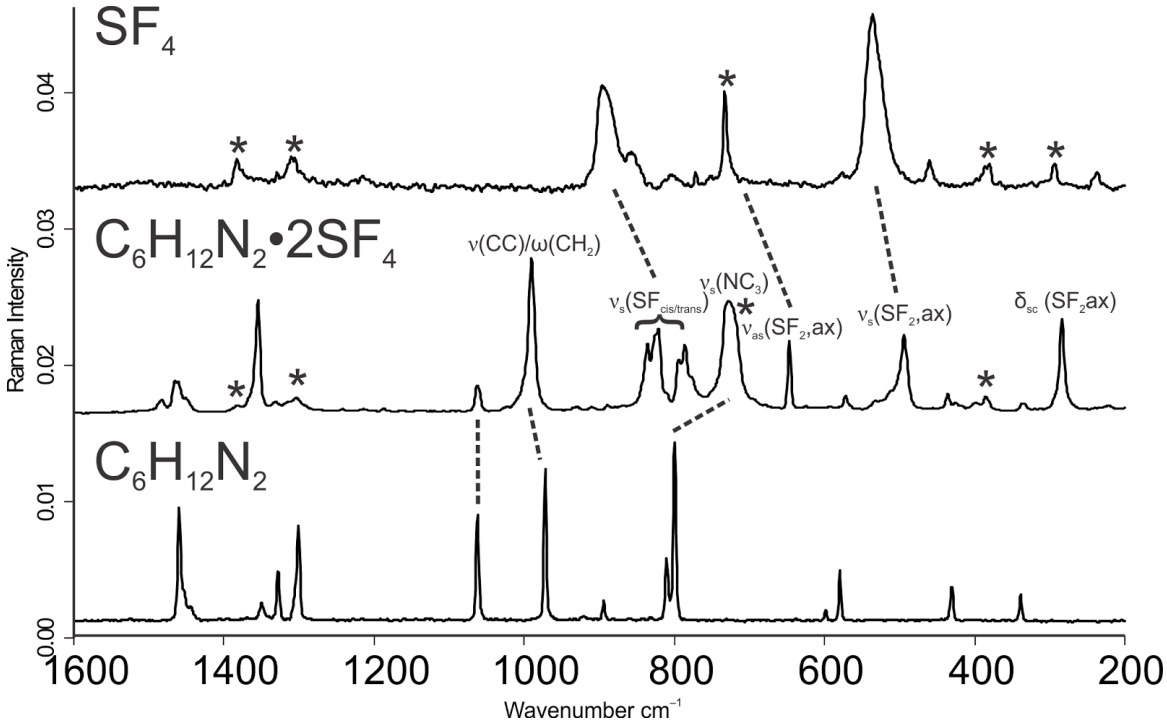

Figure 5.5 - Raman spectrum of the $C_6H_{12}N_2$•$2SF_4$ adduct in addition to the spectra for SF_4 and solid DABCO. Each spectrum was recorded at –100 °C with a minimum of 1000 scans. Signals belonging to the FEP sample tube are denoted by *.

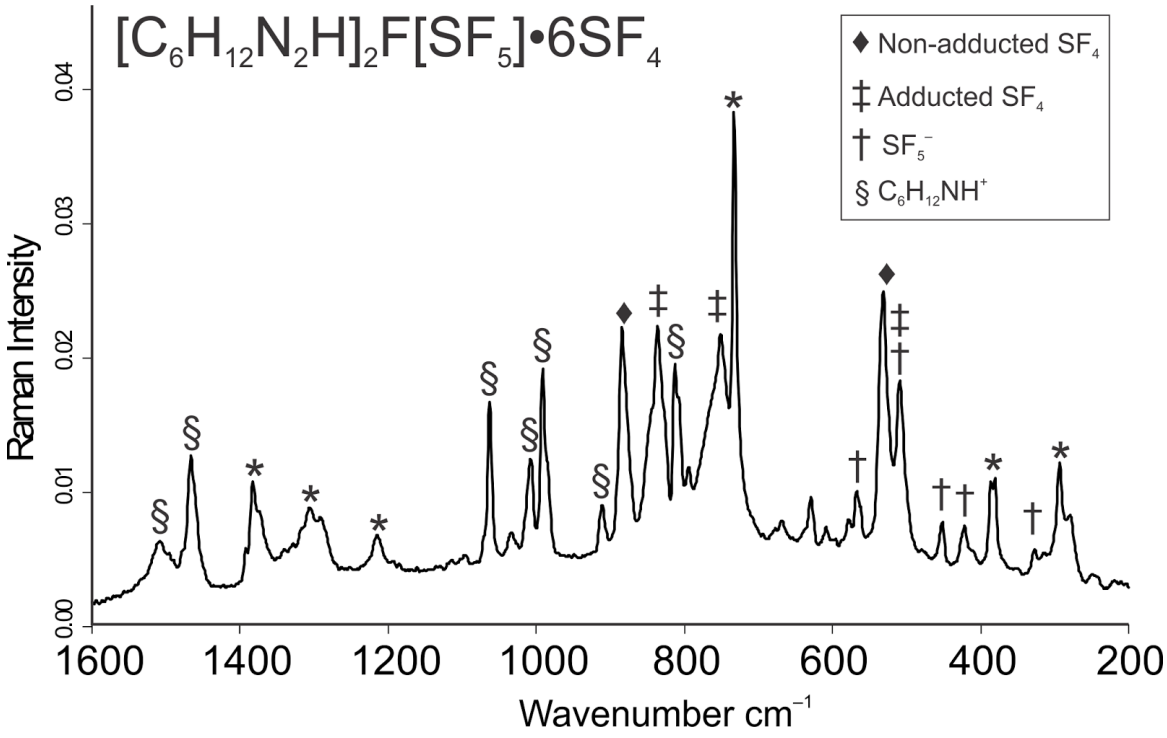

Figure 5.6 - Raman spectrum for the $[C_6H_{12}N_2H]_2F[SF_5]•6SF_4$ solvolysis product formed by the slow hydrolysis of $C_6H_{12}N_2•2SF_4$. Signals arising from the FEP sample tube are labelled with *.

The Raman spectrum of the solid from which a crystal of the $[C_6H_{12}N_2H]_2F[SF_5]•6SF_4$ salt was obtained is consistent with the composition of the crystal structure. This Raman spectrum features bands that are indicative of protonated $DABCOH^+$ at 1008 and 608 cm^{-1} arising from skeletal deformation caused by asymmetric protonation of one amine group.[13] Bands characteristic of the $[SF_5]^-$ anion are present between 800 and 250 cm^{-1},[14] most notably at 578, 452, and 422 cm^{-1} where the peaks are well differentiated from SF_4 signals.

Table 5.4 - Raman frequencies and tentative assignments for $C_6H_{12}N_2$•$2SF_4$

SF_4[b]	$C_6H_{12}N_2$	$C_6H_{12}N_2$•$2SF_4$[c]	Tentative Assignment[a]
	3001(3)	3003(18)	
	2945(81)		
	2938(82)		
	2924(82)	2977(27)	$\nu(CH_2)$ + overtones and
	2901(17)	2951(21)	combination modes
	2870(100)	2895(11)	
	2713(1)		
	2639(3)		
	2625(2)		
	2614(2)		Overtones or combination modes
	2589(3)	1482(9)	
		1465(21)	
	1457(44)	1354(73)	$\delta(CH_2)$
	1346(7)		$\nu(CH_2)/\nu(CC)/\omega(CH_2)$
	1325(15)	1331(7)	
	1299(36)	1304(10)	$\tau(CH_2)$
	1060(28)	1062(18)	$\nu_{as}(NC_3)$
	971(61)	990(100)	$\nu(CC)/\omega(CH_2)$
	918(2)		$\nu(CC)$
892		836(45)	$\nu(SF_{eq.}cis)$
		825sh	
		821(55)	$\nu(SF_{eq}$ trans)
		795sh	
		786(4)	
	829(1)		$\rho(CH_2)$
867			$\nu_{as}(SF_2$ eq)
	806(67)	728(72)	$\nu_s(NC_3)$
730		647(46)	$\nu_{as}(SF_2$ ax)
558		495(50)	$\nu_s(SF_2$ ax) + $\nu_s(SF_4)$ in phase
532			$\rho_w(SF_2$ eq), $\nu s(SF_4)$ in phase
532			$\delta_{sc}(SF_2$ eq) + $\delta_{sc}(SF_2$ ax)
	579(19)	572(11)	$\delta_{as}(NC_3)$
	430(11)	436(11)	$\delta_{as}(NC_3)$
	337(11)	337(5)	$\rho(NC_3)$
475			$\tau(SF_2)$
353		284(59)	δ_{sc} (SF_2 ax) o.o.p.
228			

[a]o.o.p. (out-of-plane); s (symmetric); as (antiymmetric); ax (axial); eq (equatorial); ν (stretch); δ (bend); ρ (rock); τ (torsion); ω (wagging), scissoring (δ_{sc})

[b]Experimental gas-phase vibrational frequencies and assignments from K. O. Christe, X. Zhang, J. A. Sheehy, R. Bau, *J. Am. Chem. Soc.* **2001**, *123*, 6338-6348 and references therein[12]

[c]Raman spectra were recorded in a ¼-in. FEP tube at –100 °C. Signals from the FEP sample tube were observed at 387(5), 733(sh), 1216(5), and 1307(2) cm^{-1}.

Table 5.5 - Raman frequencies and tentative assignments for $C_6H_{12}N_2$•$2SF_4$ and crystalline $[C_6H_{12}N_2H]_2F[SF_5]$•$6SF_4$

SF_4[b]	$C_6H_{12}N_2$	$[C_6H_{12}N_2H]_2F[SF_5]$•$6SF_4$[c]	Tentative Assignment[a]
	3001(3)	3029(32)	
	2945(81)	3019(33)	
	2938(82)	2998(69)	
	2924(82)	2972(54)	$\nu(CH_2)$ + overtones and
	2901(17)	2951sh	combination modes
		2923sh	
	2870(100)	2906(19)	
	2713(1)		
	2639(3)		
	2625(2)		
	2614(2)		Overtones or combination modes
	2589(3)		
		1508(20)	
	1457(44)	1466(53)	
	1346(7)	1392(15)	
	1325(15)	1374sh	$\nu(CH_2)/\nu(CC)/\omega(CH_2)$
	1299(36)	1292(24)	$\tau(CH_2)$
		1071sh	
	1060(28)	1063(63)	$\nu_{as}(NC_3)$
		1033(12)	
		1008(39)	Skel. def.
	971(61)	992(73)	$\nu(CC)/\omega(CH_2)$
		986sh	
	918(2)	911(19)	$\nu(CC)$
892		884(85)	
		879sh	$\nu_s(SF_2eq)$
		845sh	
		836(85)	
		827sh	ν(SF eq)
	829(1)	813(69)	$\rho(CH_2)$
		808sh	
		795(31)	SF_5^-, ν(SFax)
867		766sh	
		751(80)	$\nu_{as}(SF_2$ eq)
	806(67)	668(8)	$\nu_s(NC_3)$
		629(19)	DABCO Skel. def.
		608(8)	$DABCOH^+$
730			$\nu_{as}(SF_2$ ax)
		578(12)	SF_5^-, $\nu_{as}(SF_4)$
558		532(100)	$\nu_s(SF_{2.ax}) + SF_5^-$, $\nu_s(SF_4)$ in phase
532		510(68)	$\rho_w(SF_2$ eq) + SF_5^-, vs(SF_4) in phase
532			$\delta_{sc}(SF_2$ eq) + $\delta_{sc}(SF_2$ ax)
	579(19)		$\delta_{as}(NC_3)$
		452(17)	SF_5^- $\nu_s(SF_4)$ o.o.p.
		422(17)	SF_5^- $\delta_s(SF_4)$ umbrella
	430(11)	413sh	$\delta_{as}(NC_3)$
		328(10)	SF_5^- $\delta_s(SF_4)$ in plane
	337(11)	316(10)	$\rho(NC_3)$
475			$\tau(SF_2)$
353		280(25)	δ_{sc} (SF_2ax) o.o.p.
228		250(5)	SF_5^- $\delta_{as}(SF_4)$ in plane

[a]o.o.p. (out-of-plane); s (symmetric); as (antiymmetric); ax (axial); eq (equatorial); ν (stretch); δ (bend); ρ (rock); τ (torsion); ω (wagging), scissoring (δ_{sc})

[b]Experimental gas-phase vibrational frequencies and assignments from K. O. Christe, X. Zhang, J. A. Sheehy, R. Bau, *J. Am. Chem. Soc.* **2001**, *123*, 6338-6348 and references therein[12]

[c]Raman spectra were recorded in a ¼-in. FEP tube at –100 °C. Signals from the FEP sample tube were observed at 294(10), 387(9), 733(150), 1216(5), 1216(5), 1307(7), and 1379(10) cm^{-1}.

Signal for adducted SF_4 were observed at 836 cm^{-1} attributed to $\nu_s(SF_2$ eq.). These SF_4 stretches are sensitive to the coordination to a nitrogen base with the $\nu_s(SF_2$ eq.) stretch shifting to lower frequency when adducted to a strong base. When SF_4 was coordinated to DMAP, this stretch was observed at 797 cm^{-1} compared to the weaker 2,6-lutidine adduct in which the stretch was observed at 861 cm^{-1}.[2] This indicates that the adducted SF_4 observed in $[C_6H_{12}N_2H]_2F[SF_5]\bullet 6SF_4$ is weakly bound to the Lewis base compared to the unprotonated DABCO adducts (*vide infra*). Comparing to the previously characterized pyridine derivative adducts, the adducted SF_4 is coordinated similarly to $NC_5H_5\bullet SF_4$ and $NC_5H_4(CH_3)\bullet SF_4$ that have ν(SF eq.) frequencies of 852 and 841 cm^{-1}, respectively.[2] This is consistent with the crystal structure obtained for $[C_6H_{12}N_2H]_2F[SF_5]\bullet 6SF_4$, that shows S---N bond lengths of 2.514(5) and 2.594(5) Å similar to the S---N distances in $NC_5H_5\bullet SF_4$ and $NC_5H_4(CH_3)\bullet SF_4$: 2.514(2) and 2.513(3) Å, respectively (*vide supra*).[2]

Bands associated with non-adducted SF_4 significantly complicate the spectrum due to additional SF_4 environments. These additional Raman bands are observed in the range of 900-500 cm^{-1} with the most obvious at 531 cm^{-1}. The signal at 531 cm^{-1} is very close in frequency to the same band in the spectrum of liquid SF_4 at 535 cm^{-1}; however, the signal in liquid SF_4 is significantly broader than in the sample containing $[C_6H_{12}N_2H]_2F[SF_5]\bullet 6SF_4$. The narrowing of this signal is further indication that SF_4 is incorporated in the solid state, which is consistent with the acquired X-ray crystal structure.

The Raman spectrum of DABCO•2SF_4 presented in Table 5.4 was acquired after pumping off excess SF_4 at –76 °C for approximately 4.5 hours from a sample, from which DABCO•2SF_4 was crystallized at approximately –20 °C. Expectedly, the Raman spectrum for $C_6H_{12}N_2$•2SF_4 contains strong signals for adducted SF_4 at 495 (ν_s, SF_2 ax.), 647 (ν_{as}, SF_2 ax.), 821 (ν, SF eq. *trans*), and 836 cm^{-1} (ν, SF eq. *cis*). As observed in the study of pyridine derivative SF_4 adducts, the two equatorial fluorines on SF_4 are non-symmetry-related once adducted to DABCO, with one fluorine *trans* to the coordinating amine group and the other being *cis* with respect to the S---N contact.

The ν(SF eq. *cis*) frequency of DABCO•2SF_4 is at lower frequency of the corresponding signals in the spectrum of $[C_6H_{12}N_2H]_2F[SF_5]$•6SF_4 since the protonation of DABCO to $DABCOH^+$ causes a significant drop in basicity. Characteristic DABCO signals were observed at 990 (ν, CC / ω, CH_2) and 728 cm^{-1} (νs, NC_3) with both signals significantly shifted from the frequencies observed for pure DABCO.

The solid from which crystals of DABCO•2SF_4 were harvested was formed slowly at –20 °C before cooling to *ca.* –80 °C and pumping off solvent from the crystals. If, however, the solid is formed upon rapid cooling to low temperature in excess SF_4, it tends to incorporate significant SF_4 into the solid-state structure. For this reason, extended periods of evacuation are required for this system to remove additional non-adducted SF_4 molecules, presumably trapped in the solid by F---SF_4 chalcogen bonding. The sample was evacuated at –70 °C, –25 °C, and 20 °C, recording Raman spectra after each evacuation cycle. Raman frequencies and tentative assignments are given in Table 5.5 and shown in Figure 5.7.

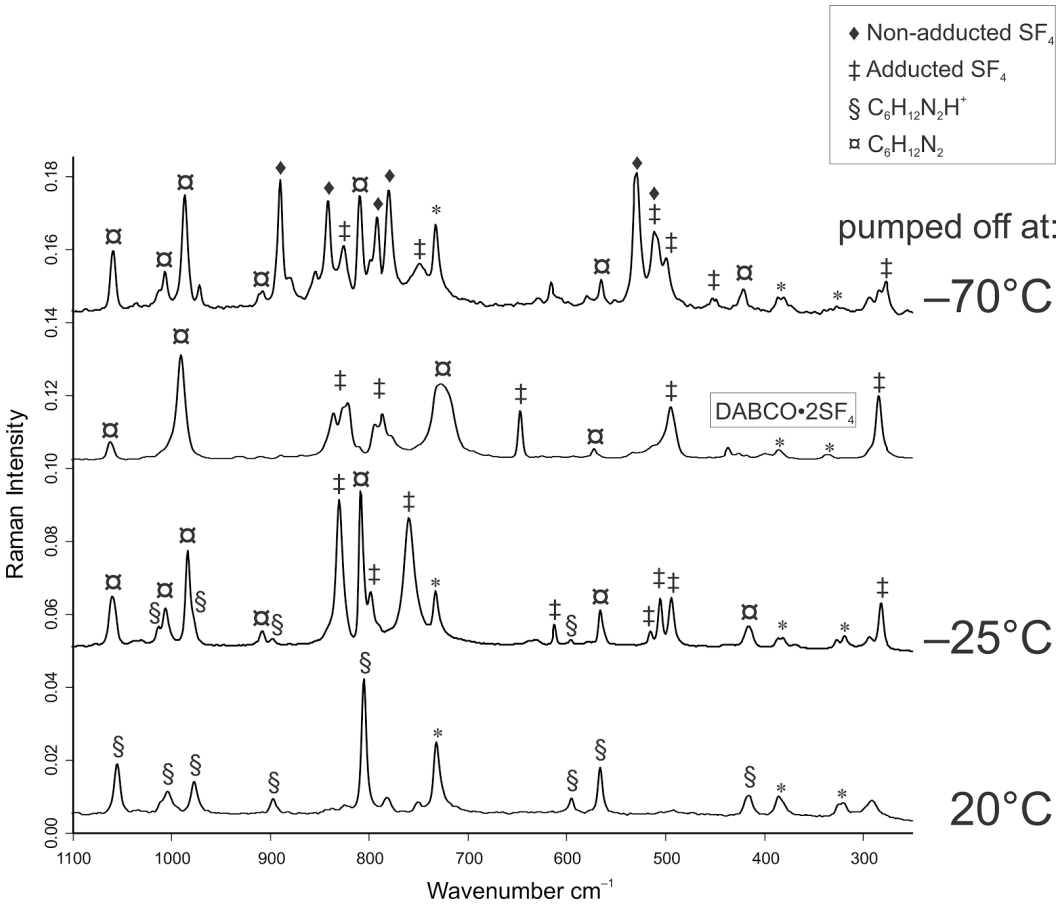

Figure 5.7 - Raman spectra for $C_6H_{12}N_2$•nSF_4 solid recorded after removal of volatiles by dynamic vacuum at –70 °C, –25 °C, and 20 °C. Signals from the FEP sample tube are denoted by *. The spectrum of DABCO•2SF_4 is included for comparison.

Upon Removal of SF_4 solvent at –70 °C for 4 hours, the primary product is the $C_6H_{12}N_2$•2SF_4 adduct, with a characteristic band at 987 cm^{-1} arising from the DABCO ν(CC)/ω(CH_2) mode. Moreover, this mode is shifted to higher frequency compared to neat DABCO (971 cm^{-1}) due to coordination of a Lewis acid to the amine groups.[13] The SF_4 regions of the –70 °C sample (900-750 and 550-250 cm^{-1}) are significantly complicated due to the additional SF_4 that appears to be incorporated into the solid. An intense band for the ν_s (SF_2 ax.) mode at 529 cm^{-1}, suggests the presence of uncoordinated SF_4. The sharpness of this band indicates the presence of SF_4 in the solid state rather than liquid SF_4.

Table 5.6 - Raman frequencies and tentative assignments for the DABCO-SF_4 system evacuated at variable temperatures

Evacuated by dynamic vacuum at [a]			Tentative Assignment [b]
–70 °C	**–25 °C**	**20 °C**	
3023(31)	3016(26)	3008(40)	
2998(38)			
2970(42)	2982(43)	2981(59)	
2944(26)	2959(37)	2956(62)	$\nu(CH_2)$ + overtones and
2924(20)	2902(9)	2902(15)	combination modes
2906(19)			
2871(20)			
	2441(5)		
		1484(11)	$DABCOH^+$, $\delta(CH_2)$
1467sh	1459(28)	1456(47)	$\delta(CH_2)$
1460(34)	1450sh		
1383(17)	1386(10)		
1367(11)		1354(20)	
1328(13)		1336(19)	
1317(18)			$\omega(CH_2)$, $\tau(CH_2)$
1300(20)	1309(12)		
1283(16)			
		1056(40)	$DABCOH^+$, $\nu_{as}(NC_3)$
1060(45)	1060(34)		$\nu_{as}(NC_3)$
1007(30)	1006(26)	1006sh	DABCO Skel. def.
1004sh	1004(5)	1004(20)	$DABCOH^+$, Skel. def.
987(84)	984(62)		coord. DABCO $\nu(CC)/\omega(CH_2)$
		978(28)	$DABCOH^+$, $\nu(CC)/\omega(CH_2)$
972(21)			DABCO, $\nu(CC)/\omega(CH_2)$
912sh			
908(10)	909(10)		$\nu(CC)$
	898(6)	898(14)	
890(94)			
881sh			ν_s (SF_2, eq.)
854(29)			
842(79)			ν (SF_2, eq.)
826(47)	831(95)		
810(82)	809(100)		
799sh		806(100)	ν_s (NC_3)
793(67)	799(35)		
780(87)	760(83)		ν(SF eq)
749(34)		781(9)	$\delta_{as}(NC_3)$
	632(6)		
629(11)	612(14)		DABCO Skel. def.
		595(15)	
579(13)	566(26)	566(38)	$\delta_{as}(NC_3)$
529(100)			ν_s (SF_2, ax.)
511(64)	515(12)		$\rho_w(SF_2$, eq)
499sh	505(33)		
453(12)	494(33)		$\nu_s(SF_2$, ax.)
421(20)	416(16)	416(18)	$\delta_{as}(NC_3)$
381(20)	381(10)		$\rho(NC_3)$
	319(22)		
284sh	282(31)		δ_{as} (SF_2 ax) o.o.p.
277(21)			
	218(5)	292(16)	
	129(12)		

[a] Raman spectra were recorded in a ¼-in. FEP tube at –100 °C. Signals from the FEP sample tube were observed at 294(10), 387(9), 733(150), 1216(5), 1216(5), 1307(7), and 1379(10) cm^{-1}.

[b] o.o.p. (out-of-plane); s (symmetric); as (asymmetric); ax (axial); eq (equatorial); ν (stretch); δ (bending); ρ (rocking); τ (torsion); ω (wagging)

Pumping at –25 °C for 3 hours removes non-adducted and some of the adducted SF_4, likely forming DABCO•SF_4 as the Raman spectrum is significantly simplified. The ν(SF eq. *trans*) mode at 760 cm^{-1} and the ν(SF eq. *cis*) at 831 cm^{-1} suggests that SF_4 remains strongly adducted. The SF_4 of DABCO•SF_4 appears to be bound stronger than in the $C_6H_{12}N_2$•2SF_4 adduct. The ν(SF eq. cis) and ν(SF eq. trans) bands are shifted to lower frequency than the analogous stretches in the Raman spectra for NC_5H_5•SF_4, $NC_5H_5(CH_3)$•SF_4, and $NC_5H_5(CH_3)_2$•SF_4, meaning the SF_4 is coordinated more strongly relative to pyridine, picoline, and 2,6-lutidine. The $\delta_{as}(NC_3)$ deformation is sensitive to change as the amine group is coordinated to a Lewis acid. This peak is shifted from 579 cm^{-1} in pure DABCO to 566 cm^{-1} in the DABCO•SF_4 spectrum, indicating the amine group remains coordinated to SF_4. The characteristic ν CC / ω CH_2 peak at 990 cm^{-1} of $C_6H_{12}N_2$•2SF_4 adduct is shifted to 984 cm^{-1} in the $C_6H_{12}N_2$•SF_4 spectrum.

The ability of DABCO•SF_4 to bind SF_4 at significantly higher temperature than previously observed for SF_4 adducts is especially interesting because of the synthetic importance of SF_4 as a deoxo-fluorinating reagent, converting OH, C=O, and COOH groups into CF, CF_2, and CF_3 groups, respectively.[15] Although SF_4 offers convenient deoxyfluorination capabilities, its low boiling point, moisture sensitivity, and dangerous hydrolysis product HF has limited its utility in a typical organic synthetic setting. The incorporation of SF_4 into a solid matrix may be method to exploit this useful reagent.

The Raman spectrum of the sample recorded after removal of volatiles under dynamic vacuum at 20 °C contains primarily $[C_6H_{12}N_2H]^+$. Since each subsequent evacuation was performed in quick succession, it is expected that some SF_4 will

hydrolyse, forming HF. The DABCO skeletal deformation mode at 1006 cm^{-1} is shifted to 1004 cm^{-1} due to protonation of the amine group by HF. Upon pumping at room temperature (and the introduction of additional moisture), the signal at 1006 cm^{-1} is lost and the signal at 1004 cm^{-1} remains.

5.3 Summary and Conclusion

The DABCO-SF_4 Lewis-acid-base system was studied by Raman spectroscopy and X-ray crystallography. By dissolving DABCO in excess SF_4 at room temperature and removing excess SF_4 at low temperature, white solid is formed containing SF_4. When cooling rapidly in excess SF_4, DABCO incorporates SF_4 in the solid state, containing non-adducted SF_4 in addition to adducted SF_4 after pumping at –70 °C. Pumping at –25 °C removed this non-adducted SF_4 but some SF_4 remains strongly coordinated to DABCO. This solid retains SF_4 at higher temperature compared to other SF_4-nitrogen base adducts. Crystals of $C_6H_{12}N_2$•$2SF_4$ were grown from excess SF_4 and characterized by X-ray crystallography, showing SF_4 coordination to both amine groups of DABCO. Slow hydrolysis of $C_6H_{12}N_2$•$2SF_4$ formed the $[C_6H_{12}N_2H]_2F[SF_5]$•$6SF_4$ solvolysis product, characterized by Raman spectroscopy and X-ray crystallography.

The DABCO-SF_4 system forms solid-state networks containing both strongly adducted SF_4 in addition to weakly bound SF_4 that is retained in the solid state. The non-adducted SF_4 can be removed by dynamic vacuum at low temperature, while the adducted SF_4 is not as easily removed, requiring pumping at elevated temperatures. This study offers insight into SF_4 chalcogen bonding expanded to non-pyridine nitrogenous

bases and may provide understanding of small molecule incorporation into solid-state networks.

References

[1] J. T. Goettel, P. Chaudhary, P. Hazendonk, H. P. A. Mercier, M. Gerken, *Chem. Commun.* **2012**, *48*, 9120-9122.

[2] P. Chaudhary, J. T. Goettel, H. P. A. Mercier, S. Sowlati-Hashjin, P. Hazendonk, M. Gerken, *Chem. - Eur. J.* **2015**, *21*, 6247–6256.

[3] E. L. Muetterties, *J. Am. Chem. Soc.* **1960**, *82*, 1082–1087.

[4] J. T. Goettel, N. Kostiuk, M. Gerken, *Inorg. Chem.* **2016**, *55*, 7126–7134.

[5] J. Bittner, J. Fuchs, K. Seppelt, *Z. Anorg. Allg. Chem.* **1988**, *557*, 182–190.

[6] M. Clark, C. J. Kellen-Yuen, K. D. Robinson, H. Zhang, Z. Y. Yang, K. V. Madappat, J. W. Fuller, J. L. Atwood, J. S. Thrasher, *Eur. J. Solid State Inorg. Chem.* **1992**, *24*, 809–833.

[7] W. Heilemann, R. Mews, S. Pohl, W. Saak, *Chem. Ber.* **1989**, *122*, 427–432.

[8] B. Bita, *Eur. J. Chem.* **2010**, *1*, 54–60.

[9] G. Laus, V. Kahlenberg, K. Wurst, T. Lörting, H. Schottenberger, *CrystEngComm.* **2008**, *10*, 1638.

[10] J. K. Nimmo, B. W. Lucas, *Acta Crystallogr., Sect. B: Struct. Sci.* **1976**, *32*, 348–353.

[11] J. T. Goettel, N. Kostiuk, M. Gerken, *Angew. Chem. Int. Ed.* **2013**, *52*, 8037–8040.

[12] K. O. Christe, X. Zhang, J. A. Sheehy, R. Bau, *J. Am. Chem. Soc.* **2001**, *123*, 6338–6348.

[13] D. A. Guzonas, D. E. Irish, *Can. J. Chem.* **1988**, *66*, 1249–1257.

[14] L. F. Drullinger, J. E. Griffths, *Spectrochim. Acta, Part A* **1971**, *27*, 1793–1799.

[15] W. C. Smith, *Angew. Chem. Int. Ed.* **1962**, *1*, 467–475.

6 Summary and Directions for Future Work

6.1 Summary

Pentafluoroethyl derivatization of sulfur(IV) fluorides was explored by $–C_2F_5$ substitution of fluoride in SF_4. An improved synthesis of $SF_3C_2F_5$ using $Me_3SiC_2F_5$ and SF_4 is presented, allowing the formation of $SF_3C_2F_5$ at low temperature. This synthetic approach also yielded $SF_2(C_2F_5)_2$. Using SOF_2 as substrate allows for the formation of thionyl pentafluoroethyl derivatives, $SOFC_2F_5$ and $SO(C_2F_5)_2$.

The characterization of these pentafluoroethyl derivatives by high-resolution ^{19}F NMR spectroscopy produced complex spin systems caused by magnetic inequivalence and long-range coupling of pentafluoroethyl groups. Via simulation of the ^{19}F NMR resonances, $SF_2(C_2F_5)_2$ was fully characterized including the determination of chemical shifts and *J*-coupling constants. The full ^{19}F NMR spectroscopic characterization of $SOFC_2F_5$ was undertaken and the correction of previously reported constants was made possible by high-field and high-resolution ^{19}F NMR experiments. Calculations were performed with B3LYP/aug-cc-pVTZ in order to compare the gas-phase geometries of the studied compounds. The pentafluoroethyl derivative, $SO(C_2F_5)_2$, was crystallized and the X-ray crystal structure was obtained. The X-ray crystal structure of $[S(OC_2H_5)_3][H_3F_4]$ was acquired after the alcoholysis of one sample at low temperature. Additionally, the crystal structure of the $Me_3SiC_2F_5$ pentafluoroethylating reagent was obtained for the first time.

The DABCO-SF_4 Lewis-acid-base system was investigated by reacting DABCO with excess SF_4, from which the $C_6H_{12}N_2 \bullet 2SF_4$ adduct was crystallized. When this adduct

is formed upon rapid cooling to low temperature in excess liquid SF_4, it tends to capture SF_4 in the solid matrix. This system contains adducted SF_4 that is strongly bound to DABCO in addition to weakly bound non-adducted SF_4. The non-adducted SF_4 can be removed under dynamic vacuum at –20 °C, at which temperature the complete loss of SF_4 was observed for SF_4 adducts with mono-basic Lewis bases.

Similar to previously characterized SF_4-nitrogen base adducts, DABCO•2SF_4 is solvolysed by HF upon the hydrolysis of SF_4. In this case, the slow hydrolysis of SF_4 was achieved incidentally by the diffusion of an ethanol cold bath through the walls of the FEP reactor, causing the hydrolysis of SF_4, the formation of HF, and ultimately the formation of crystals of $[C_6H_{12}N_2H]_2F[SF_5]•6SF_4$. This crystal structure contains both adducted SF_4, and non-adducted SF_4 molecules that are bound by weak S---F contacts to the $[SF_5]^-$ anion, which exemplifies the ability of such solids to incorporate SF_4 by weak interactions.

6.2 Directions for Future Work

The chemistry of sulfur(IV) pentafluoroethyl derivatives should be further explored. The new synthetic route to $SF_3C_2F_5$, $SF_2(C_2F_5)_2$, $SOFC_2F_5$, and $SO(C_2F_5)_2$ offers an opportunity to explore their chemical properties and possible applications. One species, $SF_3C_2F_5$, can be separated from other pentafluoroethyl-containing compounds, allowing exploration of its interactions with organic substrates.

The purification of other pentafluoroethyl derivatives $SF_2(C_2F_5)_2$, $SOFC_2F_5$, and $SO(C_2F_5)_2$ should be explored further, including attempting crystal growth of $SF_3C_2F_5$, $SF_2(C_2F_5)_2$, and $SOFC_2F_5$. The extensive utility and reactivity of SF_4, might foreshadow

the extensive reactivity of these pentafluoroethyl derivatives. Specifically, the Lewis-acid-base behaviour of these species should be investigated. Since $SF_3C_2F_5$, $SF_2(C_2F_5)_2$, and $SOFC_2F_5$ all contain sulfur-bound fluorines, reactions with strong Lewis acids may yield novel salts. Moreover, the Lewis-acid behavior of sulfur fluorides is established and the Lewis acidity of pentafluoroethyl derivatives should be probed. The properties of these pentafluoroethylated sulfur fluorides may aid the development of novel pentafluoroethylating reagents.

The included synthesis for pentafluoroethyl derivatives of sulfur fluorides should be employed for other substrates in order to synthesize other pentafluoroethyl derivatives. Harsh lithium pentafluoroethanide reactions are not suitable for all substrates and milder reaction conditions may be required for some systems. The use of $Me_3SiC_2F_5$ should be reacted with a multitude of substrates in order to explore its broader utility for nucleophilic pentafluoroethylations of inorganic fluorides.

The synthesis of $[S(OC_2H_5)_3][H_3F_4]$ and other analogous trisalkoxysulfonium salts should be investigated including the determination of which sulfur-containing species was alcoholysed by ethanol. Once determined, the species could be reacted with a selection of alcohols in order to produce similar salts.

The DABCO-SF_4 system should be investigated, including completing the characterization of DABCO•SF_4. Other polybasic bases should be employed for their ability to immobilize SF_4 in hopes of leading to a solid-state source of SF_4 at ambient temperatures. Renewed interest in metal-organic frameworks has produced a large library

of organic base struts that may be employed in crystal design, which may produce adducts with interesting properties and reactivities.